CdZnTe Detectors Development in the NNS Department

Giuseppe Camarda
A. Bolotnikov, Y. Cui, A. Hossain, K. Kim, G. Yang, and R. James
Nonproliferation and National Security Department
Brookhaven National Laboratory
February 25, 2009

BROOKHAVEN NATIONAL LABORATORY
a passion for discovery

Office of Science
U.S. DEPARTMENT OF ENERGY

Outline

Introduction

- Research areas
- Advantages of CdZnTe (CZT) gamma-ray detectors

Material characterization

- Experimental techniques
  - IR microscopy
  - White X-ray Diffraction Topography (WXDT)
  - Micro-scale X-ray mapping
  - Surface etching
- Te inclusions
- Dislocations
- Polarization effect
- E-field non-uniformities

Conclusion

Development of CZT Detectors

Three research areas:

- CZT material growth (new)

- Material characterization (samples from vendors such as Redlen, eV Products, Yinnel Tech, Acrotech, BNL)

  Others material characterization Techniques:
  Pockels Effect, Photoluminescence,I-DLTS, and TCT measurements

- Detector development and testing
  - Hand-held Gamma-ray spectrometer based on Frisch-ring CZT detector arrays
  - Gamma Camera for High-resolution Imaging of Prostate Cancer

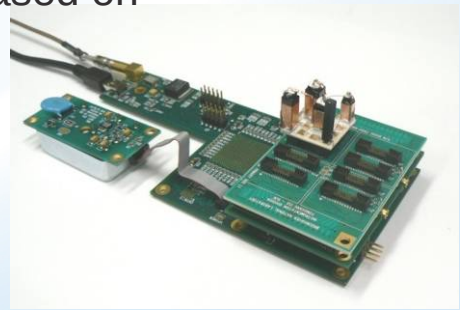

Required Material Properties for a Radiation Detector

- High density and atomic number → High efficiency
- High resistivity → Low dark current
- Photosensitive → Charge generated
- Good transport properties → Carriers collected
- Single crystals → Uniformity of response

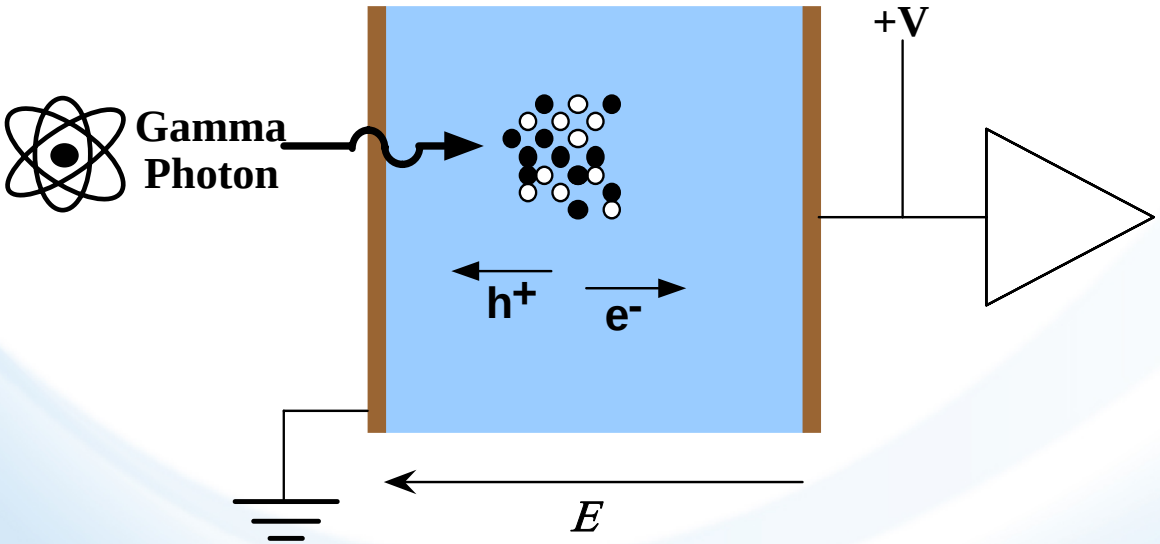

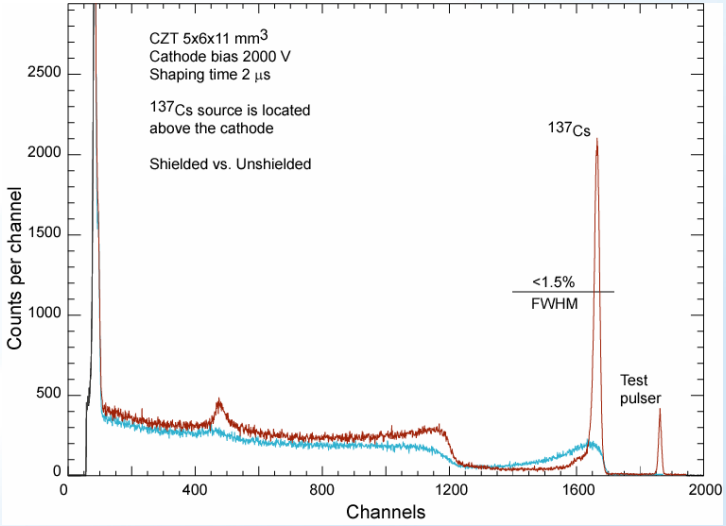

Advantages of Cadmium Zinc Telluride Material

	CZT	Ge	Si	TlBr	HgI_2
• High average Z	49.1	32	14	80	80
• High density (g/cm^3)	5.78	5.32	2.33	7.56	6.4
• High resistivity (Ω–cm)	10^{10}	47	$2.3x10^5$	10^{12}	10^{12}

- chemically reactive
- difficult to handle
- toxic

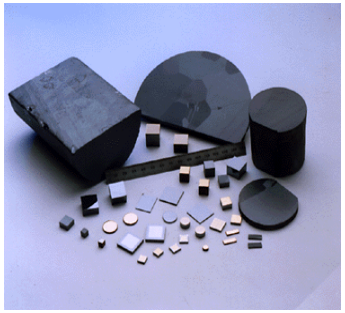

TlBr

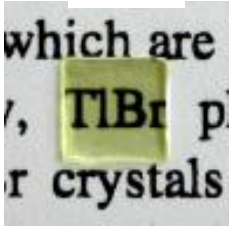

HgI_2

Important Detector Attributes:

- Large enough band gap energy (1.6 eV) to permit room temperature operation
- High atomic number (48 for Cd, 52 for Te) for photoelectric absorption up to high energies
- High density (~6 g cm^{-3}) for good stopping power
- Increased resistivity with introduction of zinc. Low leakage current at high bias
- Good energy resolution (FWHM) due to small Fano factor
- Simple, low power readout electronics
- Small size (portable devices)
- High spatial resolution (imaging devices)

Progress in CZT Detector Development

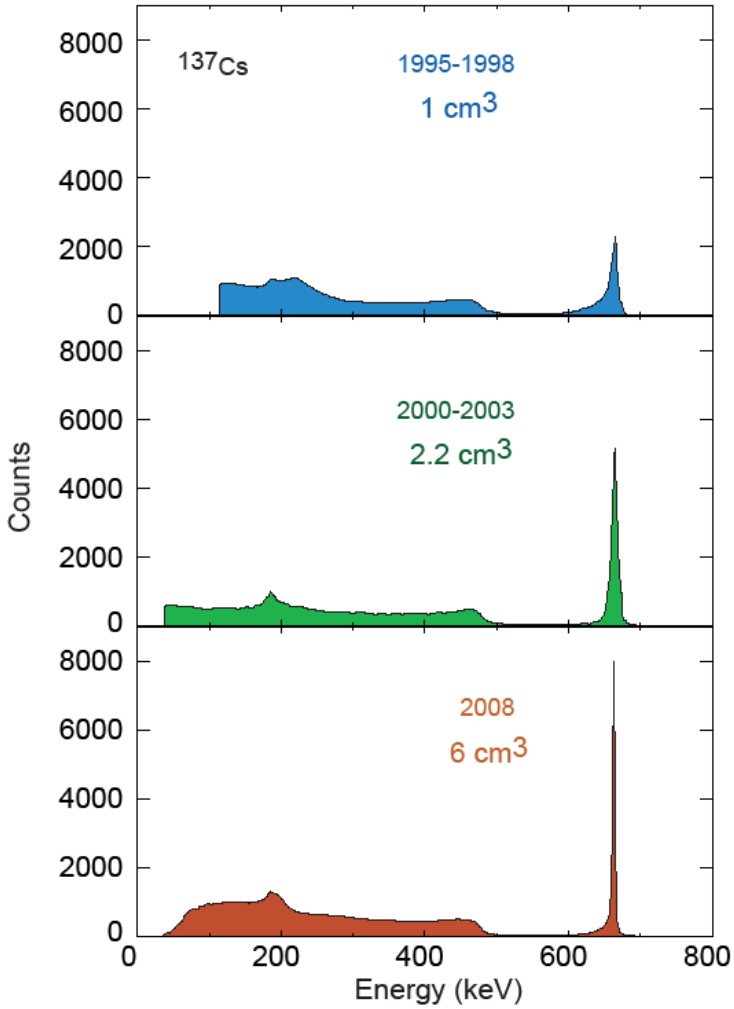

CZT detectors have been proposed more that a decade ago with a goal to replace HPGe in the field applications

Despite the significant progress in detector technologies and electronics we are still far from achieving this goal

We believe, that today's commercial CZT material have excessively high concentrations of the **extended defects**, which limit the size and performance of CZT detectors

Extended Defects in Commercial CZT Material

- Several types of the extended defects that can be found in a typical commercial CZT crystal:
  - twins,
  - sub-grain boundaries,
  - Te inclusions,
  - and dislocations which are usually arranged in dislocation walls or mosaic structures

- Most of these defects are not readily seen with visible or IR microscopes => they are often overlooked by vendors

- The extended defects are less important in thin detectors, but their critical role increases with device thickness

Operation Principle of Ionization Detectors

- Low mobility of holes (single-charge carrier device)
- This makes CZT detectors different from HPGe

$$Q_{out} = Q_{col} + Q_{ind}$$

Collected charge (mostly electrons)

Charge induced by trapped carriers (mostly holes). It is function of coordinates

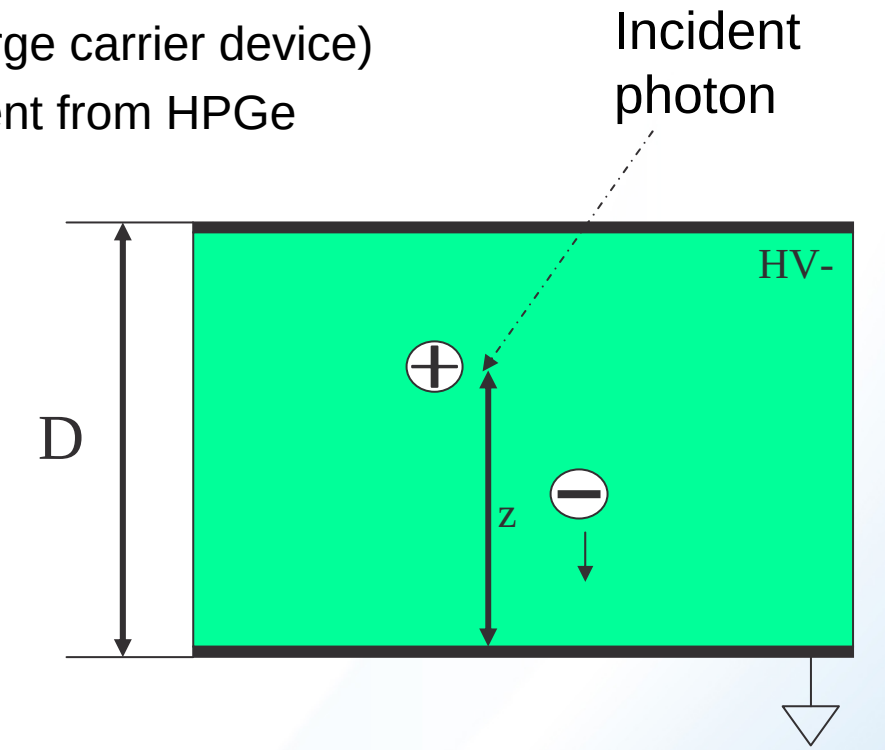

$$Q_{ind} = \frac{E_{ph}}{D} z$$

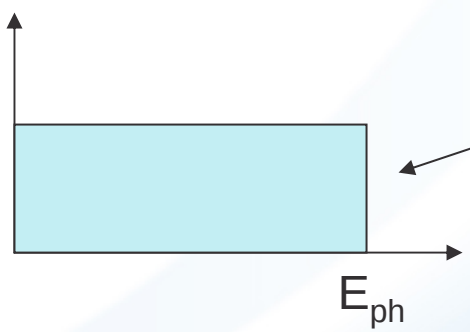

The electrodes design should provide an efficient way for eliminating the effect of holes!

Elimination of the Influence of the Uncollected Holes

Electron-only carrier device

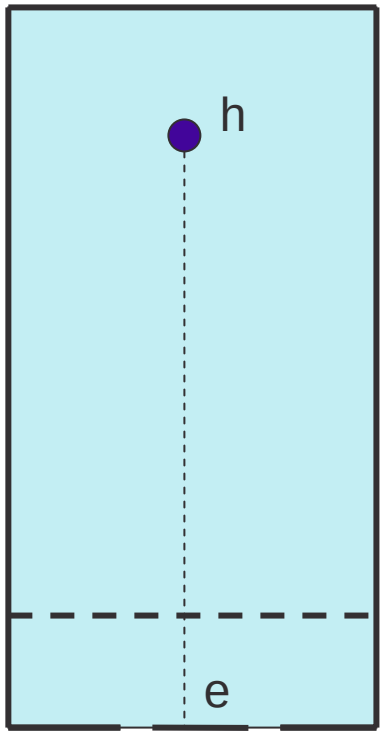

Anode

$$A \sim Q_{col}^{el} + \cancel{Q_{ind}^{hol}}$$

(1) Electrostatic shielding

- Frisch-grid ionization chambers
- Virtual Frisch-grid detectors
  - Spherical, Hemi-spherical, Three-terminal, CAPture, Frisch-ring, Capacitive Frisch-grid, Pixel detectors and their modifications

(2) Electronic subtraction

- Coplanar-grid detectors

Theoretically, all these designs should provide an energy resolution close to its statistical limit determined by the Fano-factor (FWHM ~0.5% at 662 keV)

Experimental Techniques for Material Characterization

- Experimental techniques are used to identify the extended defects and to measure their effect:
  - **IR microscopy**
  - White X-ray diffraction topography
  - Micro-resolution X-ray mapping
  - Surface etching

IR Microscopy

CZT is transparent to NIR and Te inclusions are opaque.

CCD camera

Motorized X-Y-Z translational stage

Microscope Objective lens (large working distance)

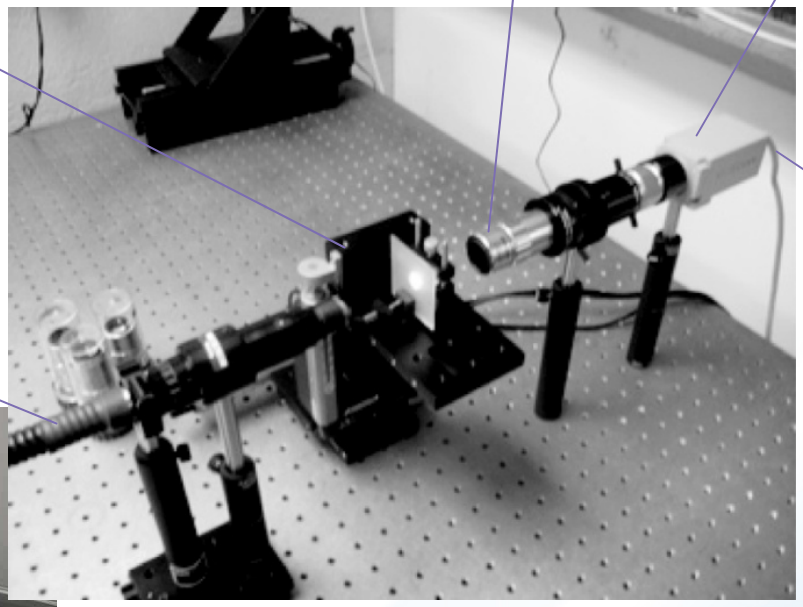

Light source

Connected to PC

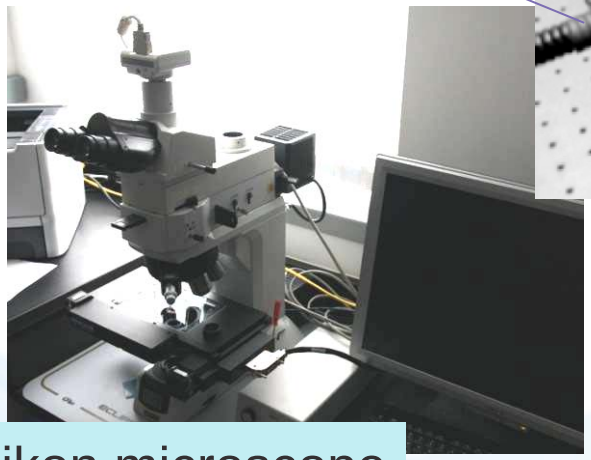

Nikon microscope

Te Inclusions Concentration Measurement

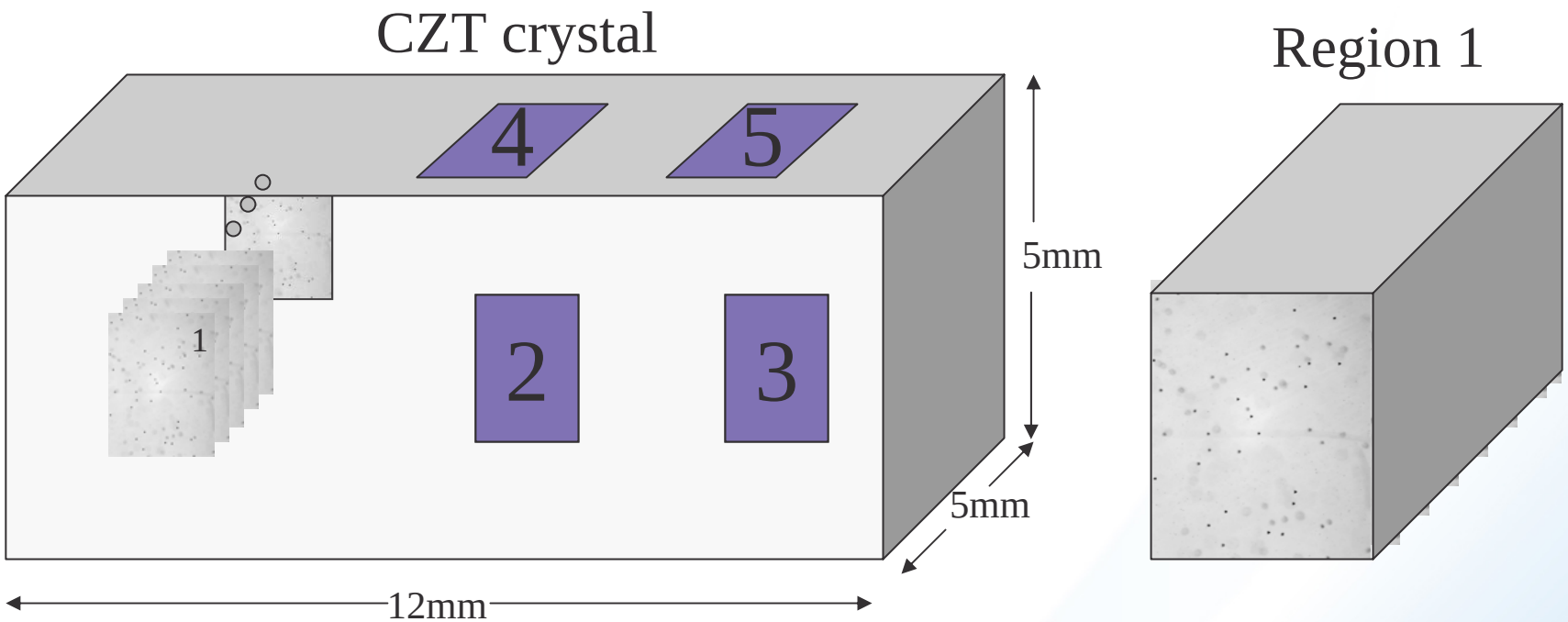

1. We count the number and size of Te inclusions in each volumetric region (or stack of images)
2. We calculate the concentration of Te inclusions in each of the 5 volumetric regions
3. We average over these 5 regions to estimate the concentration of Te inclusions per cm^3

Results:

Concentration/cm^3
Distribution of sizes

Example of a Stack of 100 Images Projected on one Plane

Volume 1.1x1.5x10 mm^3

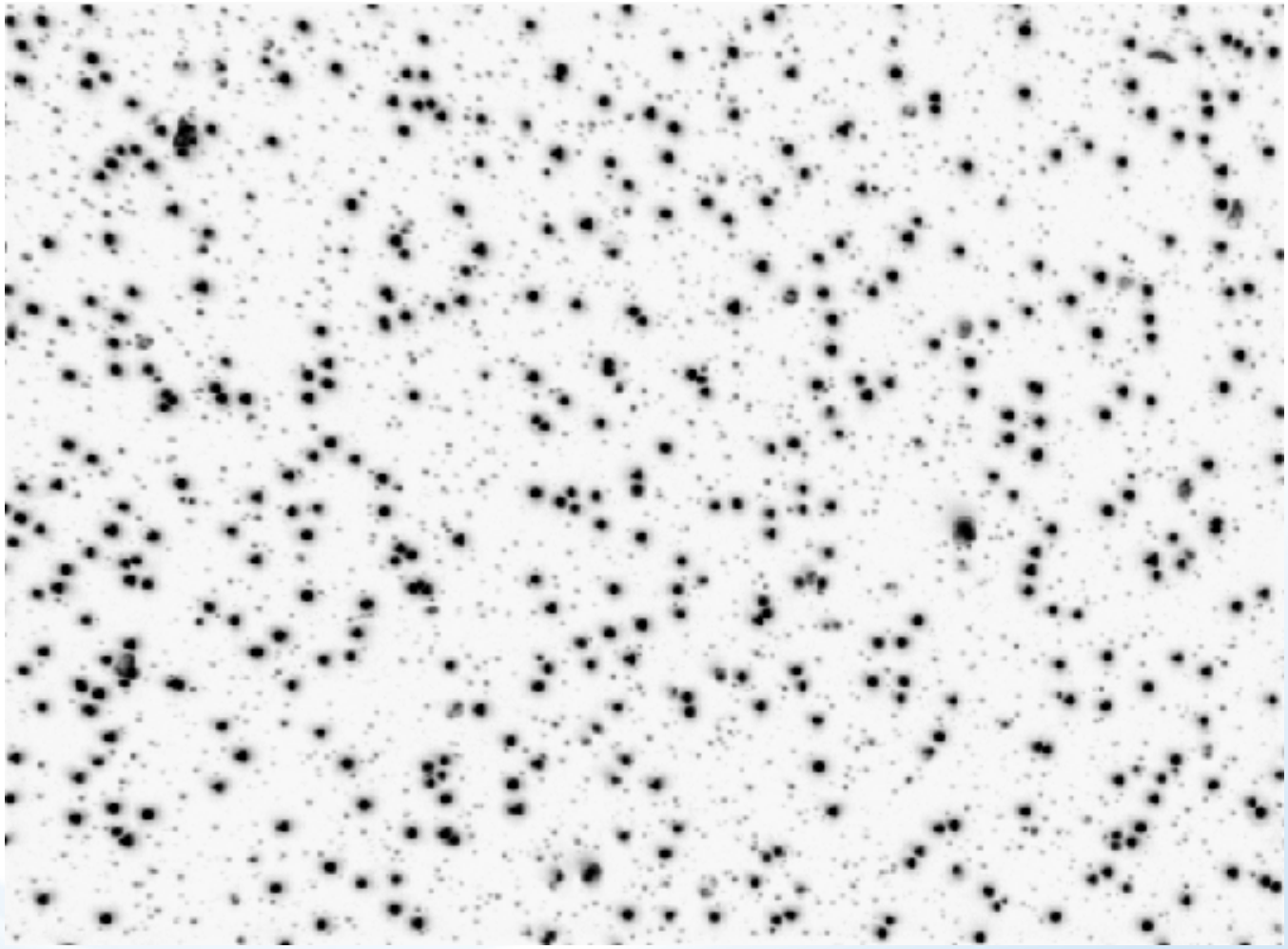

IR Image Analysis

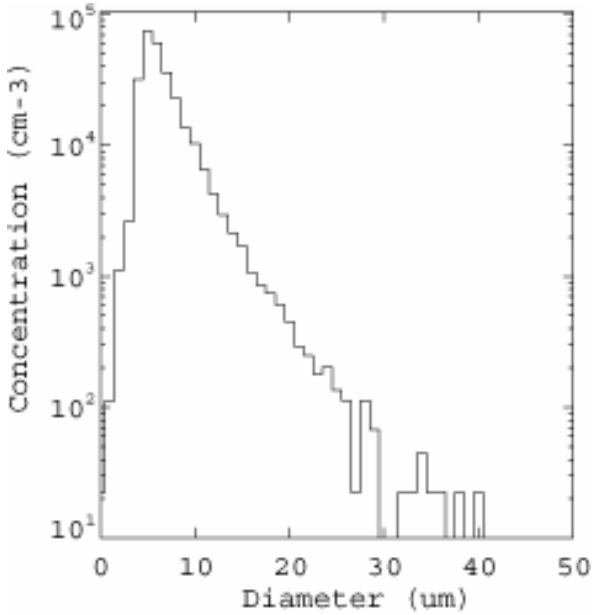

- Size distribution of Te inclusions
- Resolution is limited by the wavelength
- Min. size is ~1 μm

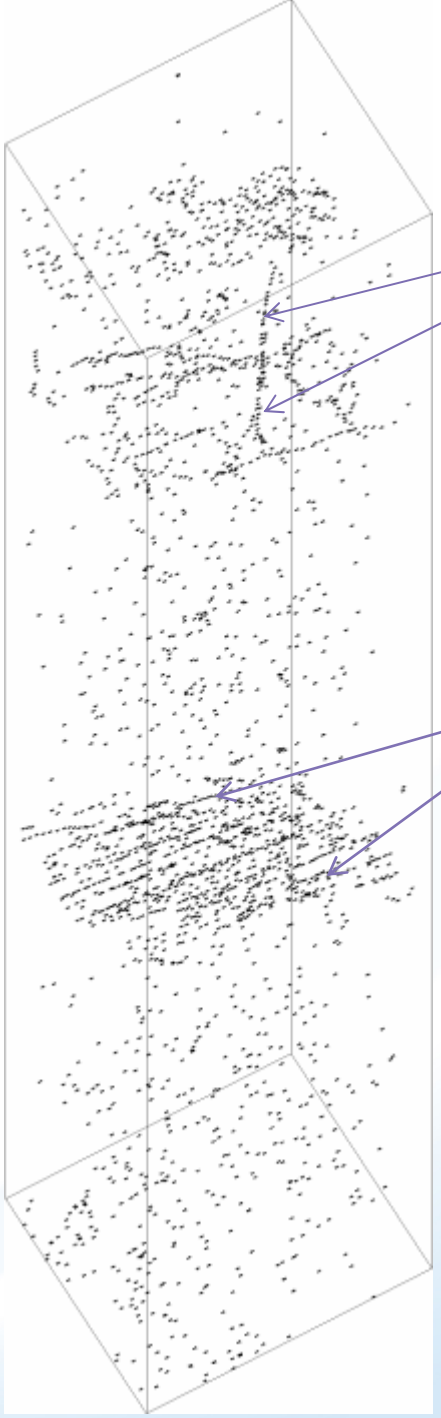

Grain boundaries decorated by Te inclusions

Twins decorated by Te inclusions

1.1x1.5x6 mm^3 volume

Synchrotron Radiation at NSLS

What is a synchrotron? It is a source of tiny beams of very bright X-rays, UV, visible and IR light

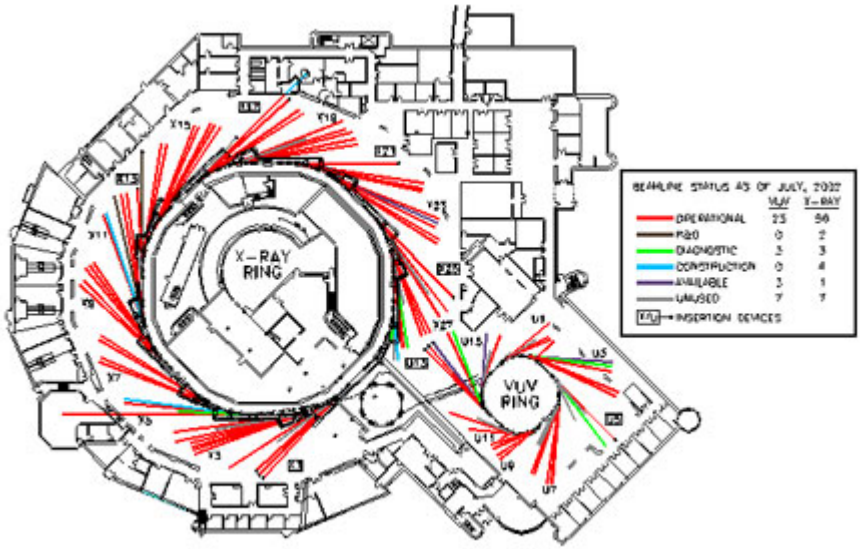

NSLS is a user facility

- X27B – PRT
- X17B1, X27A, X19C – General users

http://www.nsls.bnl.gov/users/usersguide/bt-gu.asp

Experimental Techniques for Material Characterization

- Experimental techniques are used to identify the extended defects and to measure their effect:
  - IR microscopy
  - **White X-ray diffraction topography**
  - Micro-resolution X-ray mapping
  - Surface etching

White X-ray Diffraction Topography

Energy:

white X-ray **from** 50keV **to** 200keV

Beam-size:

200μm x 15mm (max: 4mm x 12cm)

Scan in z and 2θ

z from 0mm to 22mm

2θ from 0 to 0.97 degree

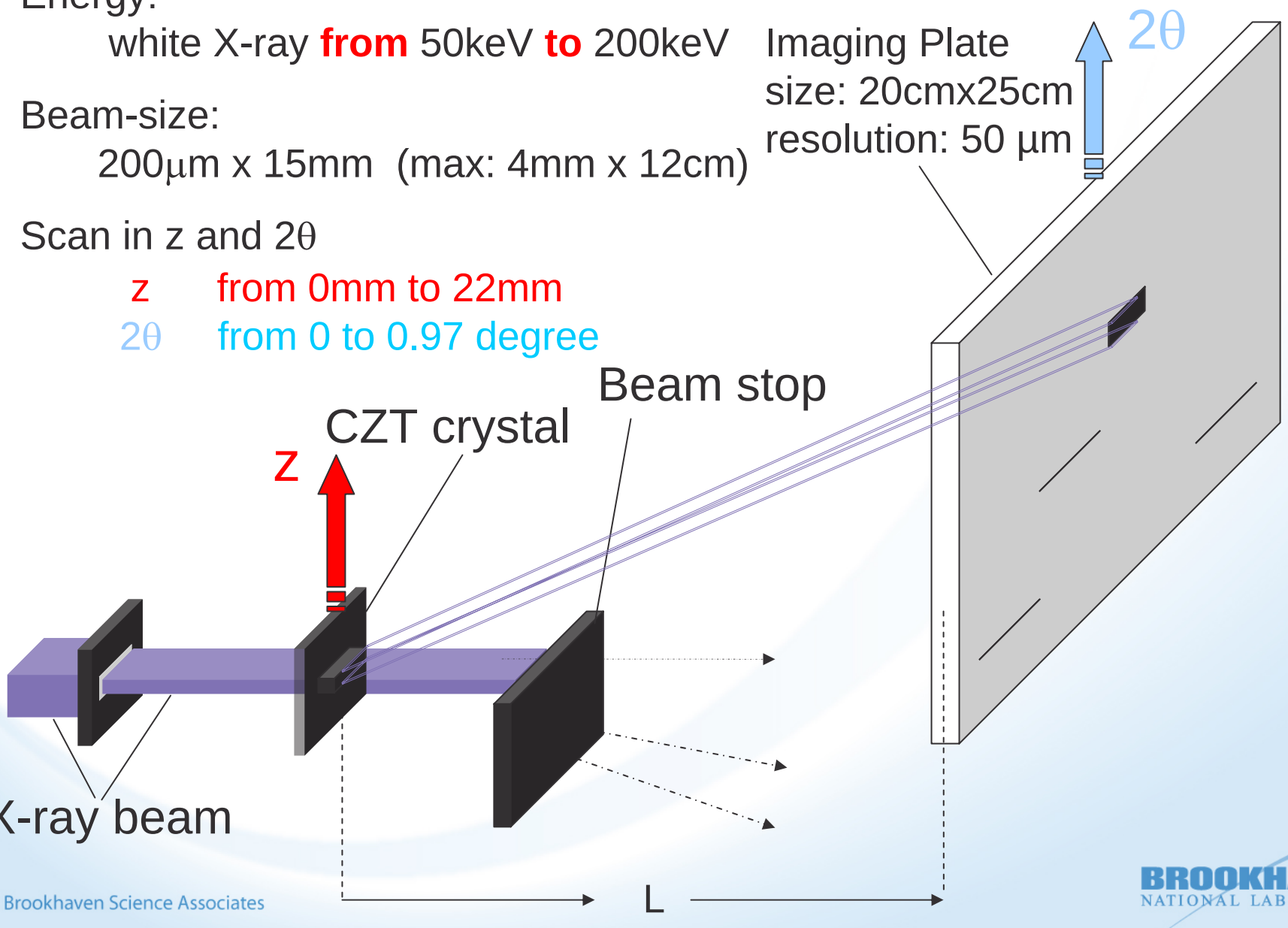

White X-ray Diffraction Topography

- Very quick measurement: it takes a few seconds to scan a detector
- Nondestructive
- Resolution of the imaging plate is only 50 µm

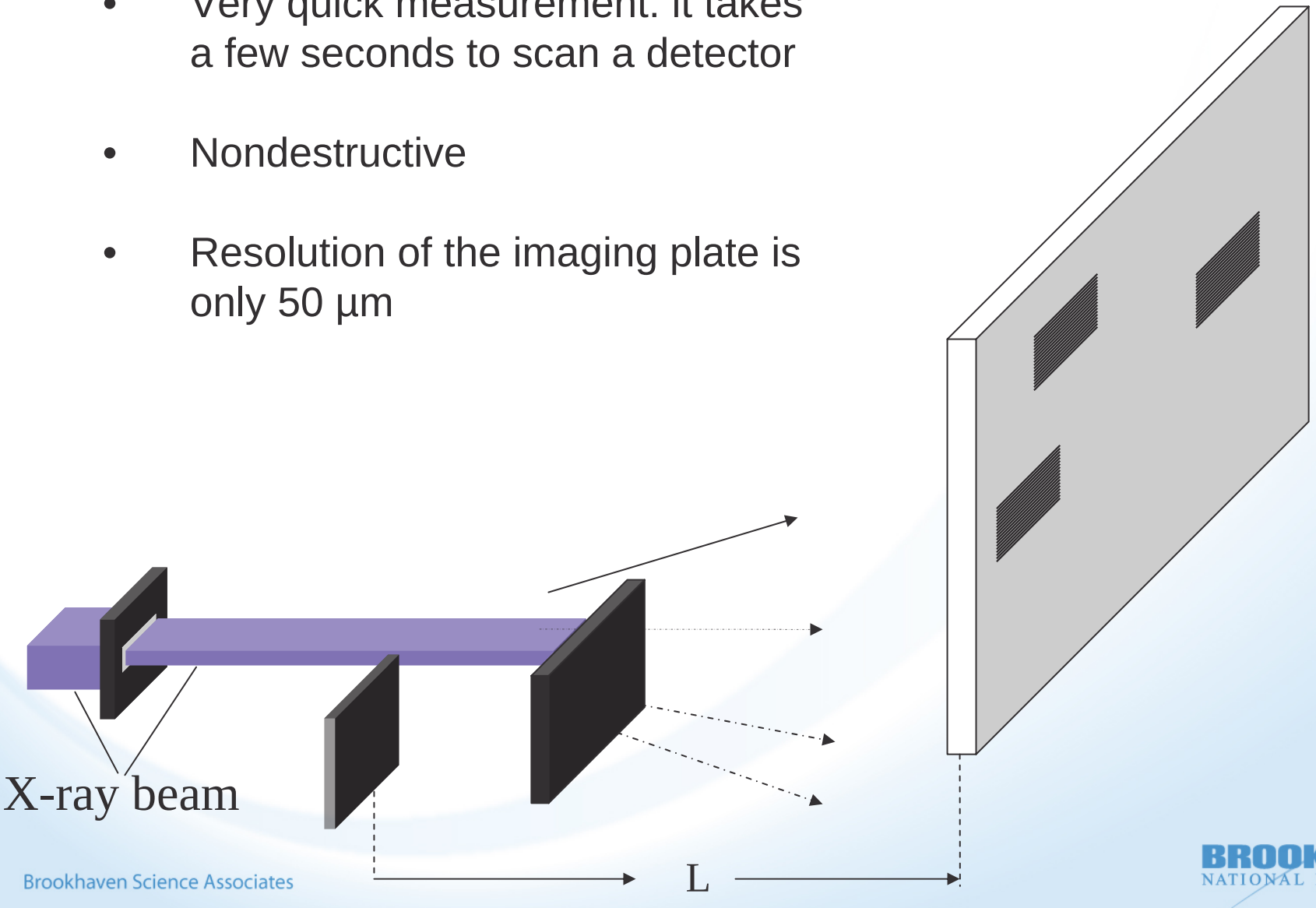

White X-ray Diffraction Topography Images

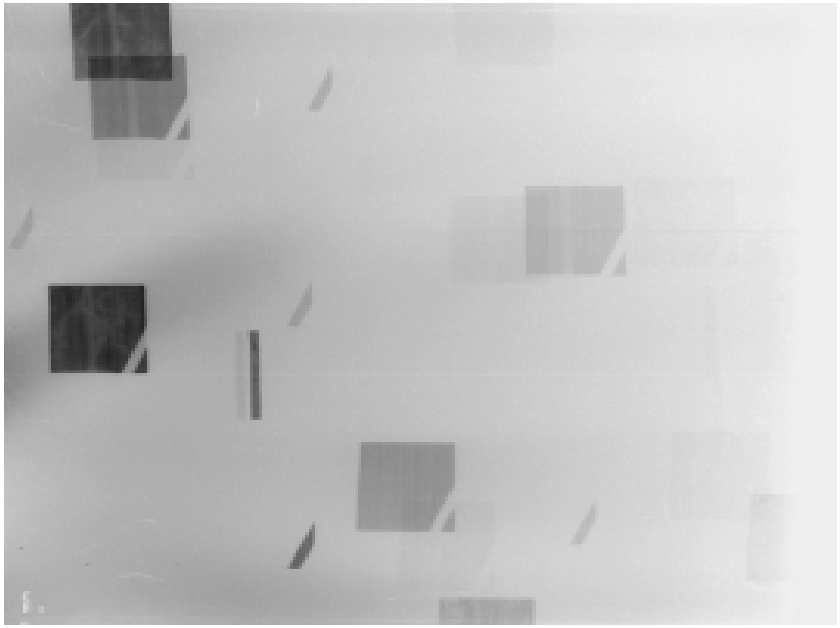

20 cm

25 cm

Perfect crystal:

the WXDT image is the replica of the crystal geometry

CZT crystal

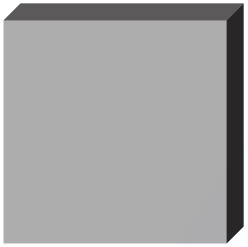

WXDT image

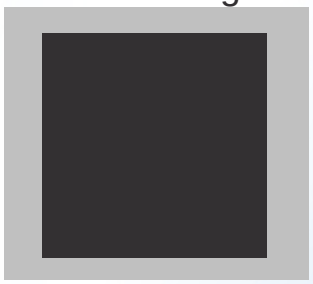

Imperfect crystal:

CZT crystal

WXDT image

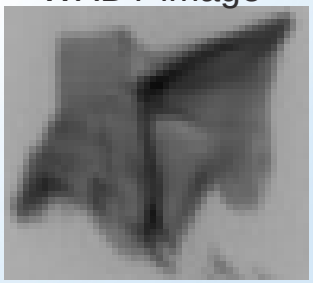

With WXDT we can screen quickly CZT crystals to make sure they have only one domain; we need high resolution imaging plates to see some extended defects and strains fields.

Examples of Diffraction Topography Images

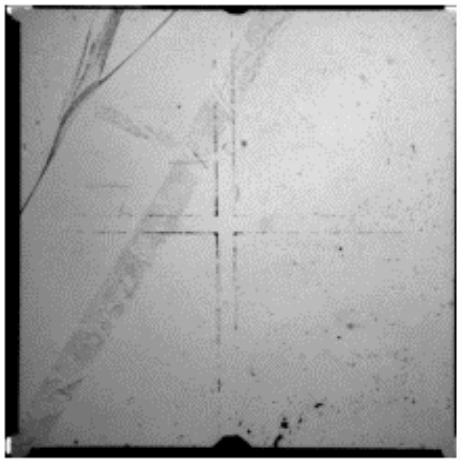

IR Transmission Map

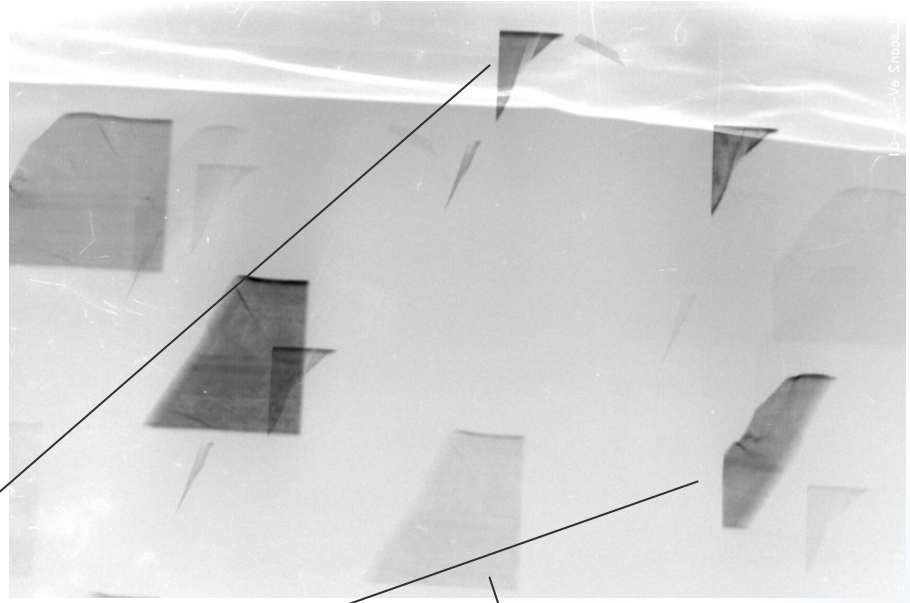

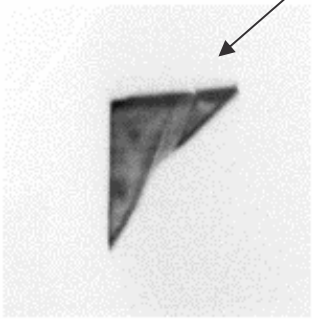

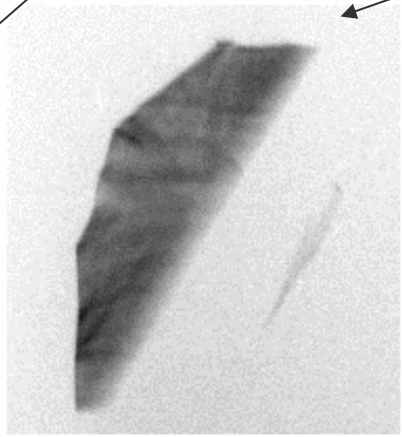

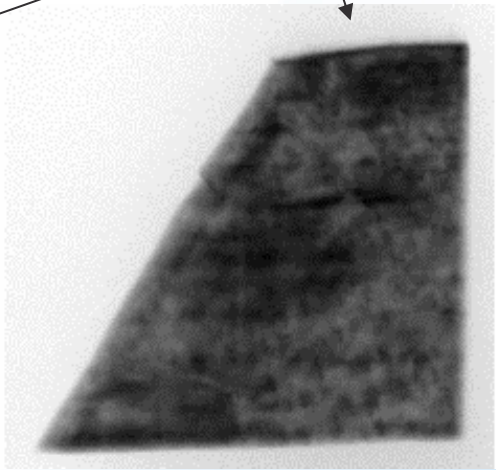

Experimental Techniques for Material Characterization

- Experimental techniques are used to identify the extended defects and to measure their effect:
  - IR microscopy
  - White X-ray diffraction topography
  - **Micro-resolution X-ray mapping**
  - Surface etching

Micro-resolution X-ray Mapping System

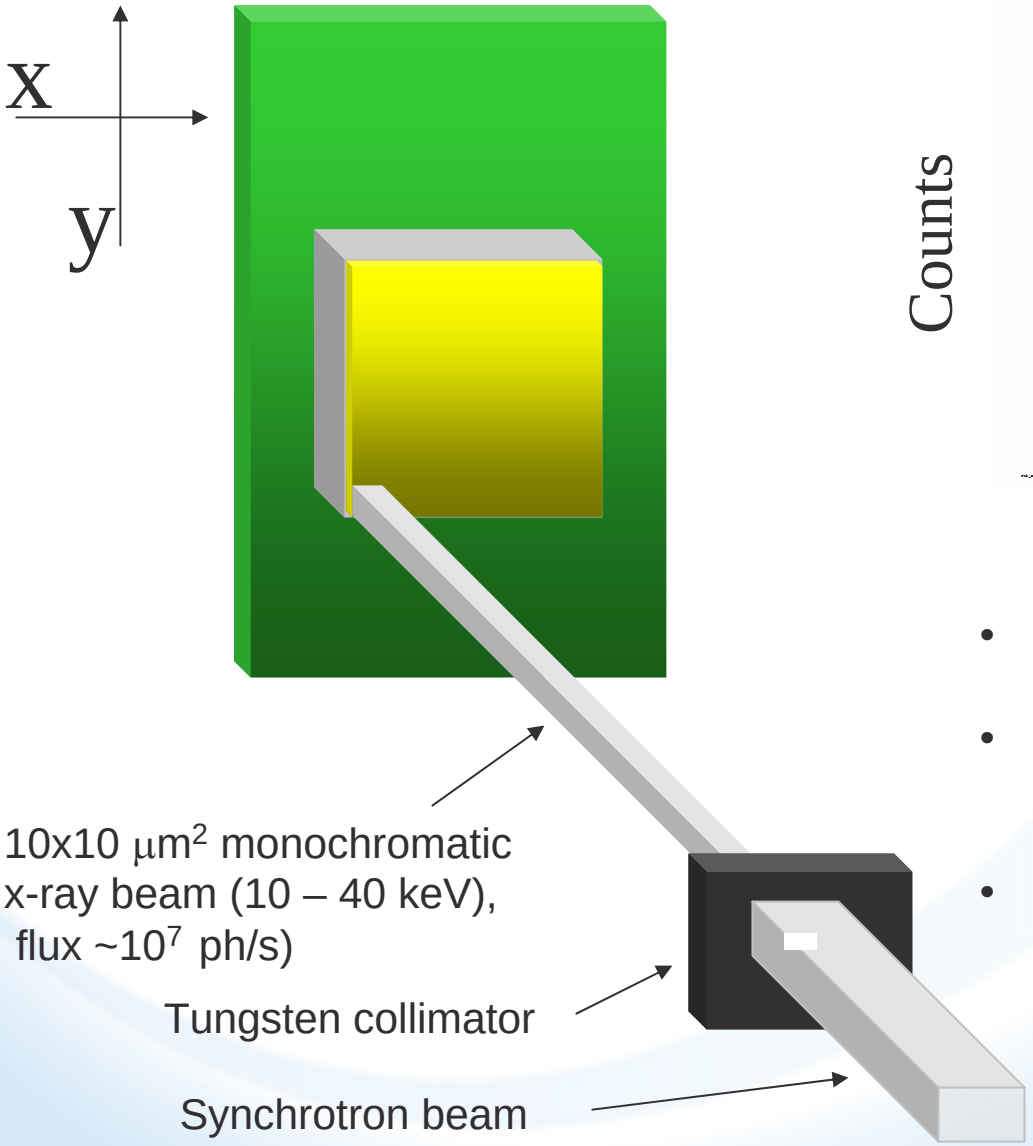

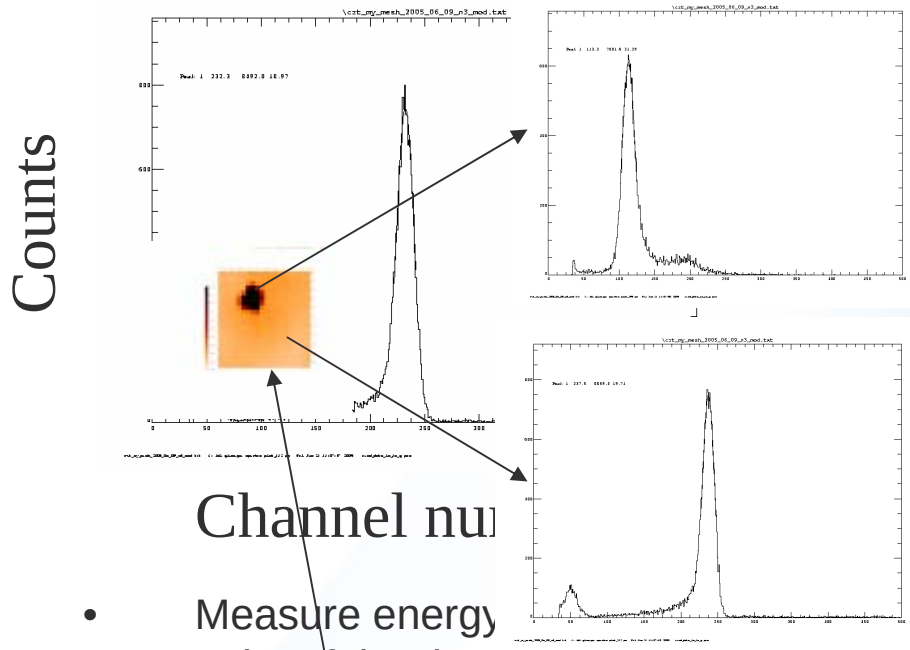

- Measure energy
point of the detector area
- Analyze the data and record the peak channel for each point of the detector area
- Next we plot the peak-channel vs. XY-position.

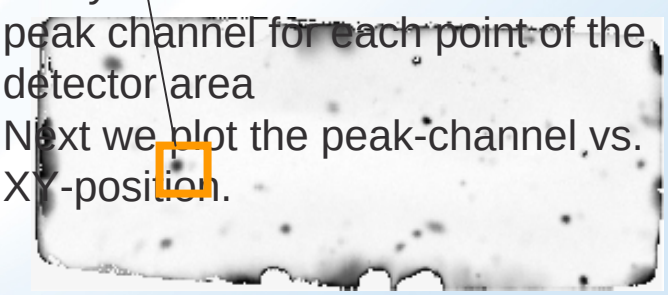

3x3x7mm³ CZT detector

Advantage of Using an X-ray Beam as Probe for Testing CZT Detectors

X-ray mapping technique is our main tool that provides high spatial resolution, limited by the diffusion only (low in the case of X-rays) and lets us control the interaction depths of X- rays (avoid surface and polarization effects).
We can collect electrons or holes.
By collecting the holes at very high biases we can minimize the diffusion

$$\sigma = \sqrt{2Dt} = \sqrt{\frac{4kTZ}{E}}$$

$$Q_{col} = Q_0 \exp\left(-\frac{L}{E\mu\tau}\right)$$

and significantly increase sensitivity to the charge trapping defects.

Alpha-particles (also used to probe CZT detectors) ~10 times less spatial resolution than X- or gamma-rays.

Charge spread due to diffusion and repulsion

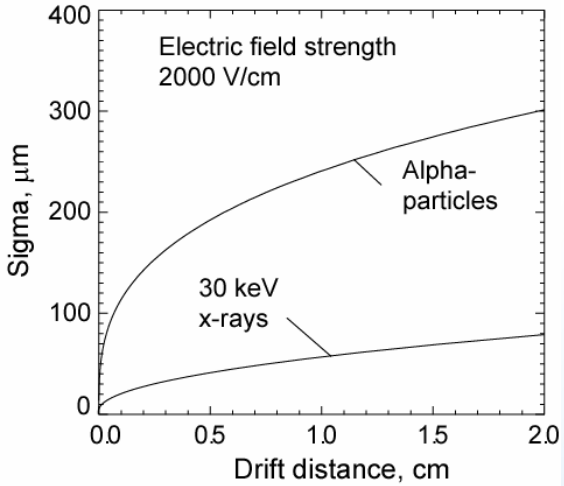

X-ray attenuation length

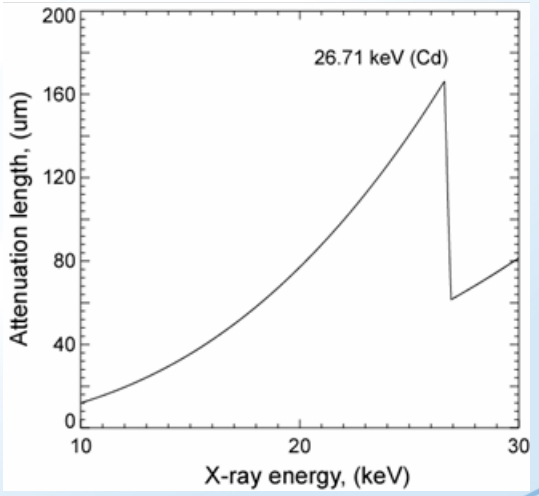

Typical Response over a Te Inclusion

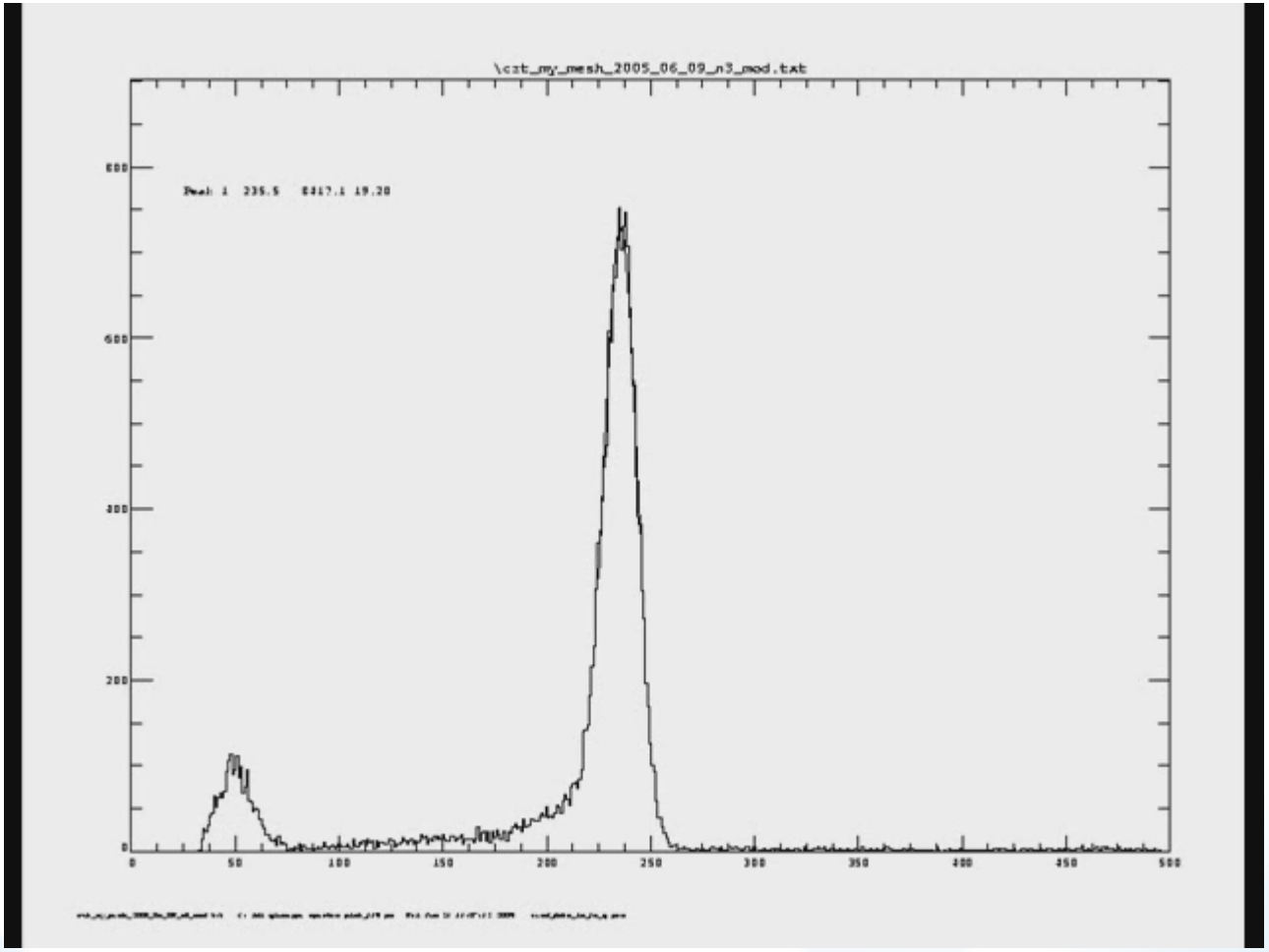

Te inclusion

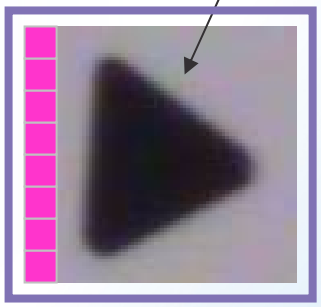

100 µm x 100 µm area
10-µm x 10-µm pinhole
5-µm step size

Role of Te Inclusions

- Te inclusions are formed during the growth in the melt phase and trapped by the melt-solid interface
- Typical sizes in commercial crystals are 1-20 μm, concentrations are 10^3-10^6 cm^{-3}
- In the past, it was believed that Te inclusions do not affect the device performance (based on the results from alpha-particle measurements)
- We proved that Te inclusions are opaque to the drifting electrons and reduce the total collected charge in CZT detectors

X-ray map

1.5 mm x 1.5 mm area
10-μm x 10-μm pinhole
10-μm step size

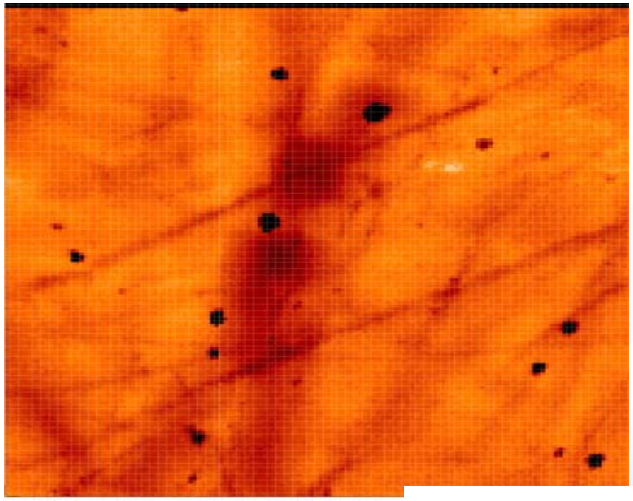

IR micrograph

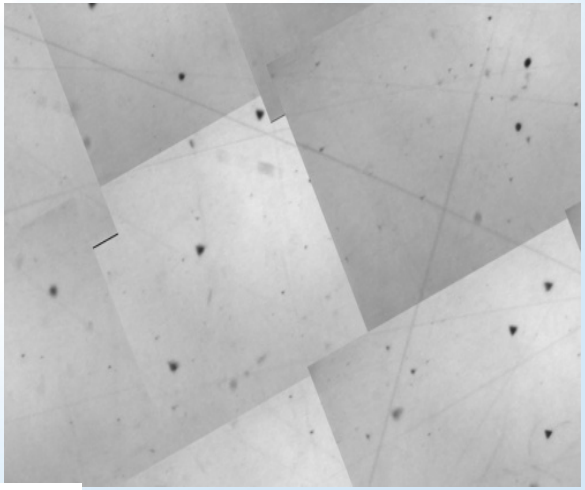

One to one correlation

Fluctuations Introduced by Te Inclusions

- Drifting electron cloud impinges on Te inclusions which are opaque to electrons:

  1) Reduction in total collected charge (or output signal) which can be electronically corrected
  2) Fluctuations in total collected charge which cannot be electronically corrected

- Small Te inclusions should behave as ordinary point defects

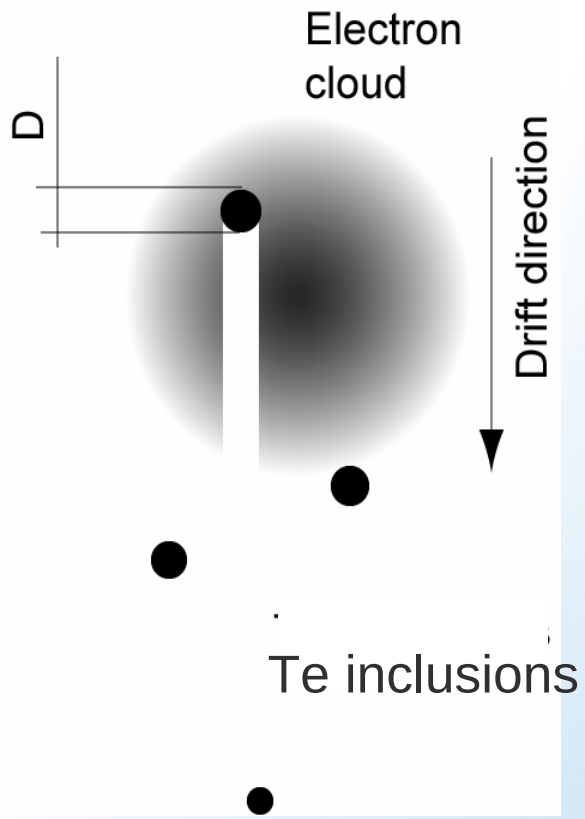

Prediction of the Effects of Te Inclusions

Expected fluctuation caused by Te inclusions in 15-mm long CZT device

Inclusions below 3 μm can be neglected!

Inclusions >10 μm are the most harmful.

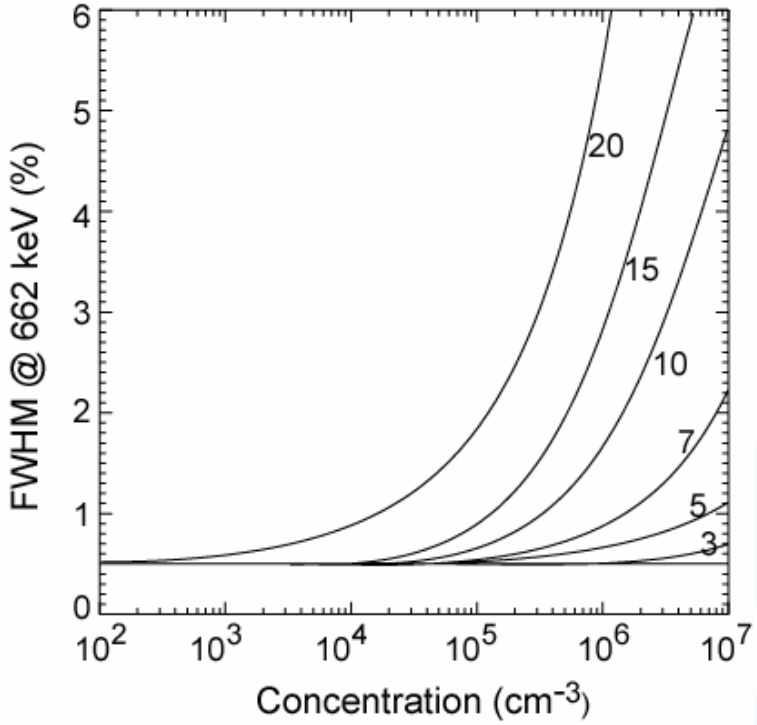

Variations of the spatial distribution of inclusions can significantly increase the effects!

Comparison Between Two Detectors

Detector A
4x4x11 mm^3
Energy resolution 0.8% at 662 keV

Detector B
6x6x12 mm^3
Energy resolution 3.8% at 662 keV

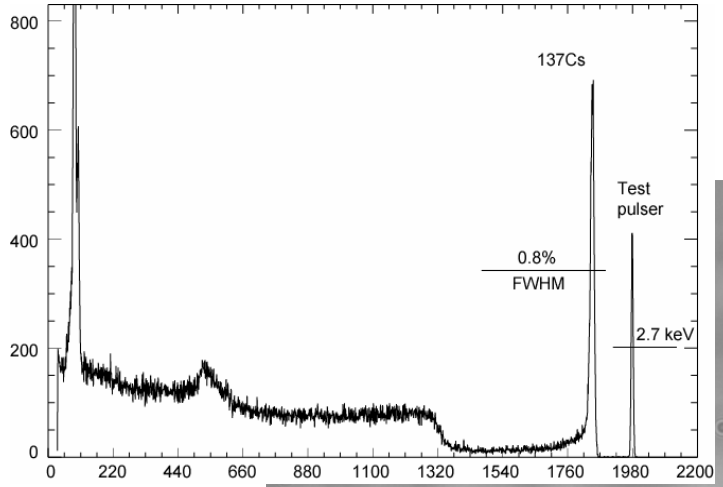

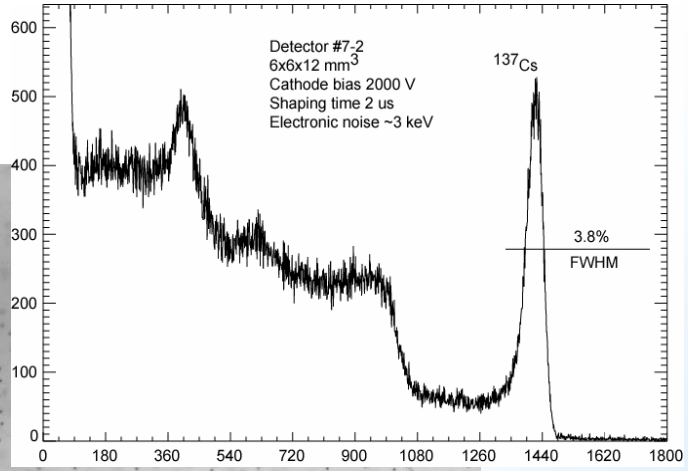

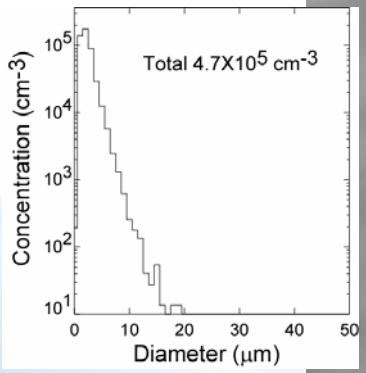

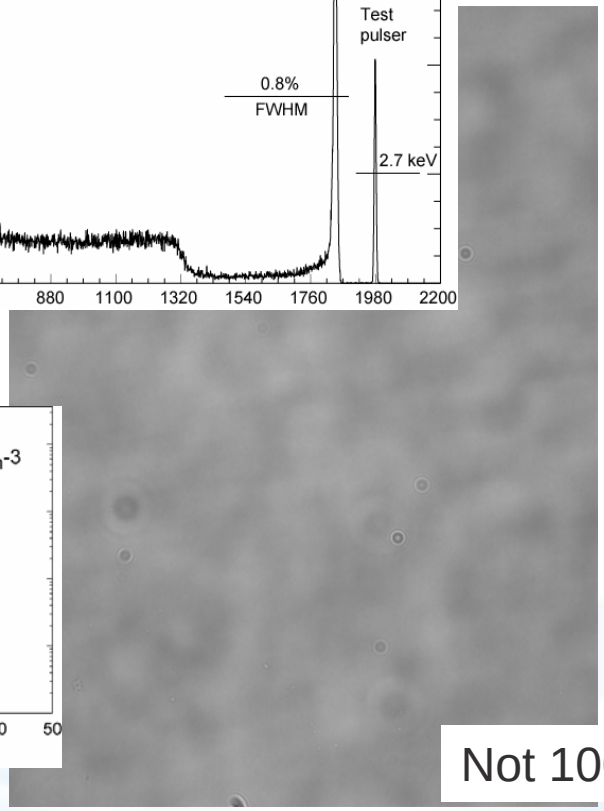

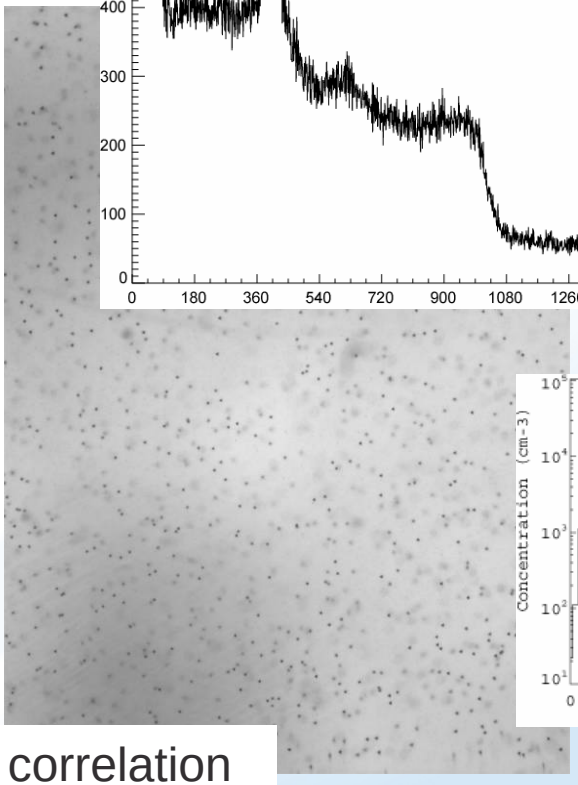

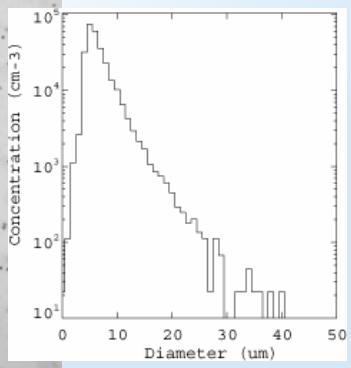

Not 100% correlation

Electron Trapping by Te Inclusions in the Case of Thin Detectors

X-ray scan of 10x10x1.2 mm^3
Cathode 200 V, 20 μm step

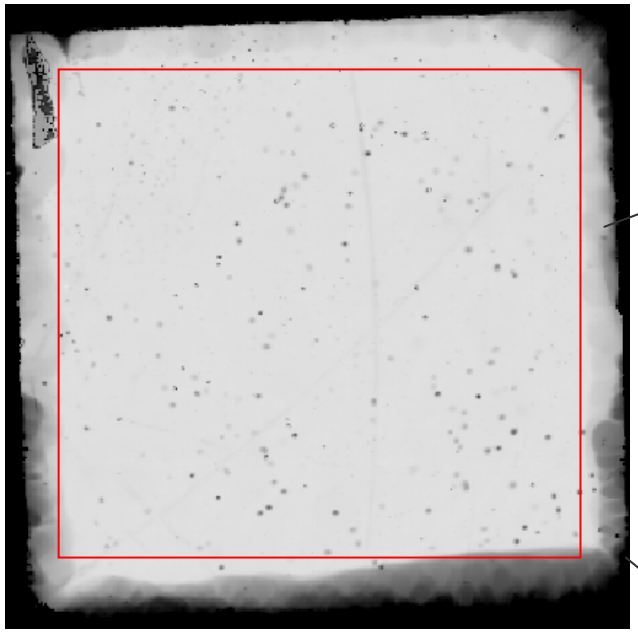

3-D representation of the response map

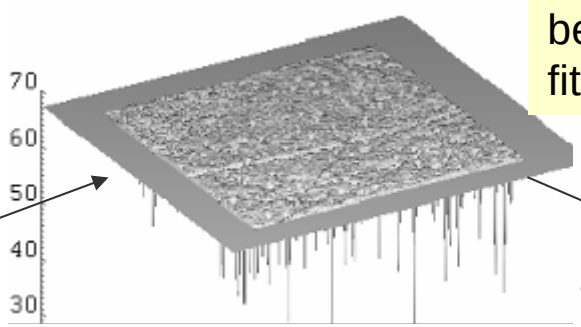

Histogram of the response map. Effect is negligible in thin detectors. 0.5% can be attributed to the peak fitting errors.

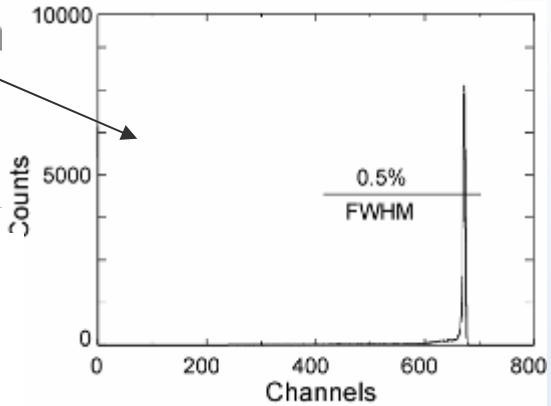

How important are these peaks for the device spectral response?

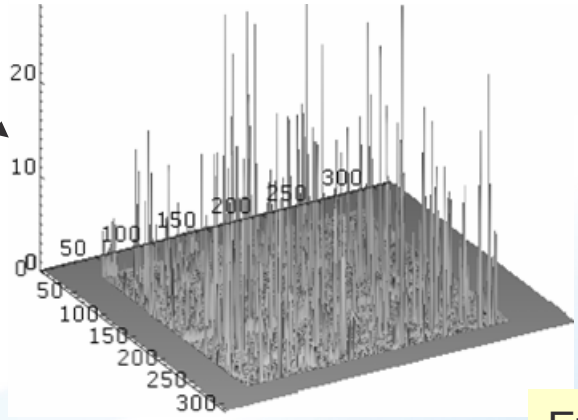

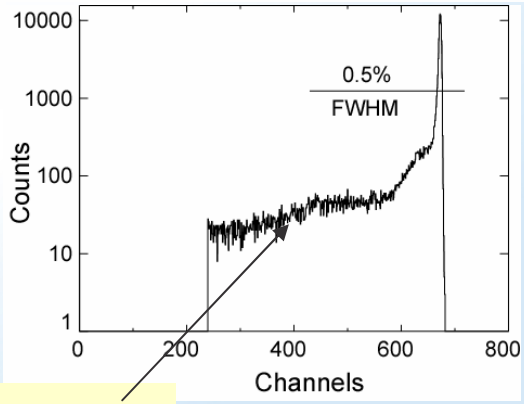

This X-ray map represents the intrinsic response of the detector without electronic noise contribution.

Efficiency loss

Response Map in the Case of a 10-mm Thick Detector

28 keV
1000 V,
50 μm step

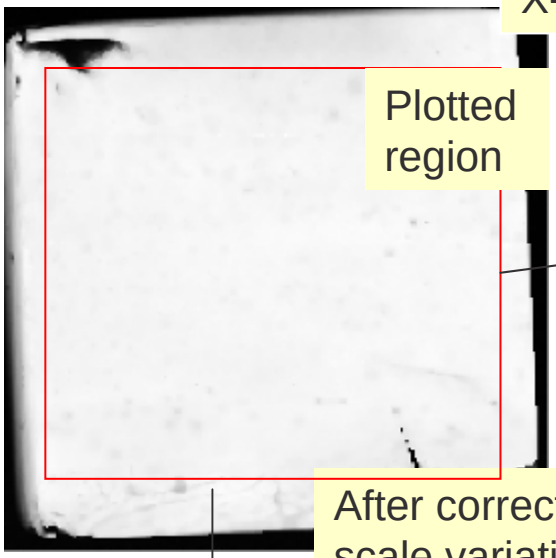

X-ray scan of 10x10x10 mm^3

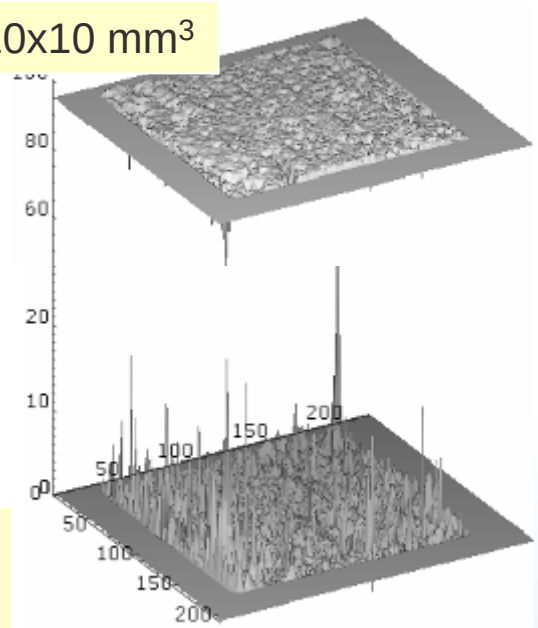

After correction for large–scale variations, which is equivalent to the response from a pixel detector made of this crystal, 1x1 mm^2.

Histogram of the response map

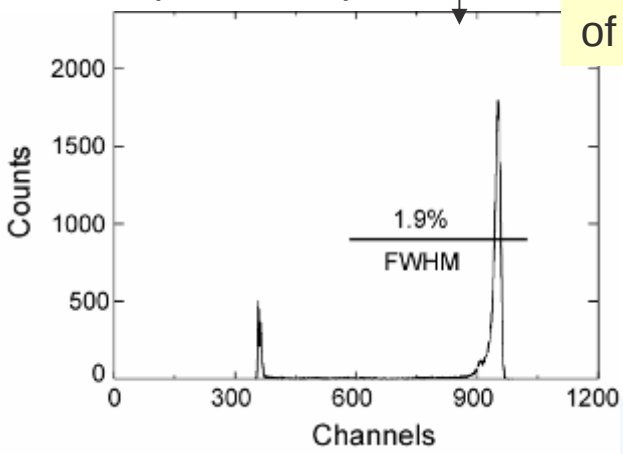

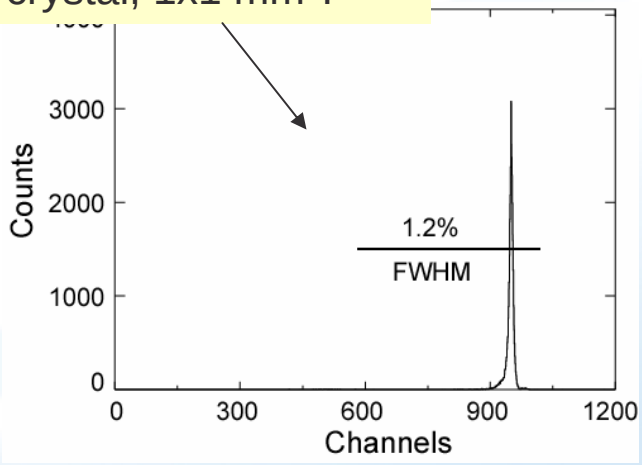

Fluctuations is ~1.2%, compared to 0.5%.

The fluctuations are primary attributed to Te inclusions.

Detector response degrades with device thickness.

1x1x1 cm^3 Detector with High Concentration of Te Inclusions

X-ray scan of 10x10x10 mm^3
28 keV, 1000 V, 50 μm step

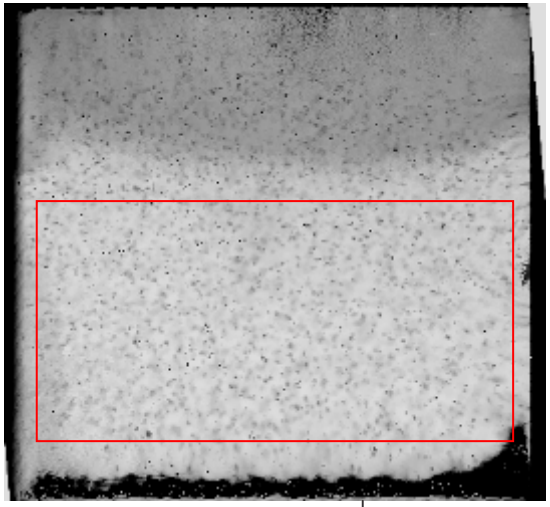

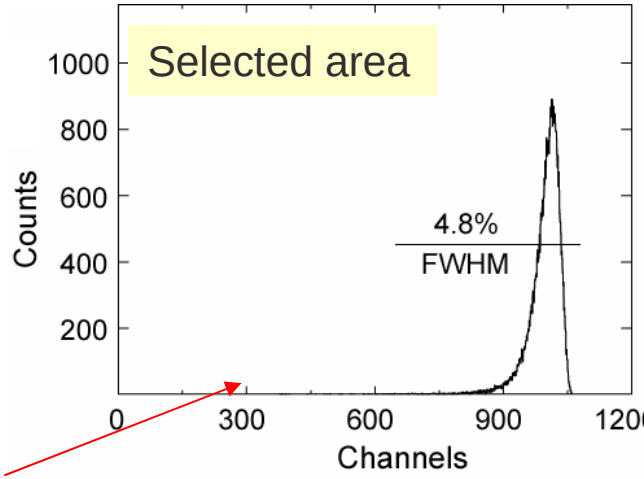

After dividing selected area in small pixels and normalizing the responses generated from each pixel

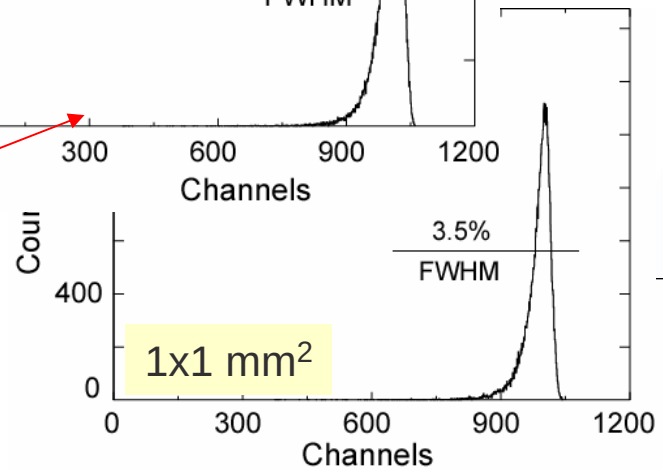

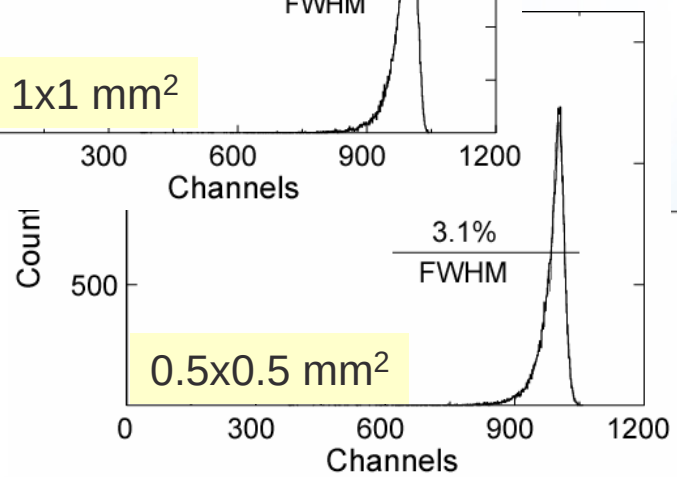

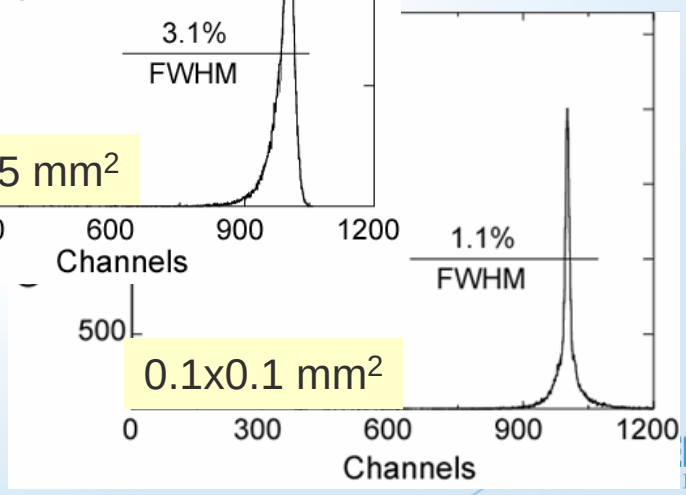

Histogram of a whole area

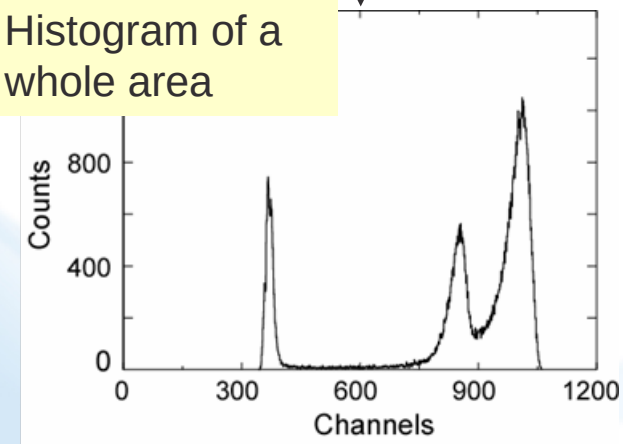

Electron Vs. Hole Collection Response Maps

Electron collection maps measured for 1.2-mm thick detector. Cathode 180 V.

0.5x0.5 mm^2

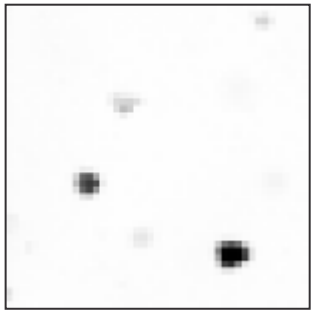

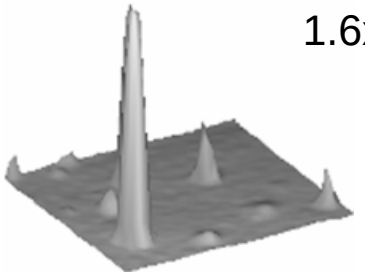

1.6x0.5 mm^2

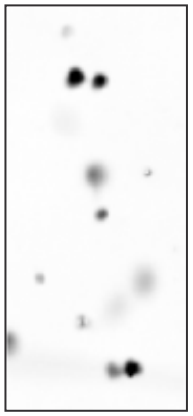

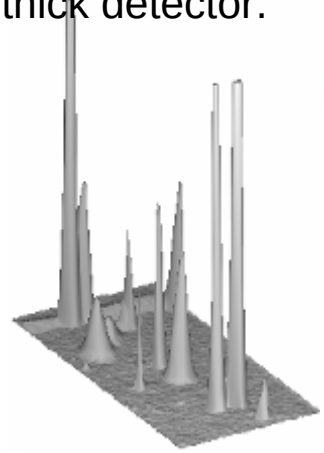

Inclusions look similar to their actual size.

Hole collection, cathode 260 V

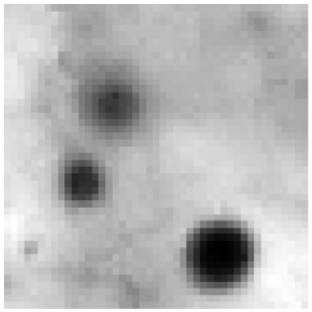

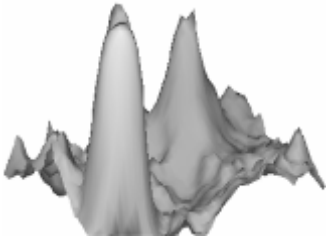

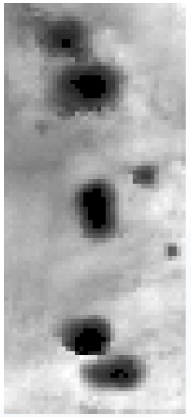

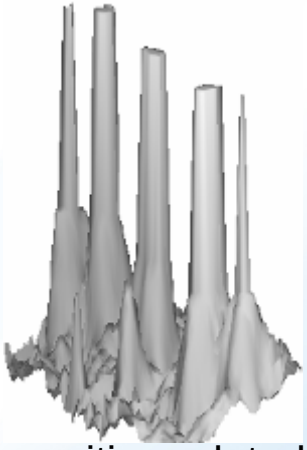

Inclusions look much bigger that their actual size.

The discrepancies could be explained by the presence of impurities-related trapping centers around inclusions. Inclusions accumulate impurities during growth and release them during cooling. This is in agreement with our measurements of impurities in Te inclusions.

G. Yang et al, accepted by J. Cryst. Growth, 2008

Effects of Twins and Sub-grain Boundaries on 12-mm Long Virtual Frisch-grid Detector

Pulse-height spectrum

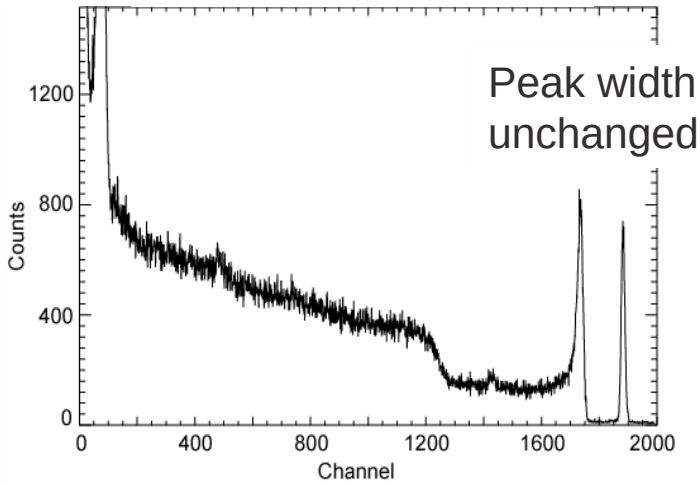

Peak width is unchanged!

X-ray mapping of 5x5x12 mm^3 detector by using a highly collimated beam

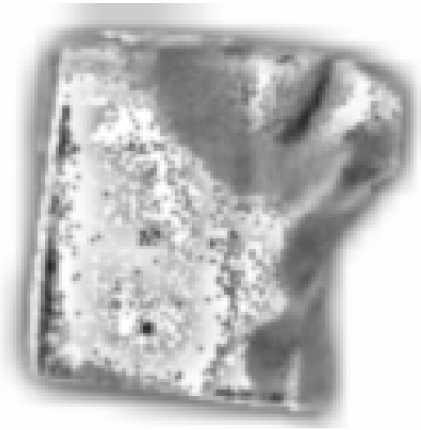

Diffraction topography image

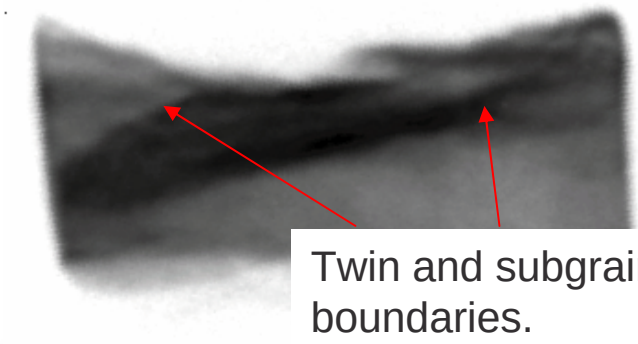

Twin and subgrain boundaries.

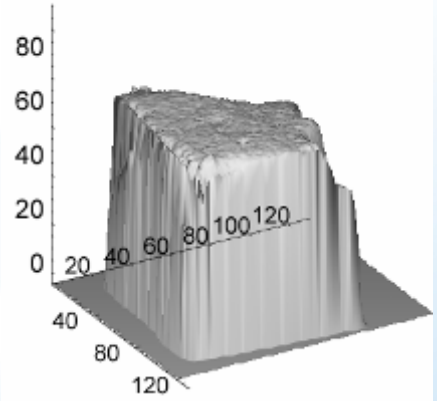

More Results…

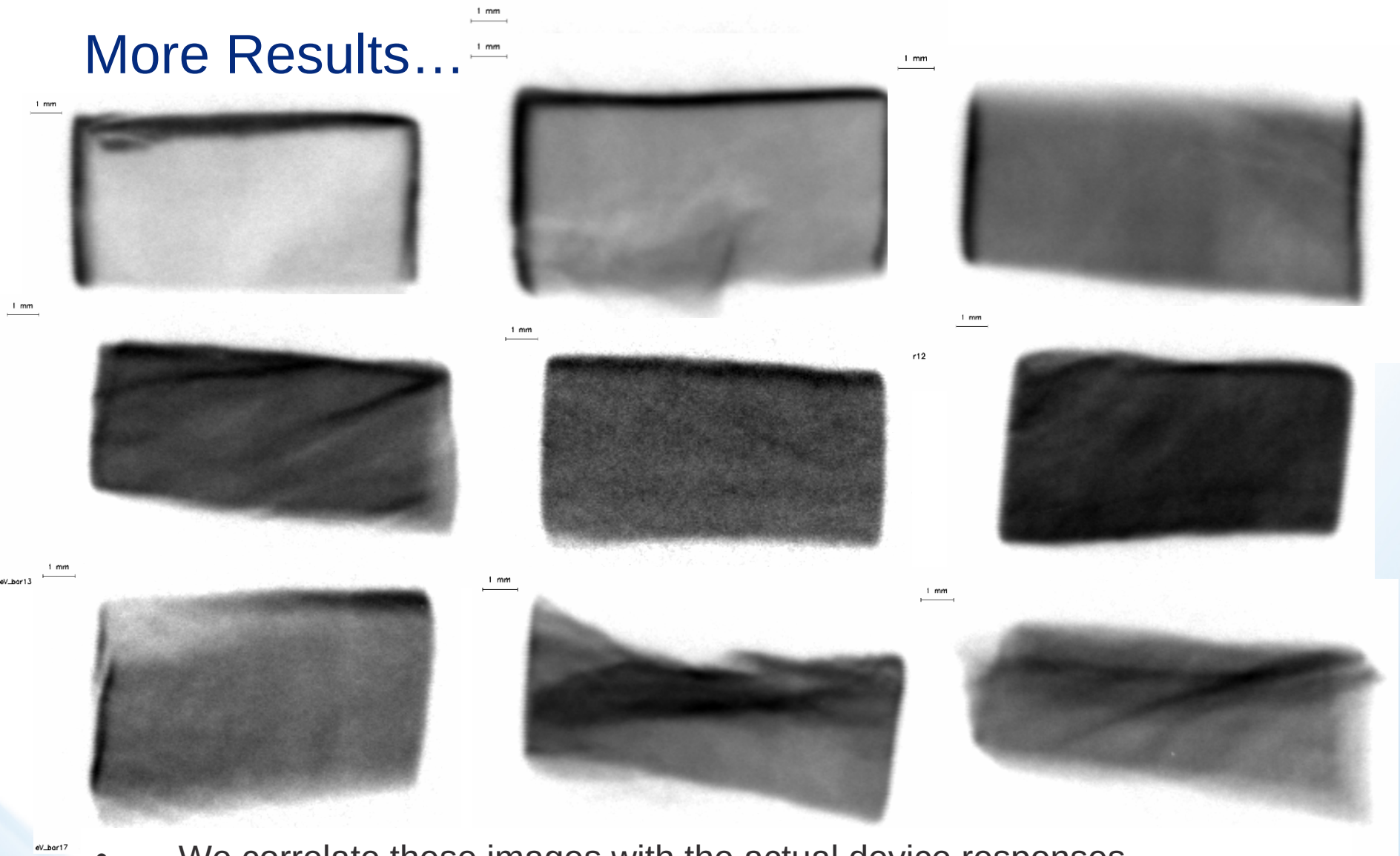

- We correlate these images with the actual device responses
- By measuring X-ray maps we confirm that large linear features in diffraction images corresponds to the twins or subgrain boundaries

Results from 5x5x12 mm^3 Virtual Frisch-grid Detector

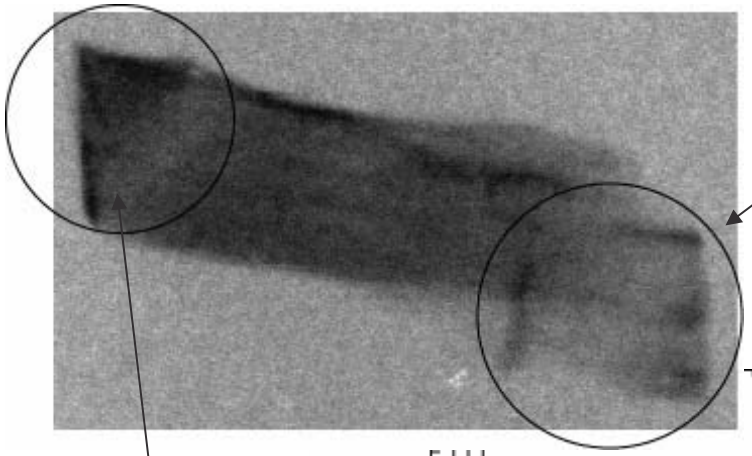

X-ray map

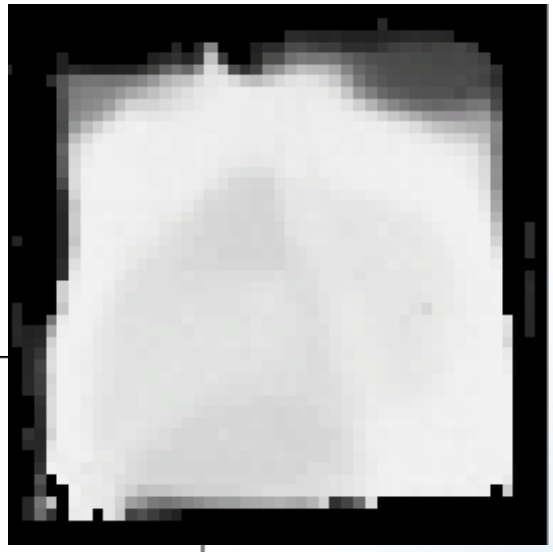

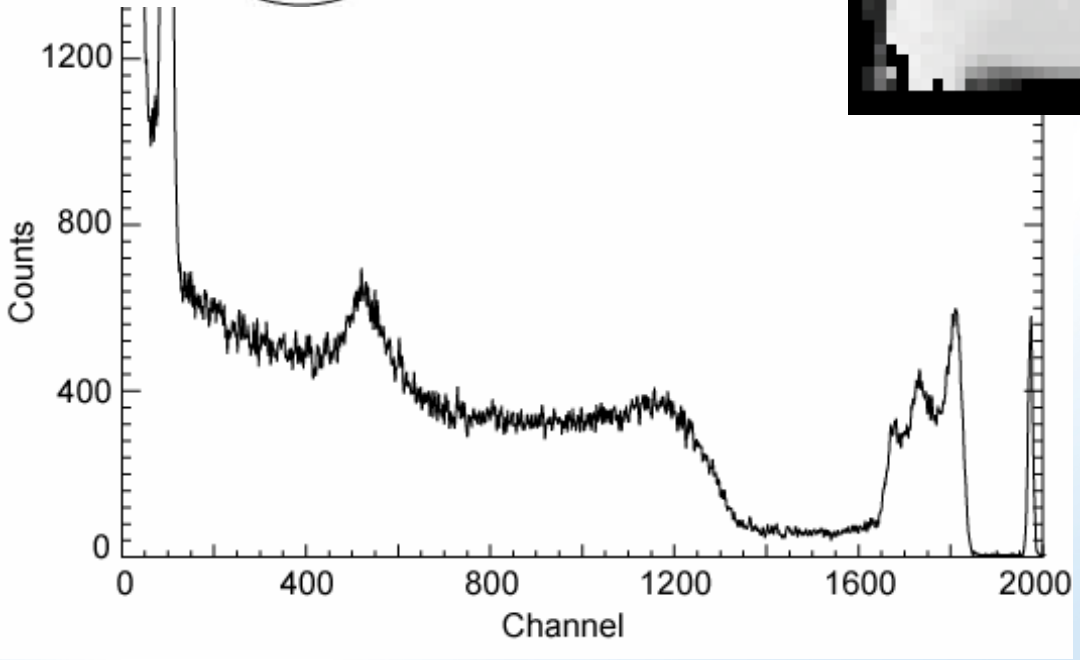

Results from 5x5x12 mm^3 Virtual Frisch-grid Detector

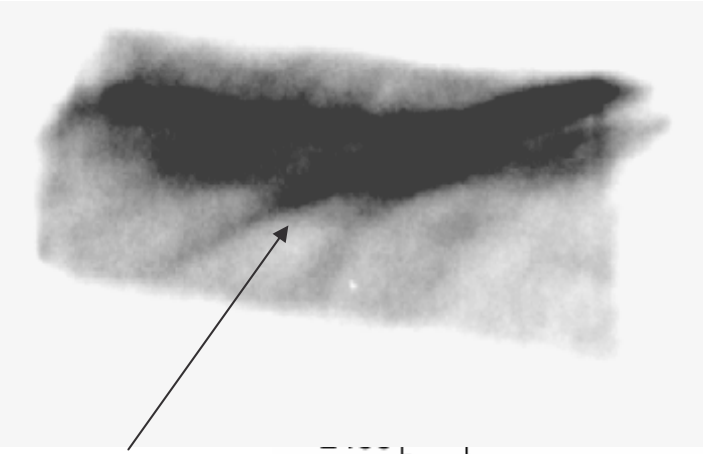

Subgrain boundary

X-ray map

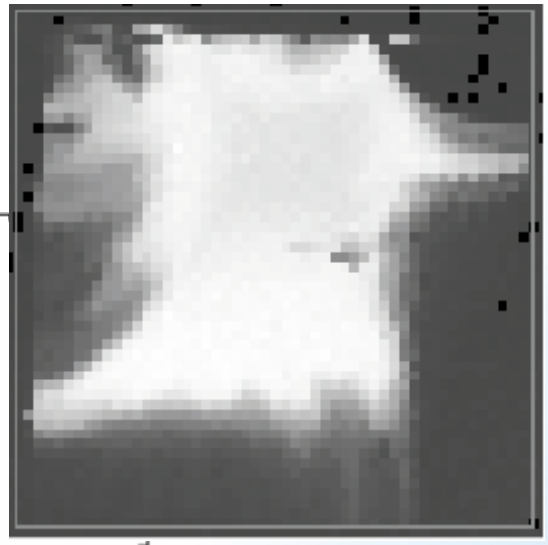

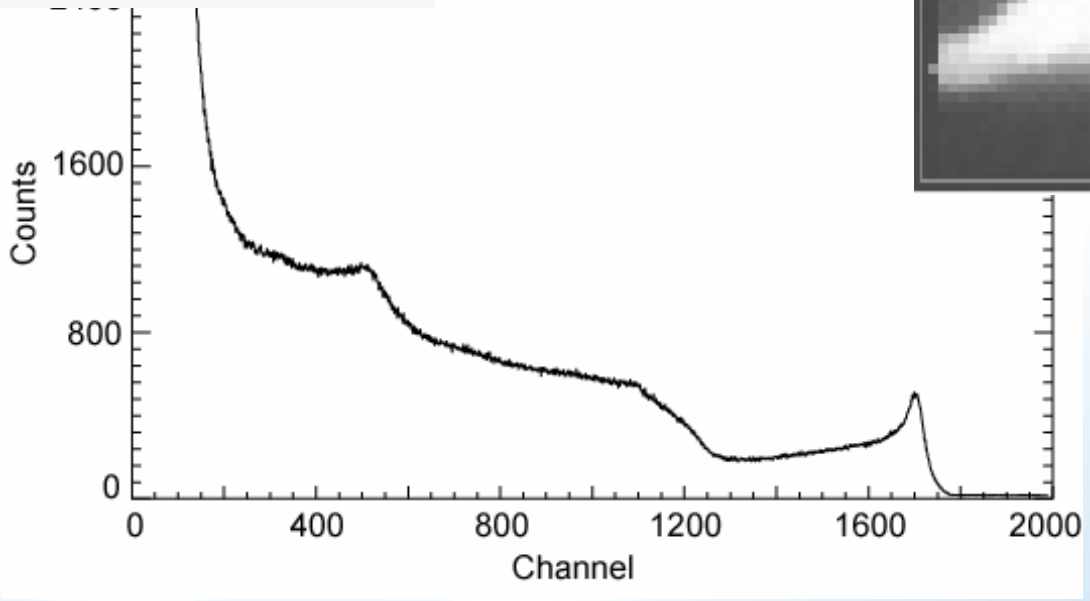

Results from a Good 6x6x14 mm^3 Bar Detector

Full scan

25umx25um resolution
28 keV photons

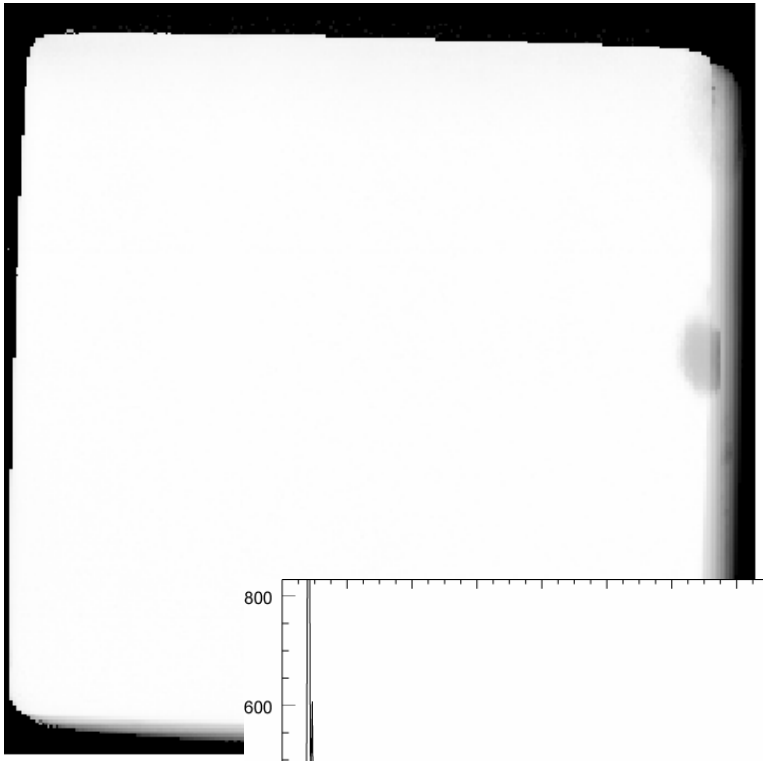

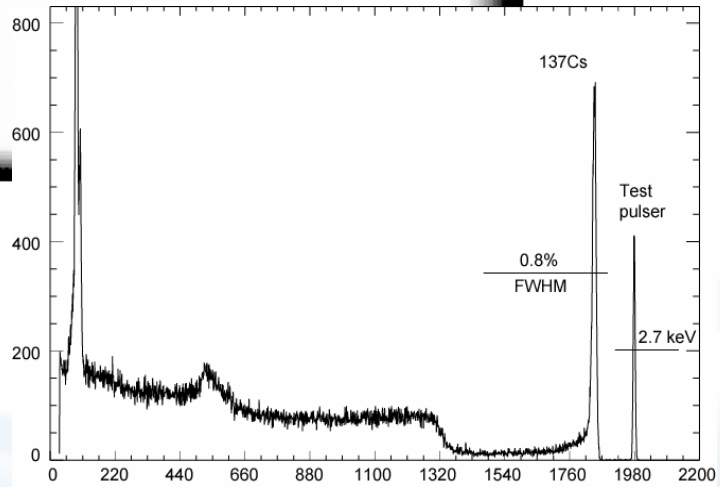

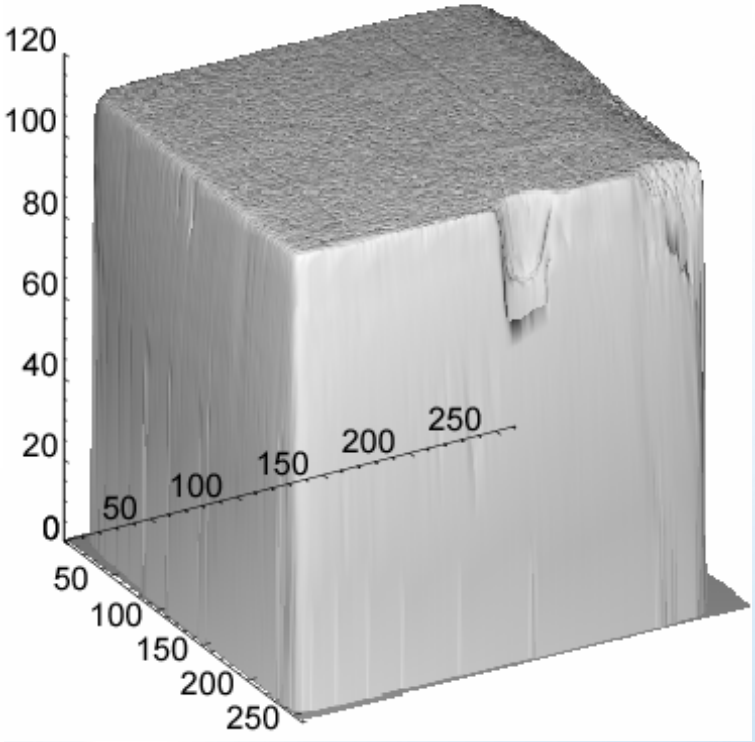

Visible linear feature is an artifact due to the beam injection

Results from a Good 6x6x14 mm^3 Bar Detector

Partial area scan (no edge effect)

Dislocation patterns

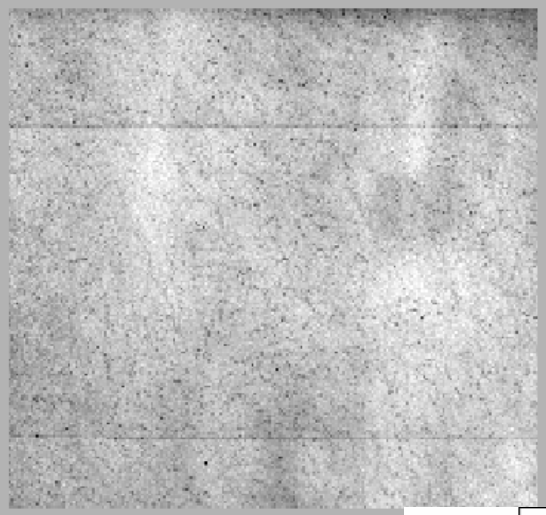

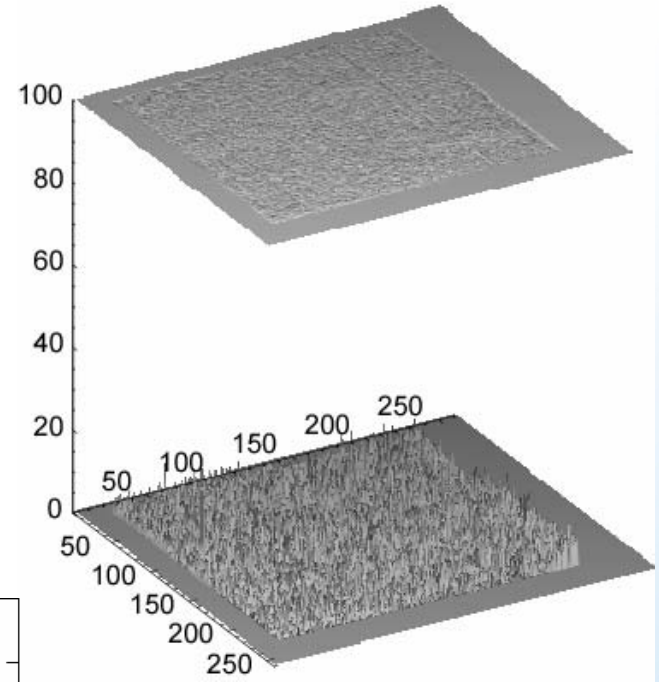

3D plot of partial area scan

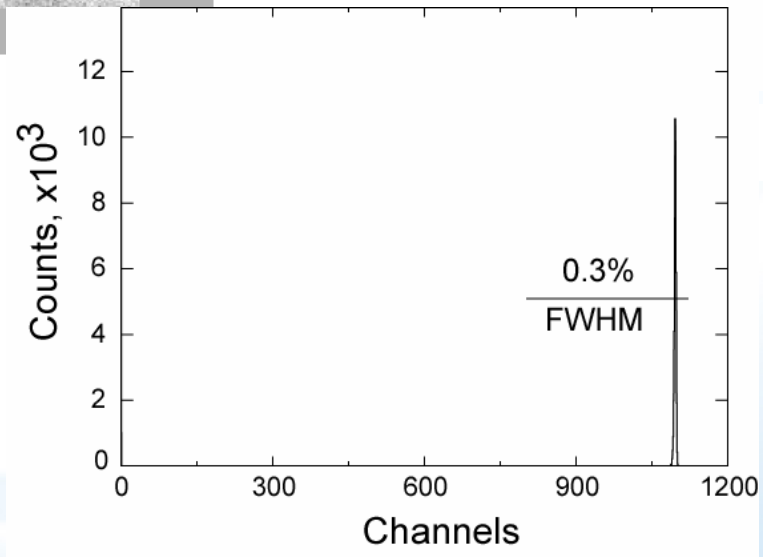

Histogram of the response map of the partial area (no edge effect)

Experimental Techniques for Material Characterization

- Experimental techniques are used to identify the extended defects and to measure their effect:
  - IR microscopy
  - White X-ray diffraction topography
  - Micro-resolution X-ray mapping
  - **Surface etching**

Roles of Dislocations

- Low concentration of Te inclusions
- No boundaries
- X-ray map response is uniform
- But resolution is still poor

5x5x12 mm^3 virtual Frisch-grid detector

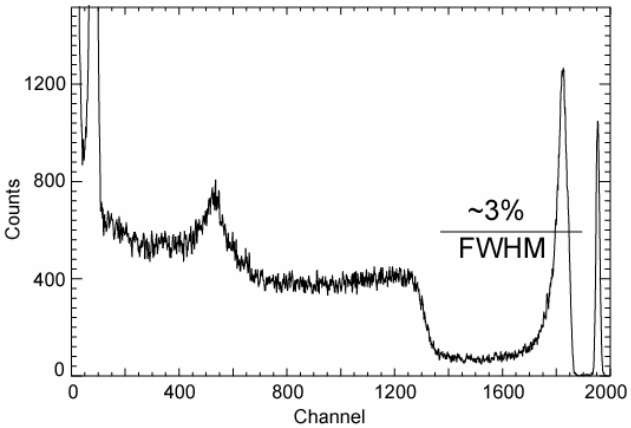

X-ray map

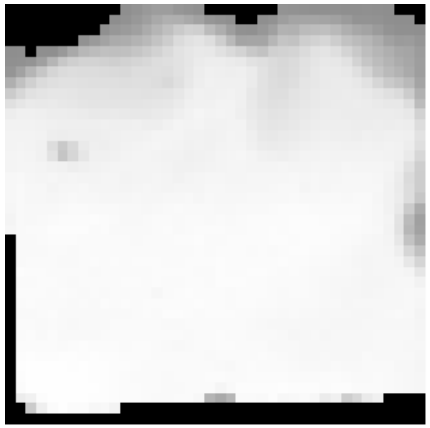

Inclusion distribution

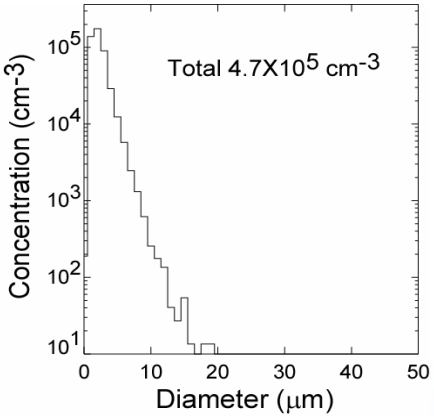

Dynamic contrast typical for the strained crystals with dislocations

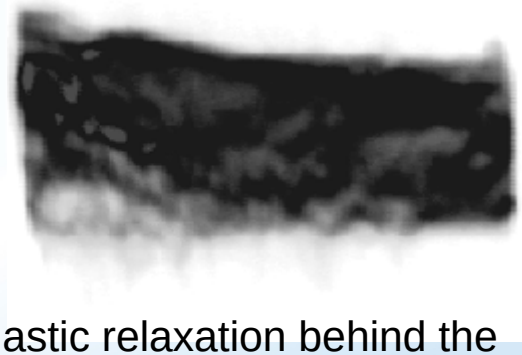

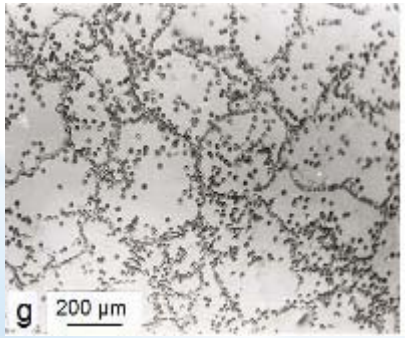

The fact that dislocations are present in CZT is well known

The dislocations are formed during thermoplastic relaxation behind the cooling. At high concentrations, the dislocations arrange themselves into dislocation walls (polygonization). The dislocation walls are similar to the twin and subgrain boundaries

P. Rudolph, Cryst. Res. Tech, 40, p.7, 2005

Dislocation Walls Revealed by Etching

We used the Nakagawa solution (H_2O:H_2O_2:HF) to reveal dislocations on the CZT surface. The effect of etching depends on the crystallographic surface orientation and surface preparations. This solution works on (1 1 1) surfaces

A. Hossain et al., J. Cryst. Growth, 2008.

Etch pits correspond to dislocations terminated on the surface.

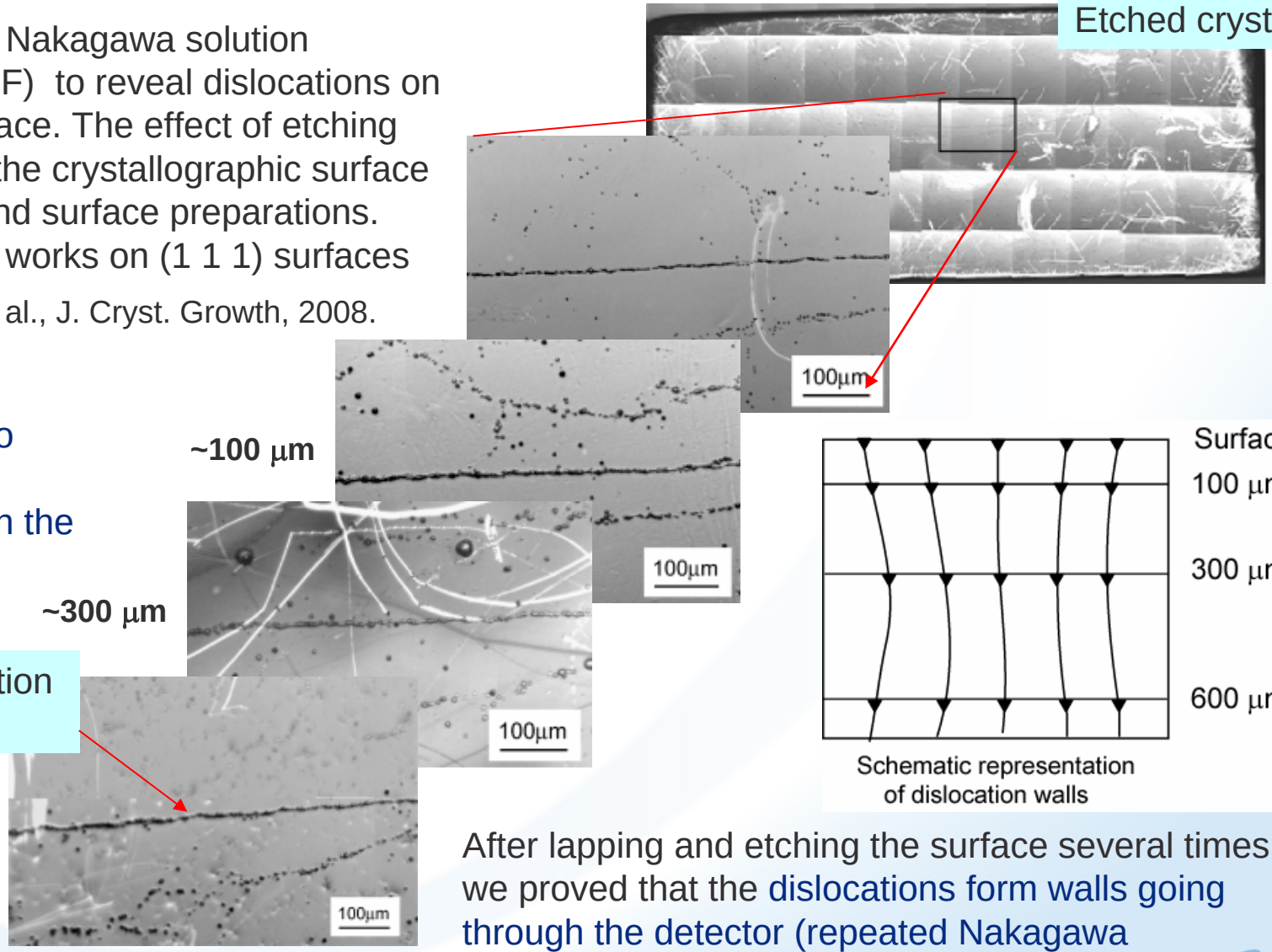

Schematic representation of dislocation walls

After lapping and etching the surface several times we proved that the dislocations form walls going through the detector (repeated Nakagawa procedure).

Prismatic Punching Dislocation Patterns

Photograph of the etched surface of a 5x5x12 mm^3

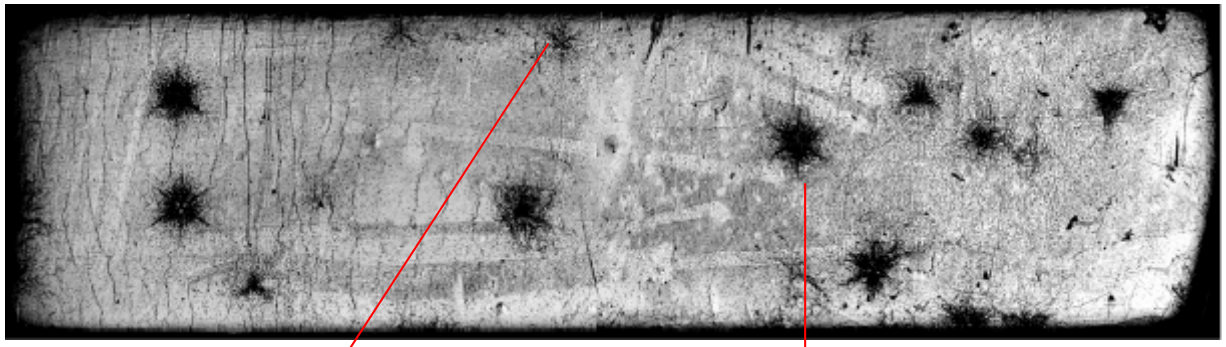

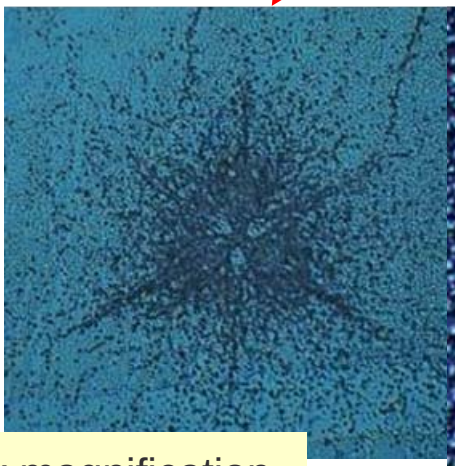

50x magnification

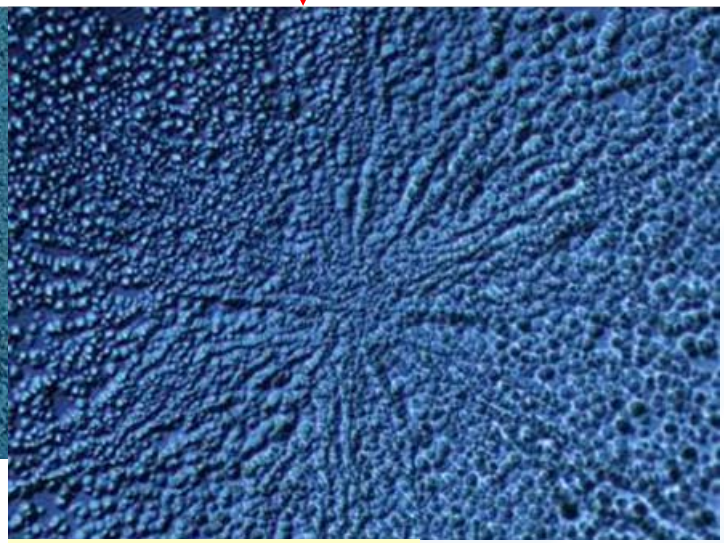

500x magnification

The origin of such defects is unclear. Two mechanisms are discussed in the literature: 1) caused by high pressure built inside inclusions (R. D. S.Yadava et al., J. Electron. Mater 21, p. 1001, 1992); 2) moving dislocations interact with inclusions or precipitates (P.B. Hirsh, J. Inst. Metals 86, p. 7, 1957).

No remnants of inclusions or precipitates are observed inside the “stars”.

Prismatic Punching Defects

2x2 mm^2

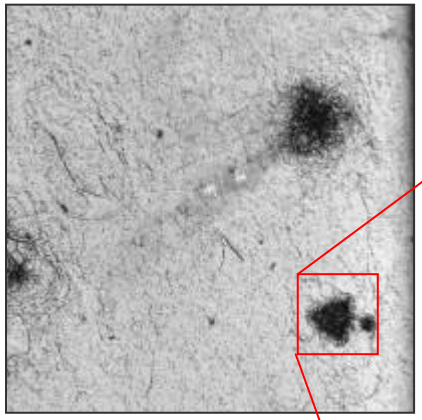

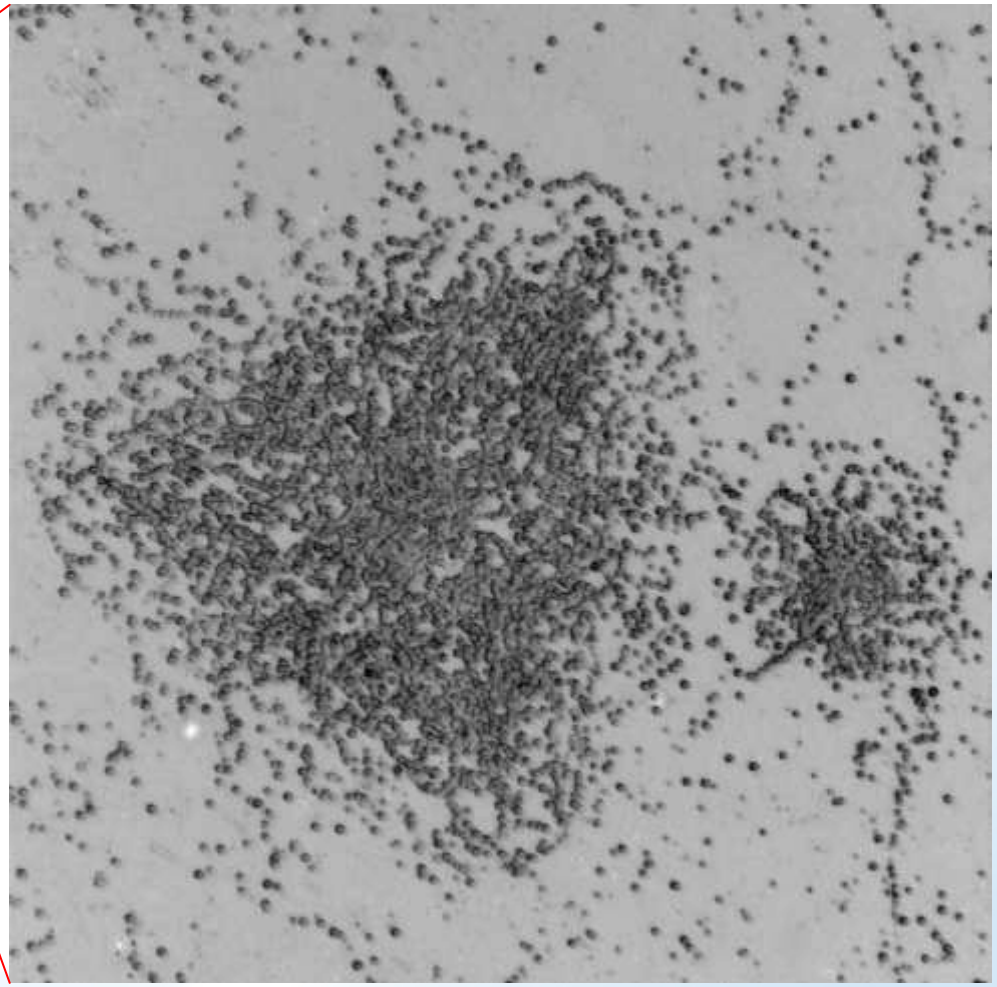

Photograph of the Etched Surface

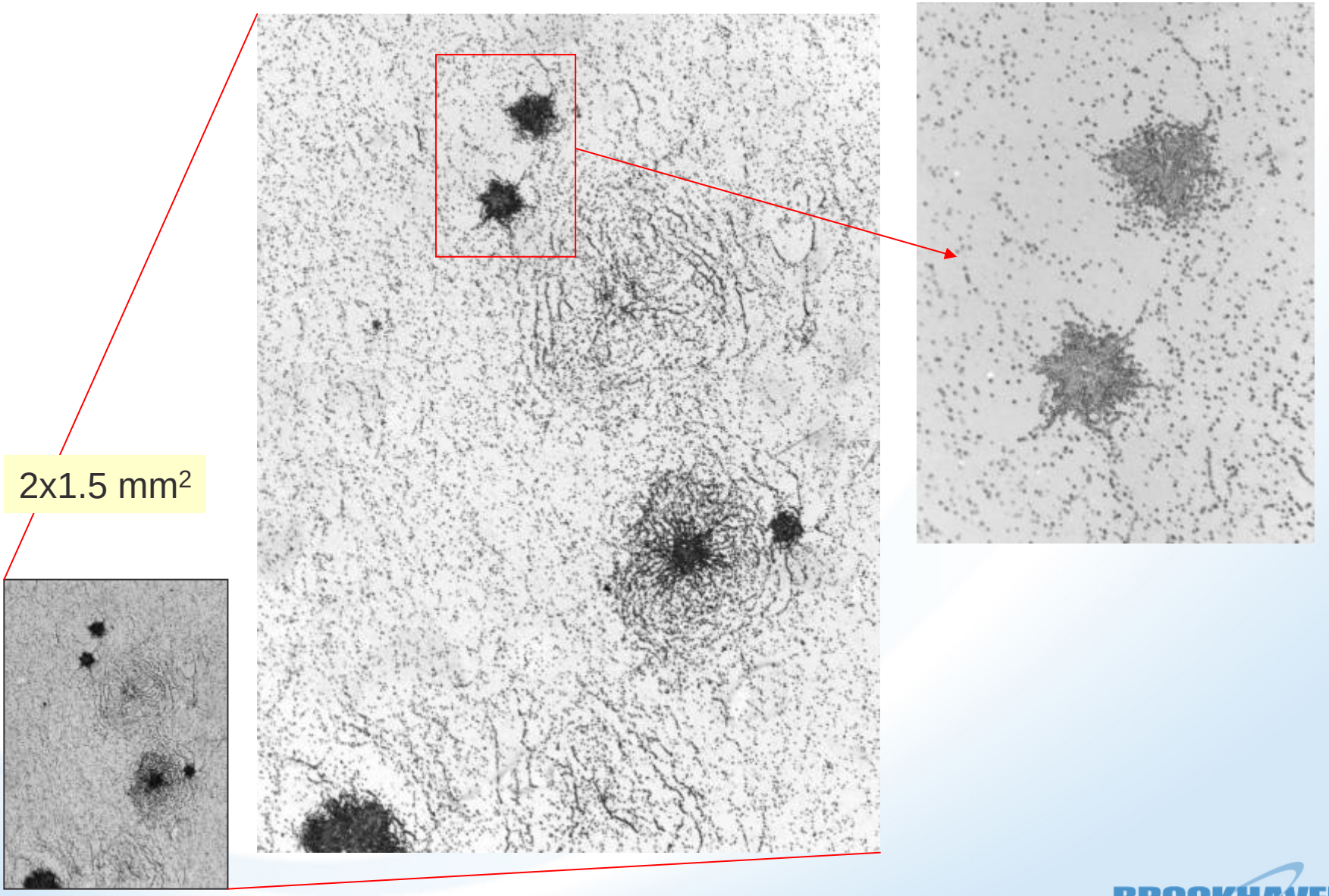

Outline

Introduction

- Research areas
- Advantages of CdZnTe (CZT) gamma-ray detectors

Material characterization

- Experimental techniques
  - IR microscopy
  - White X-ray Diffraction Topography
  - Micro-scale X-ray mapping
  - Surface etching
- Te inclusions
- Dislocations
- **Polarization effect**
- E-field non-uniformities

Conclusion

Polarization Effect

In some medical and industrial applications high flux is needed to perform very quick measurements. CZT when irradiated with high flux might show a polarization effect. “Polarization effect” i.e. when we observe gradual changes in the electron charge collection efficiency while exposing a fix area.

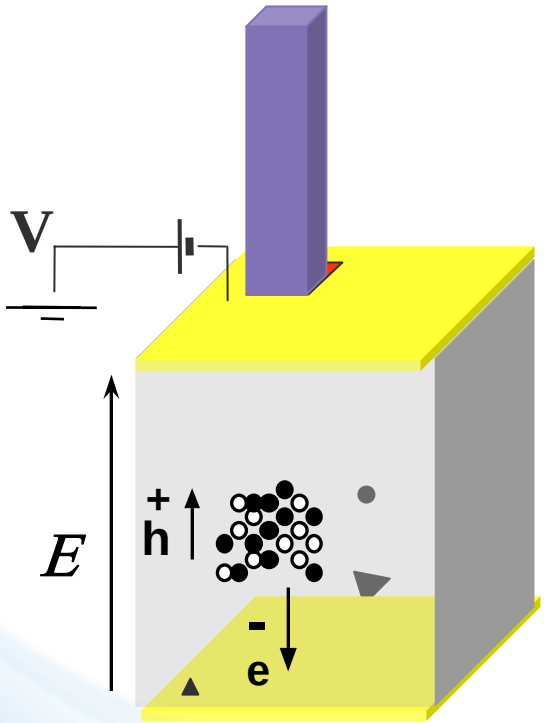

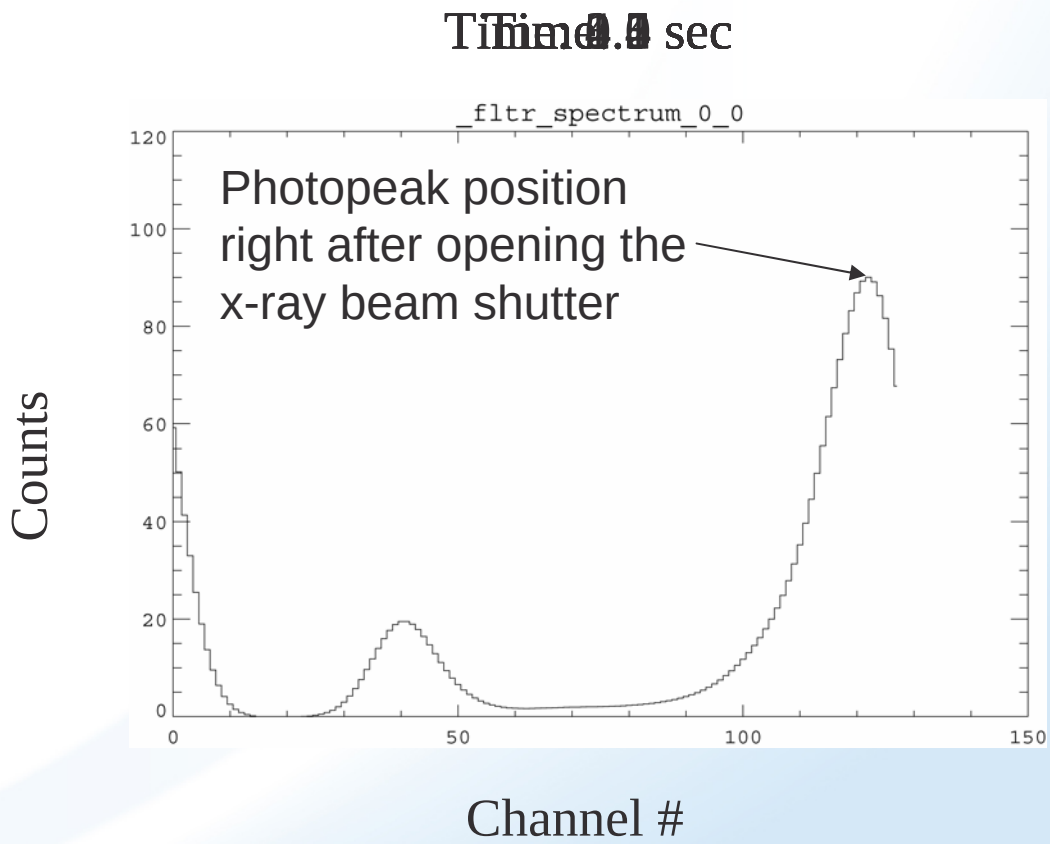

Electron Collection of Detector HX2

Very low bias x-ray maps

~10^{10} ph/sec*mm^2

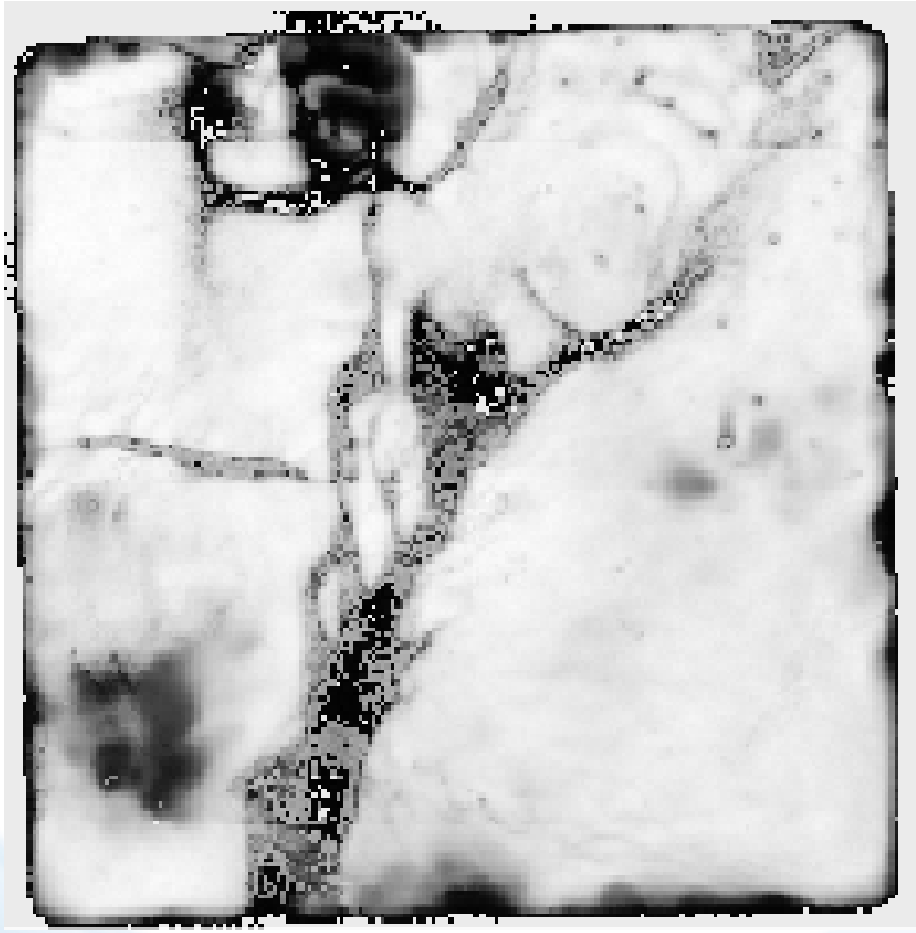

27keV; 12V; coll10um; step: 50um

~10^{10} ph/sec*mm^2

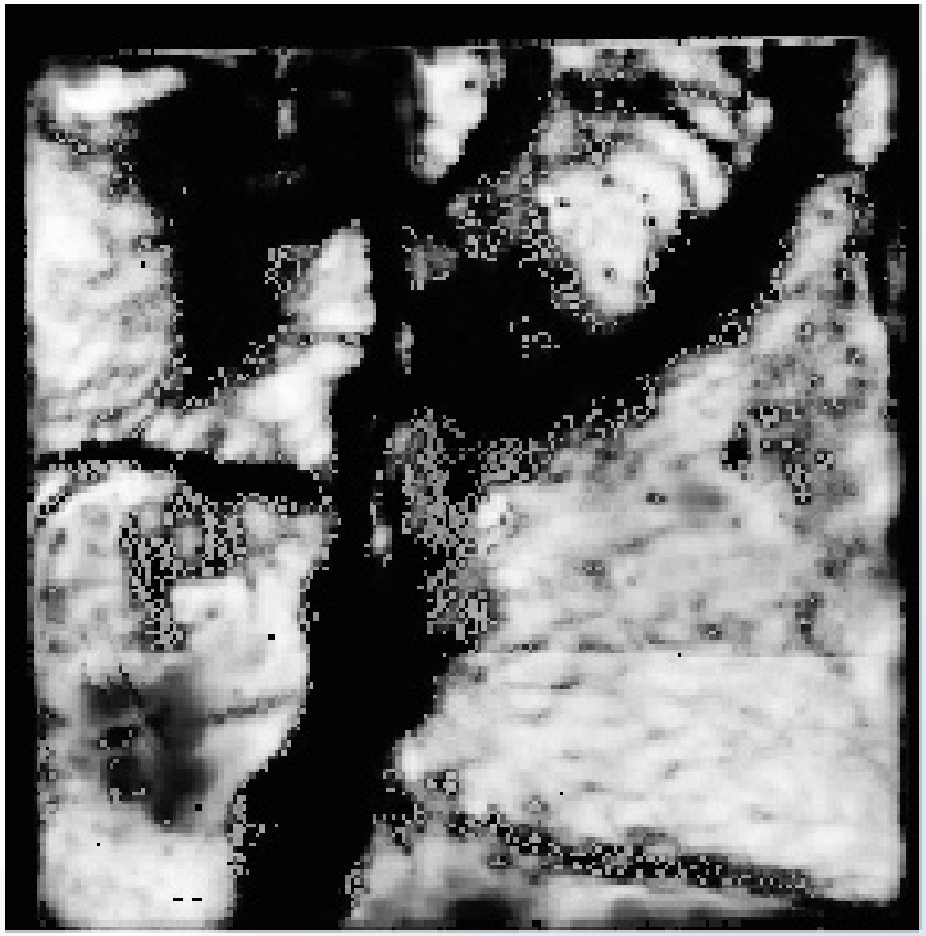

27keV; 12V; coll25um; step: 50um

Hole collection Map and WXDT Image of Detector HX2

12x12x1 mm^3 CZT

Hole collection map

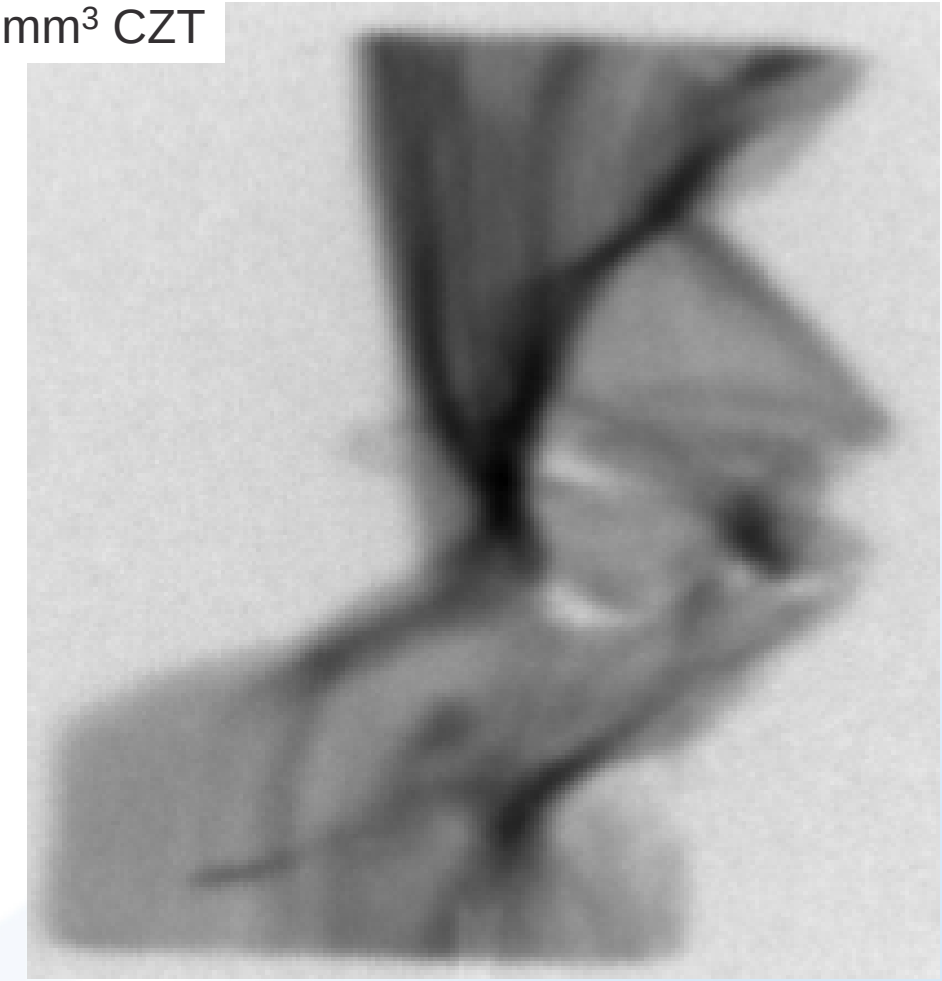

WXDT image

Not easy to see this structure with the IR!

Outline

Introduction

- Research areas
- Advantages of CdZnTe (CZT) gamma-ray detectors

Material characterization

- Experimental techniques
  - IR microscopy
  - White X-ray Diffraction Topography
  - Micro-scale X-ray mapping
  - Surface etching
- Te inclusions
- Dislocations
- Polarization effect
- **E-field non-uniformities**

Conclusion

Charge Loss with X27B X-ray Beam

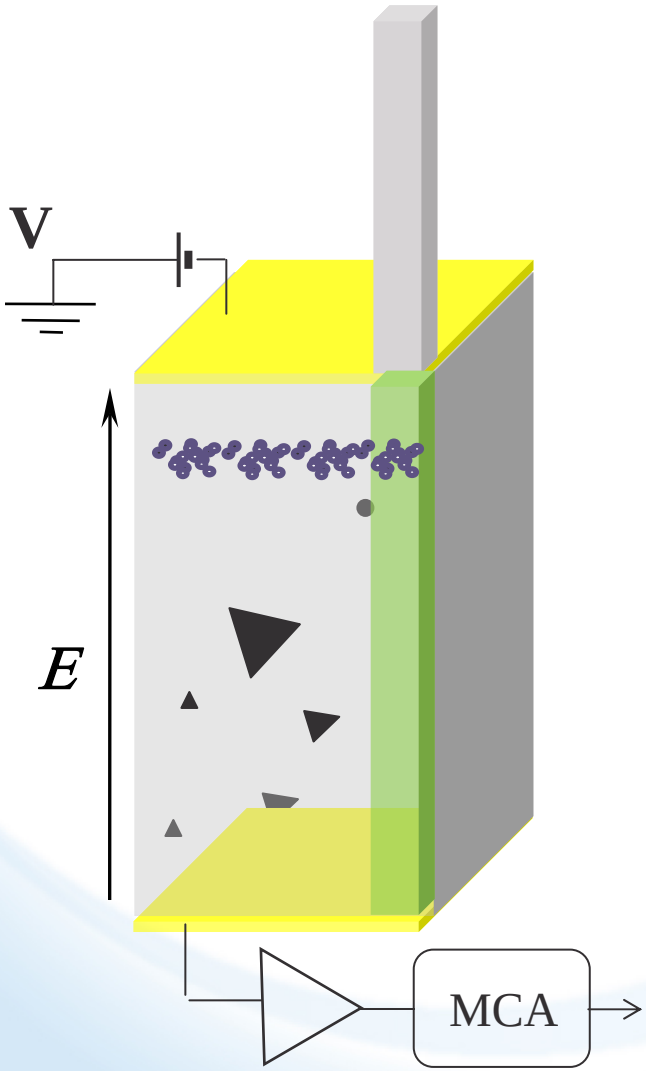

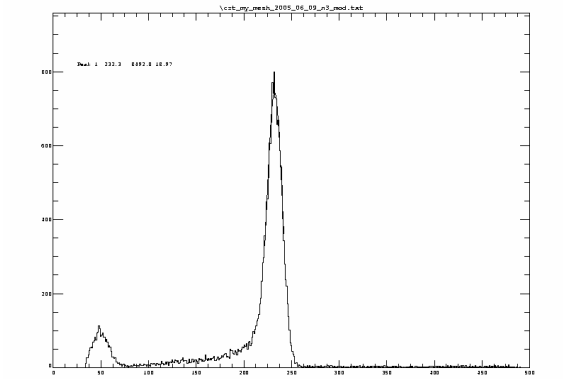

Full charge collection:

Photopeak at ch 480:

No defect is in the path

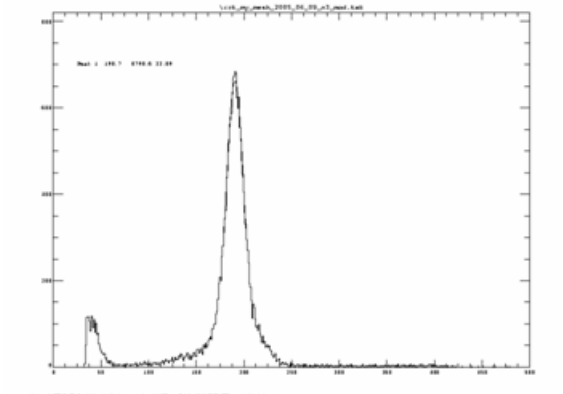

Some charge is trapped:

Photopeak at ch 350:

Some small defect is in the path

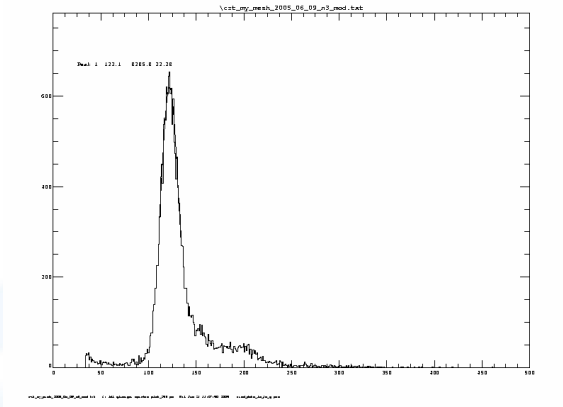

More charge is trapped:

Photopeak at ch 150:

Large defect is in the path

Internal E-field in Detectors with Planar Contacts

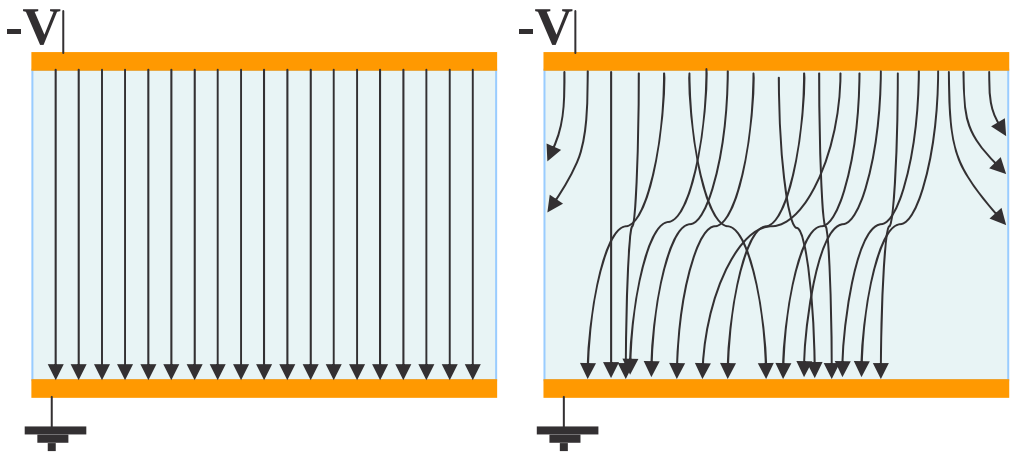

The arrowed lines represent the electron cloud drift trajectory and give an idea of the internal E-field (they are not field lines)

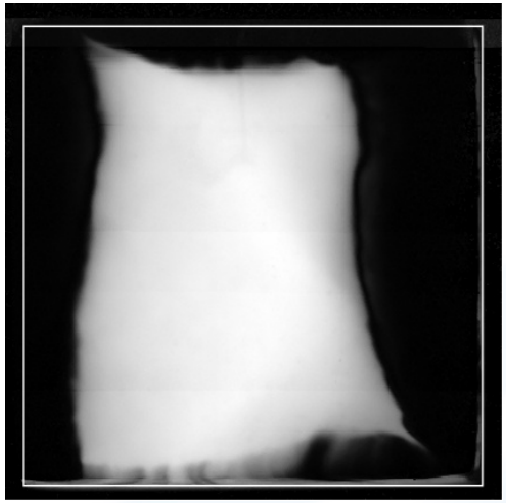

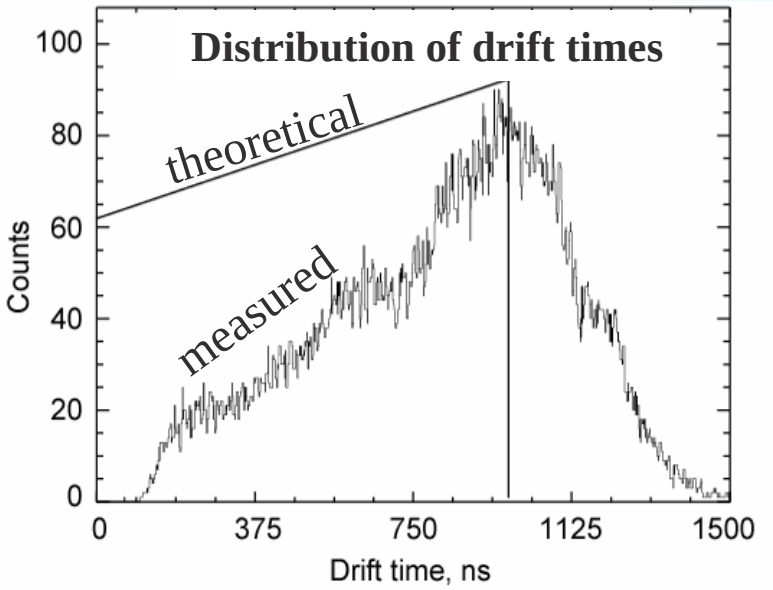

Correlation Between Dislocation Walls and Charge Loss

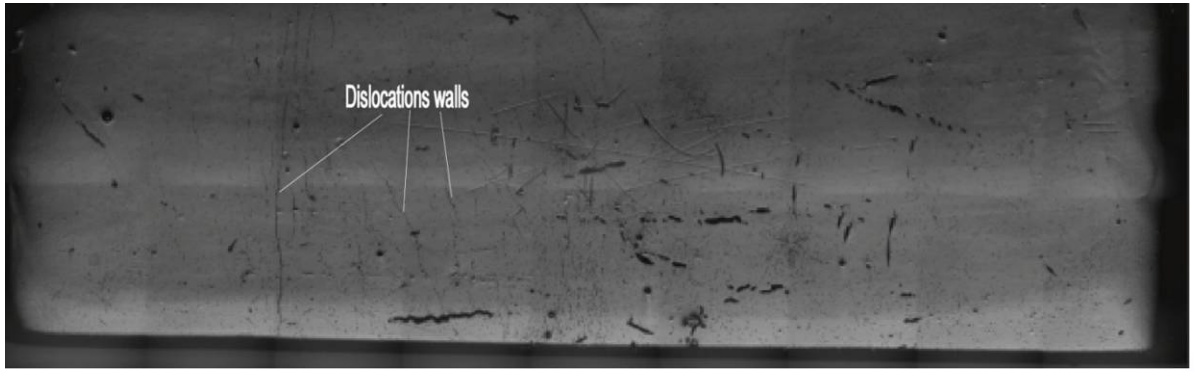

EPD image of a 12x5x3 mm^3 CZT sample

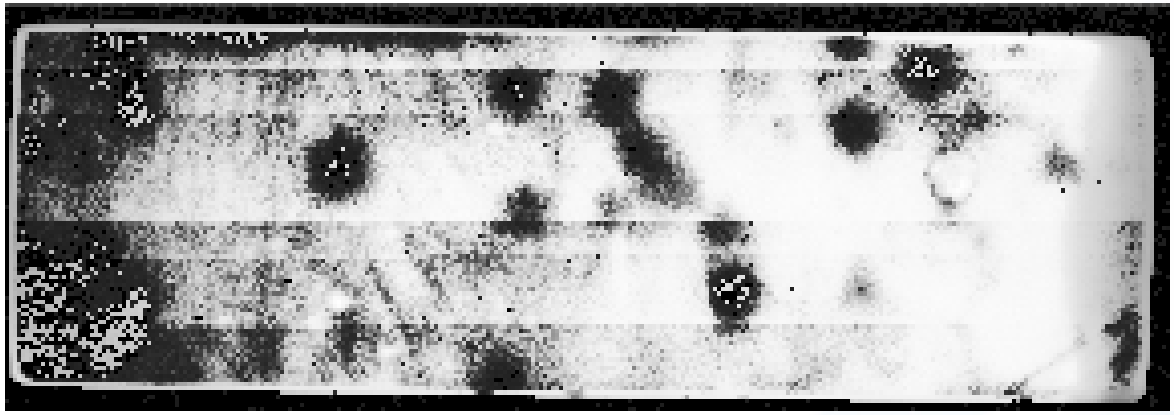

Electron collection map of a 12x5x3 mm^3 CZT detector

Dislocation walls affect carriers transport. Charge loss is very small. We did non observe direct match between IR and X-ray maps => changes of E-field (well know in Ge and Si semiconductors)

X-ray Maps of the Grid Detector

Illuminating from the grid-electrode side

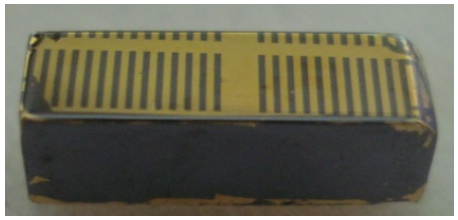

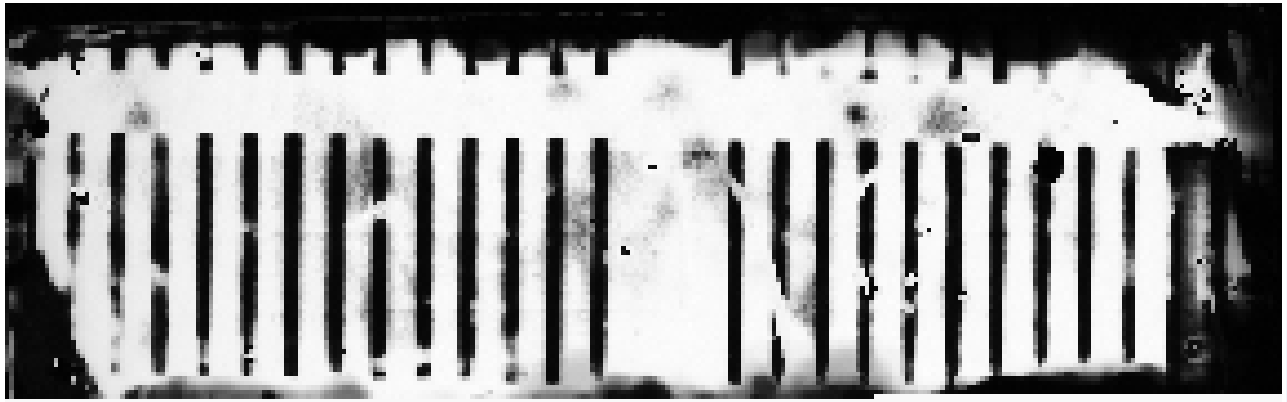

Raster scan area: 11.8mm x 4mm

Step size: 25 µm; Bias: 500 V; Energy: 15 keV

Illuminating from the planar-electrode side

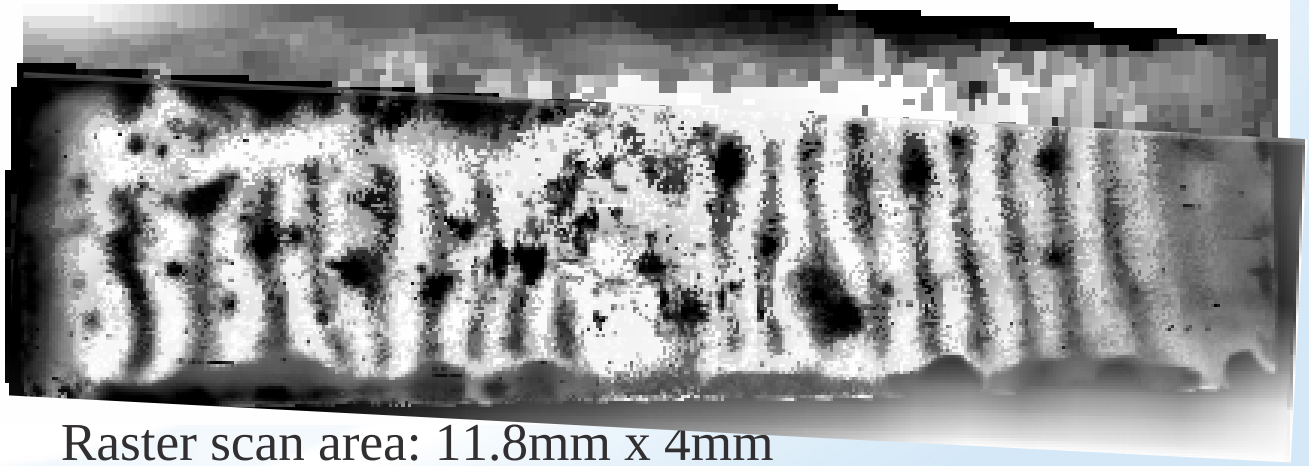

Raster scan area: 11.8mm x 4mm

Step size: 25 µm; Bias: 500 V; Energy: 15 keV

Internal E-field and X-ray Maps of a Grid Detector

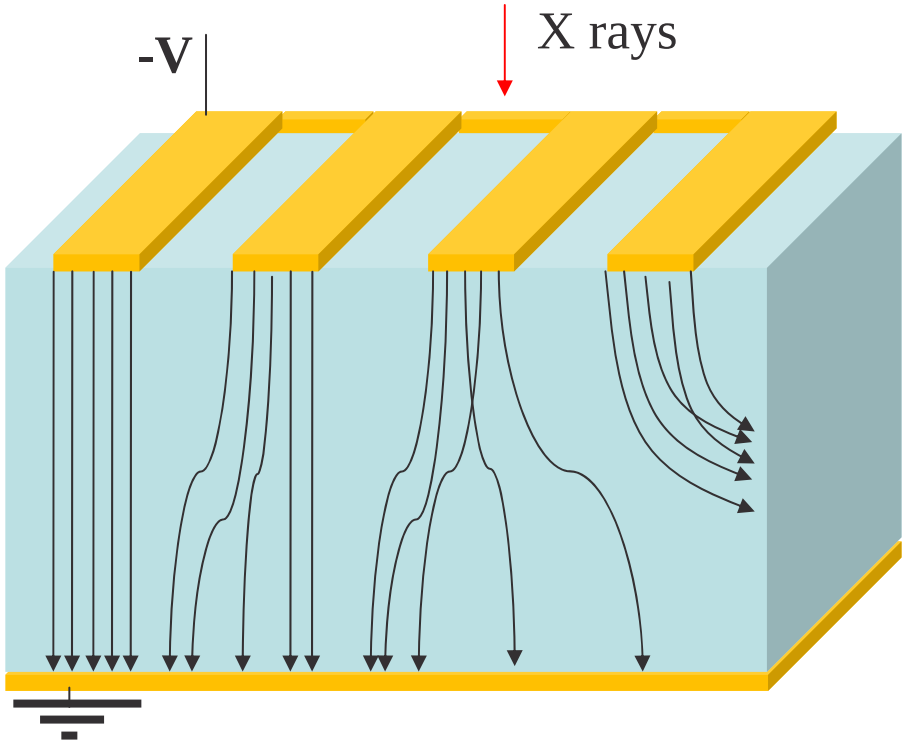

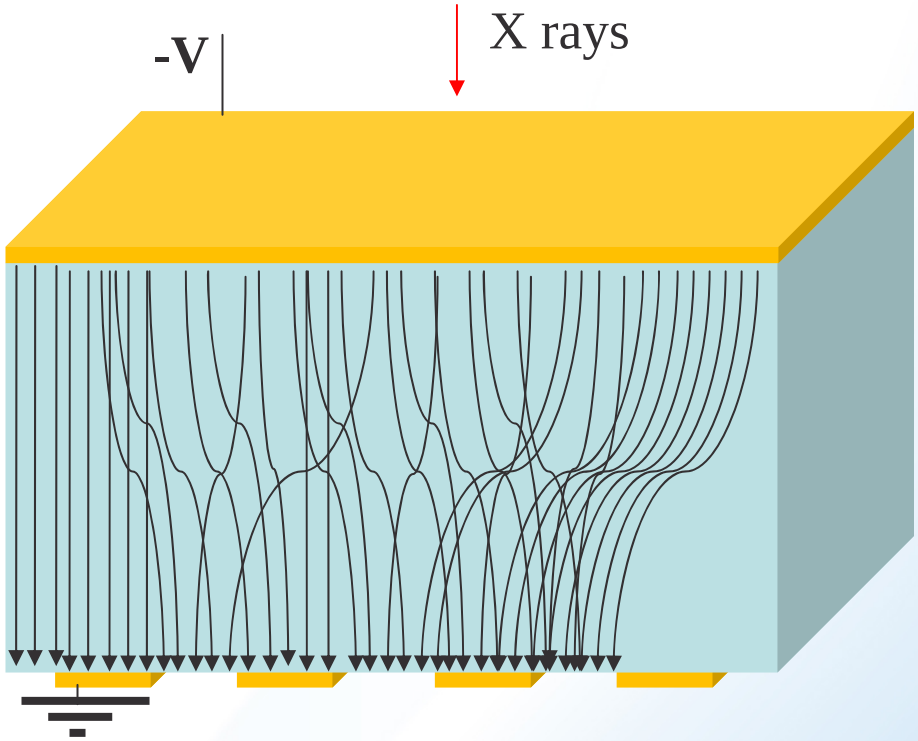

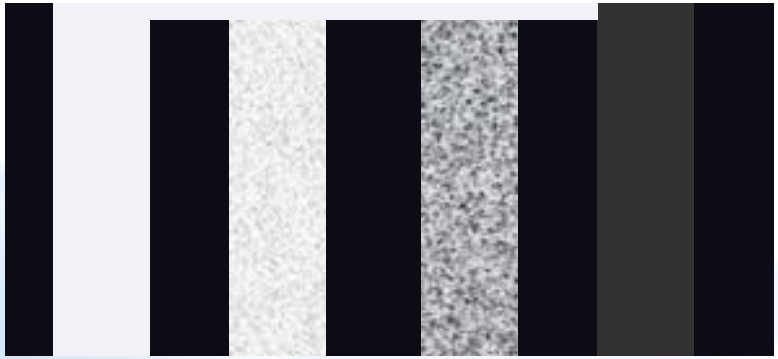

X-ray maps

Some of the Large Volume CZT Detectors Tested

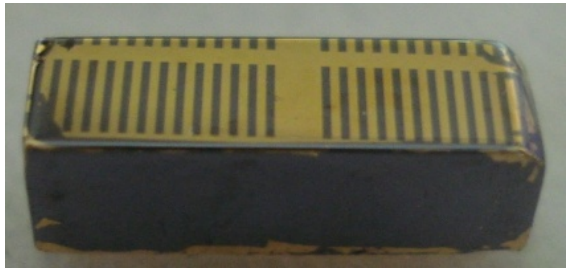

Grid detector
5x12x3 mm^3

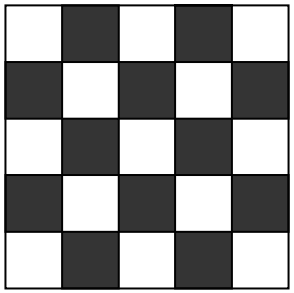

Two pixel detectors
10x10x10 mm^3

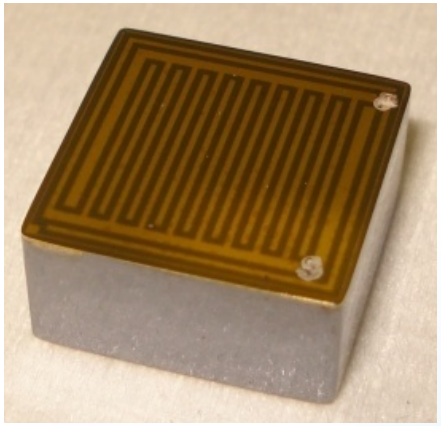

Two CPG detectors
15x15x7.5 mm^3

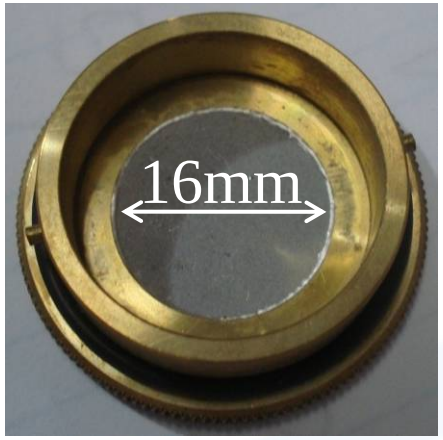

eV Products device holder

X-ray Maps of Two 1x1x1 cm^3 Pixel Detectors

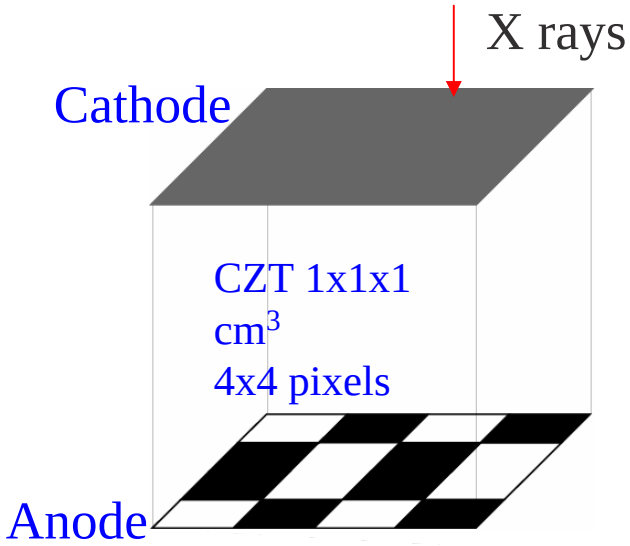

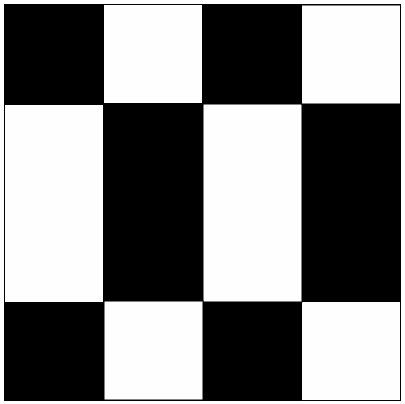

Pixel contacts are connected to form two electrodes: dark (grounded) and white (signal).

X-ray scan conditions
Energy 27 keV
Spatial resolution 25 μm

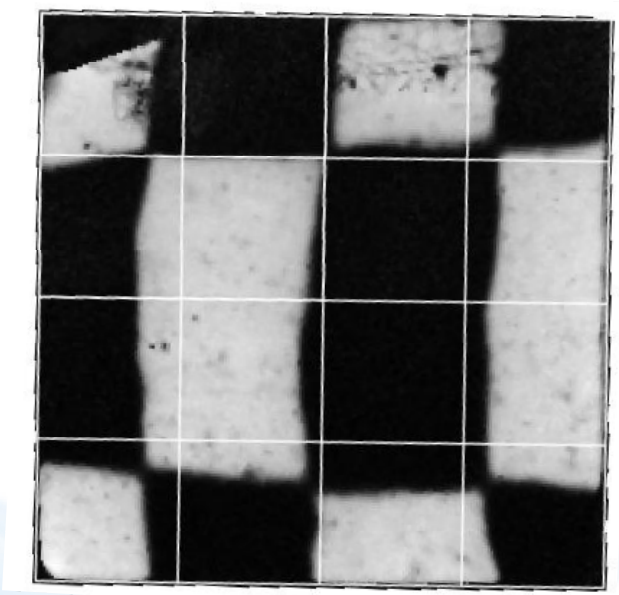

Detector 1

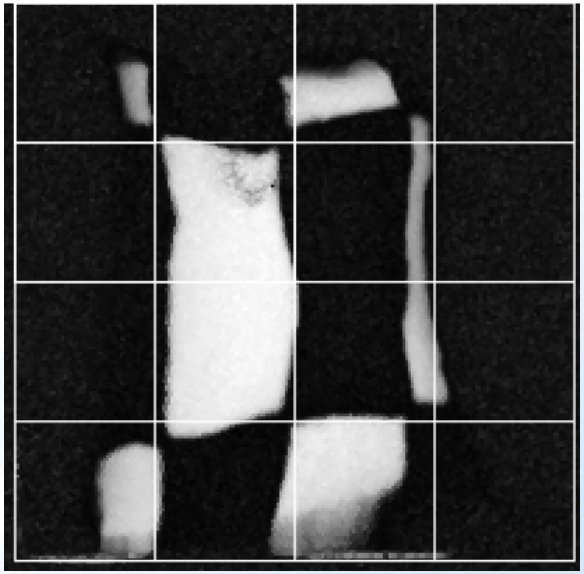

Detector 2

X-ray Maps of two 1x1x1 cm^3 Pixel detectors

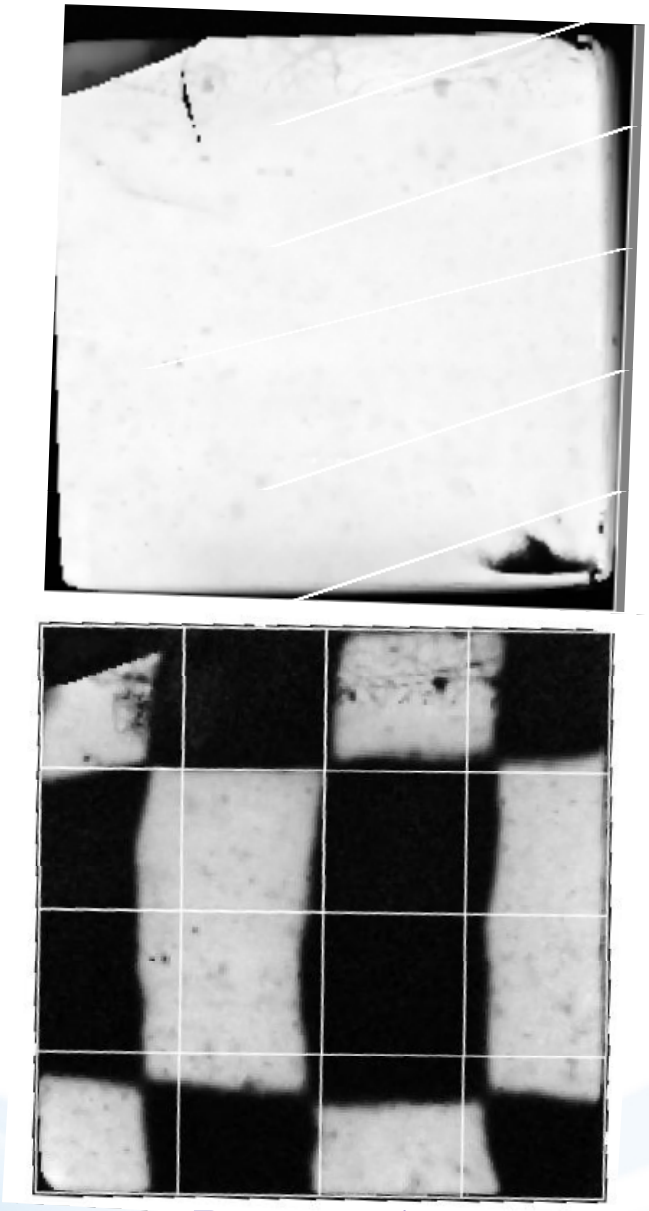

Detector 1

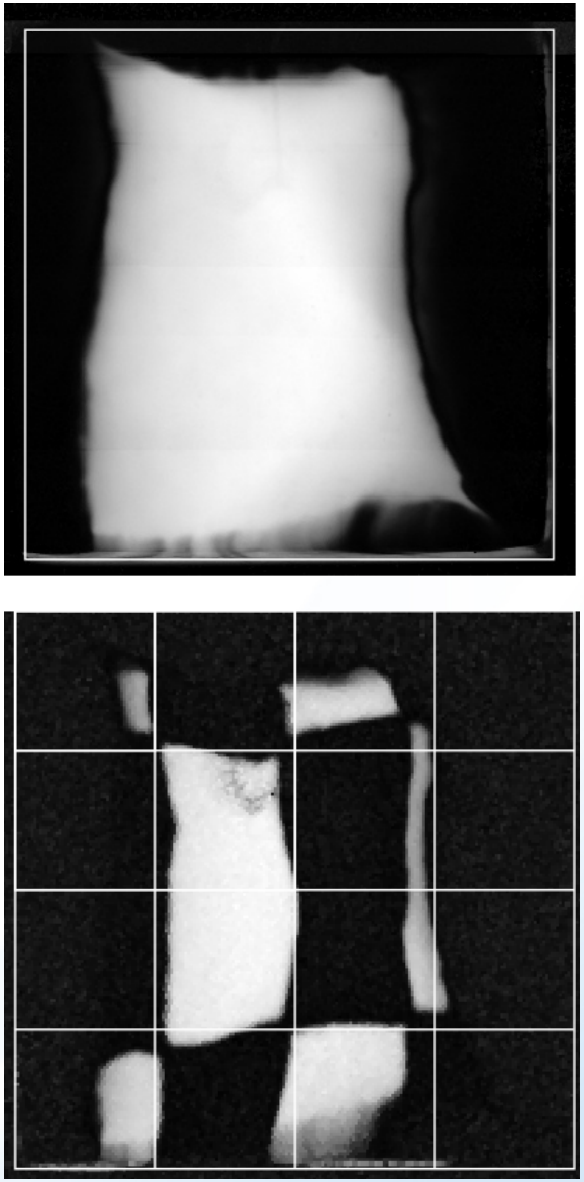

Detector 2

2D X-ray Maps of CPG2

Illuminating from the grid-electrode side

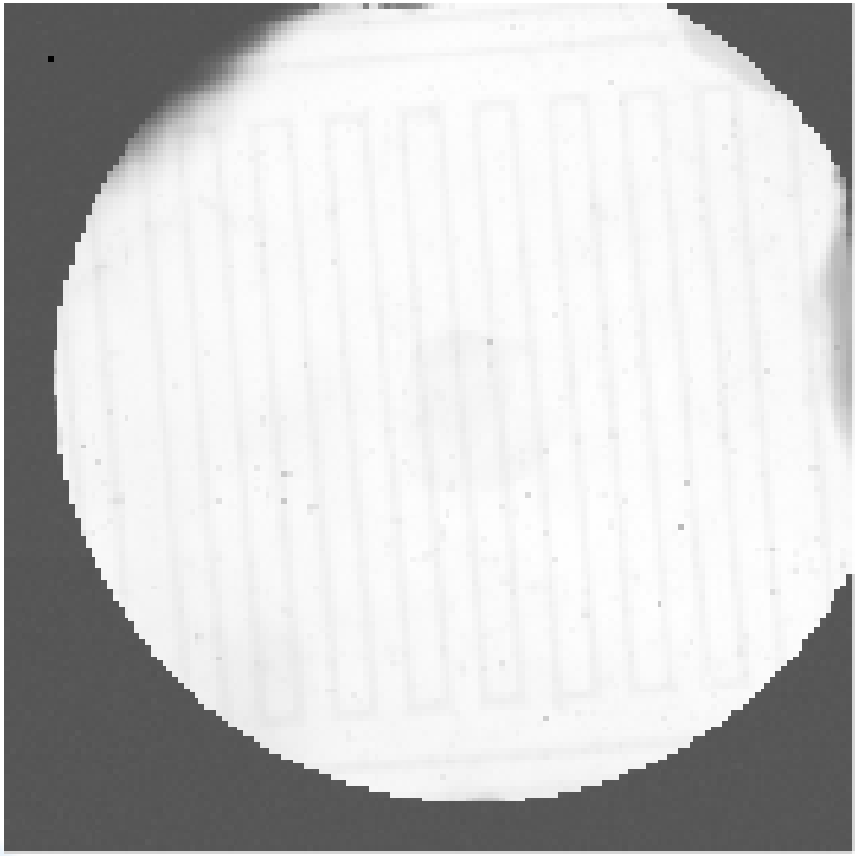

Raster scan area: 16mm x 16mm
Step size: 50 µm; 600 V; 18keV

Illuminating from the planar-electrode side

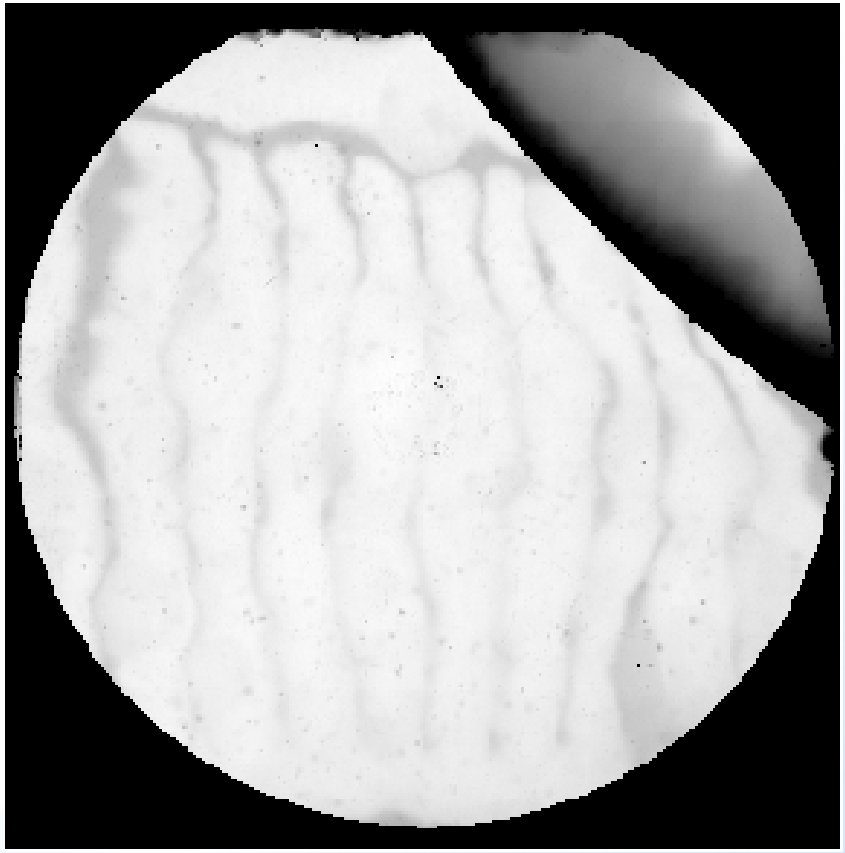

Raster scan area: 16mm x 16mm
Step size: 50 µm; 600 V; 18keV

3D X-ray Maps of CPG2

Illuminating from the grid-electrode side

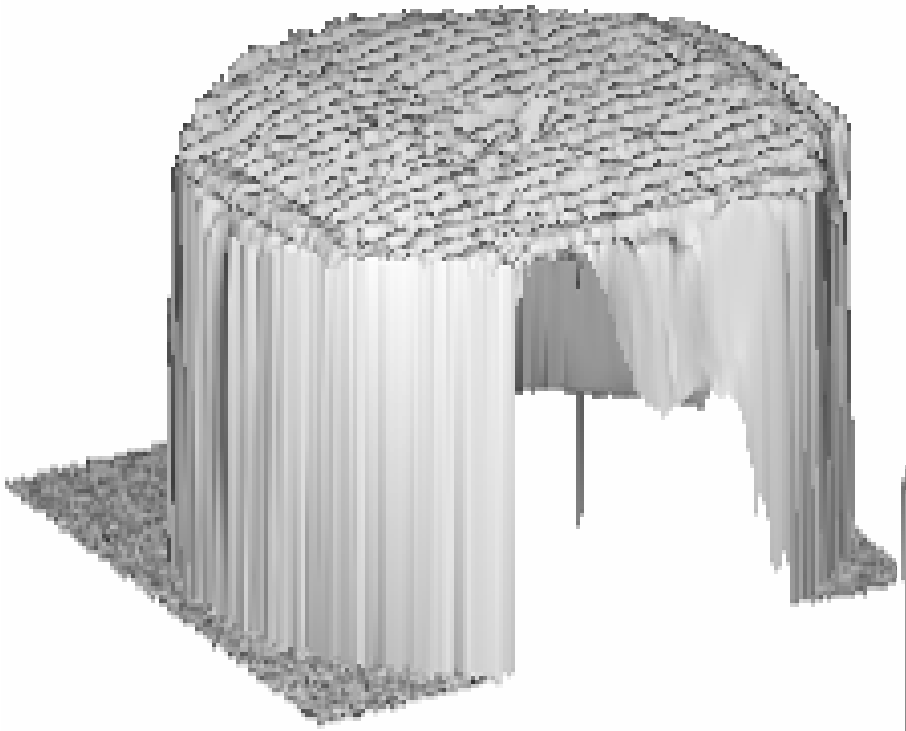

Raster scan area: 16mm x 16mm
Step size: 50 µm; 600 V; 18keV

Illuminating from the planar-electrode side

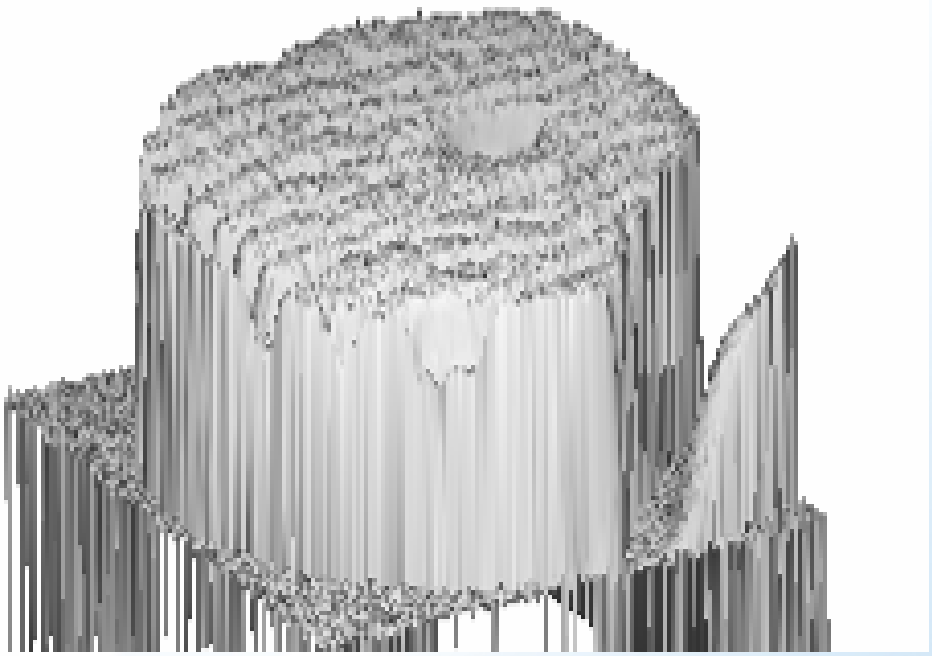

Raster scan area: 16mm x 16mm
Step size: 50 µm; 600 V; 18keV

2D X-ray Maps of CPG2 with Filter

Illuminating from the grid-electrode side

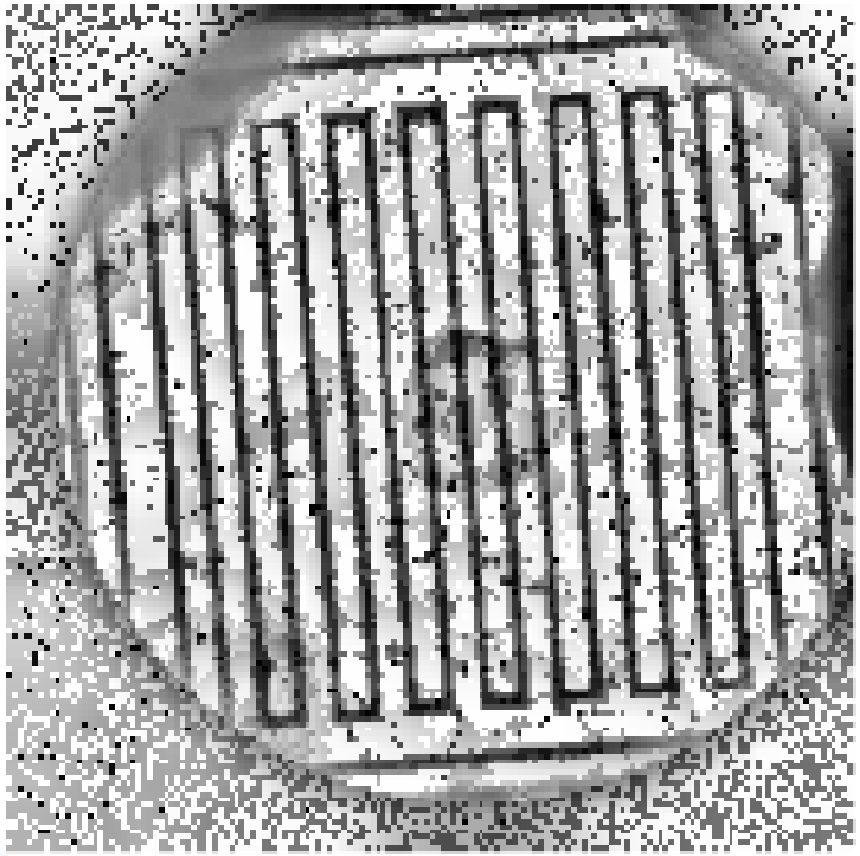

Raster scan area: 15.5mm x15.5mm
Step size: 100 µm; 600 V; 18keV

Illuminating from the planar-electrode side

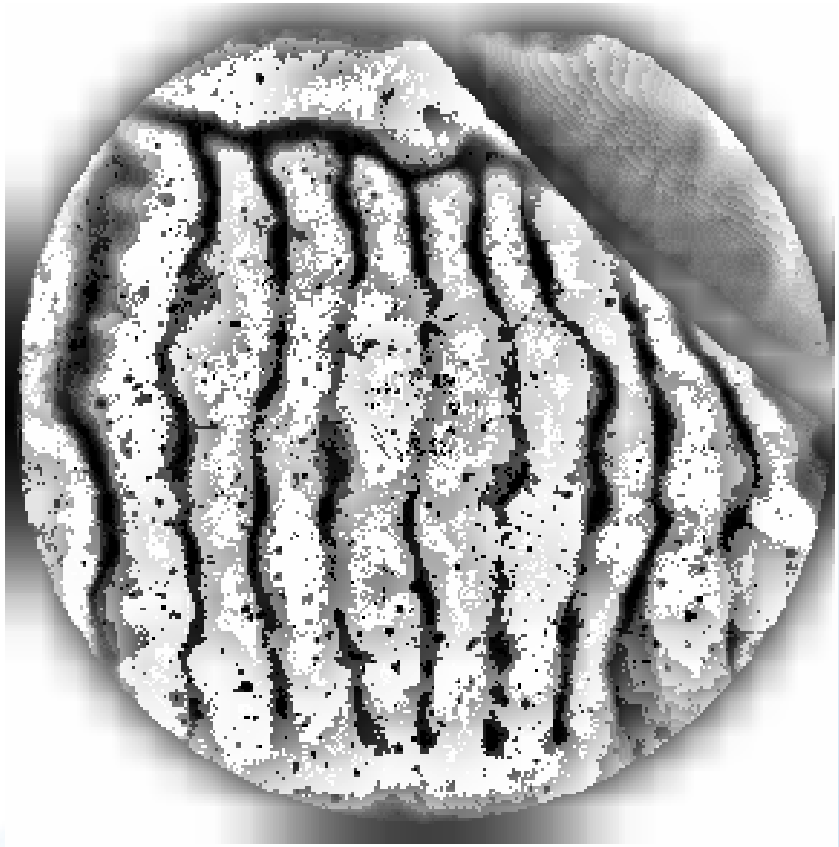

Raster scan area: 15.5mm x 15.5mm
Step size: 50 µm; 600 V; 18keV

Conclusions

•We demonstrated that several types of extended defects exist in commercial crystals: twins, sub-grain boundaries, dislocation walls, prismatic punching dislocations and Te inclusions. They affect charge transport and detector performance.

•Te inclusions trap charge and reduce output signals. They also cause fluctuations in the collected charge.

•We observed correlation between the onset of polarization and hole trapping.

•Dislocations distort local E-field which also causes fluctuations in collected charge.

Acknowledgments

This work was supported by the Defense Threat Reduction Agency and by the U.S. Department of Energy, Office of Nonproliferation Research and Development, NA-22.

And

Istvan Dioszegi, Peter Vanier, Carl Czajkowski, Joseph Indusi

Zhong Zhong, Zhijian Yin, Randy Smith, Balaji Raghothamachar, Pete Siddons, Abdul Rumaiz, Gabriella Carini, Tony Lanzirotti, Tony Lenhard, Shu Cheung, Rick Greene

Gianluigi De Geronimo, Zheng Li, Rubi Gul, Rolf Beuttenmuller, John Triolo, Don Pinelli, Pavel Rehak, Sergio Rescia, Graham Smith

Don Elliott, Paul Vaska, Nick Simos, Genda Gu, Stephen Babalola, Petro Fochuk, Stephen Egarievwe

Thank you

Extra slides

Why do we need a collimated source?

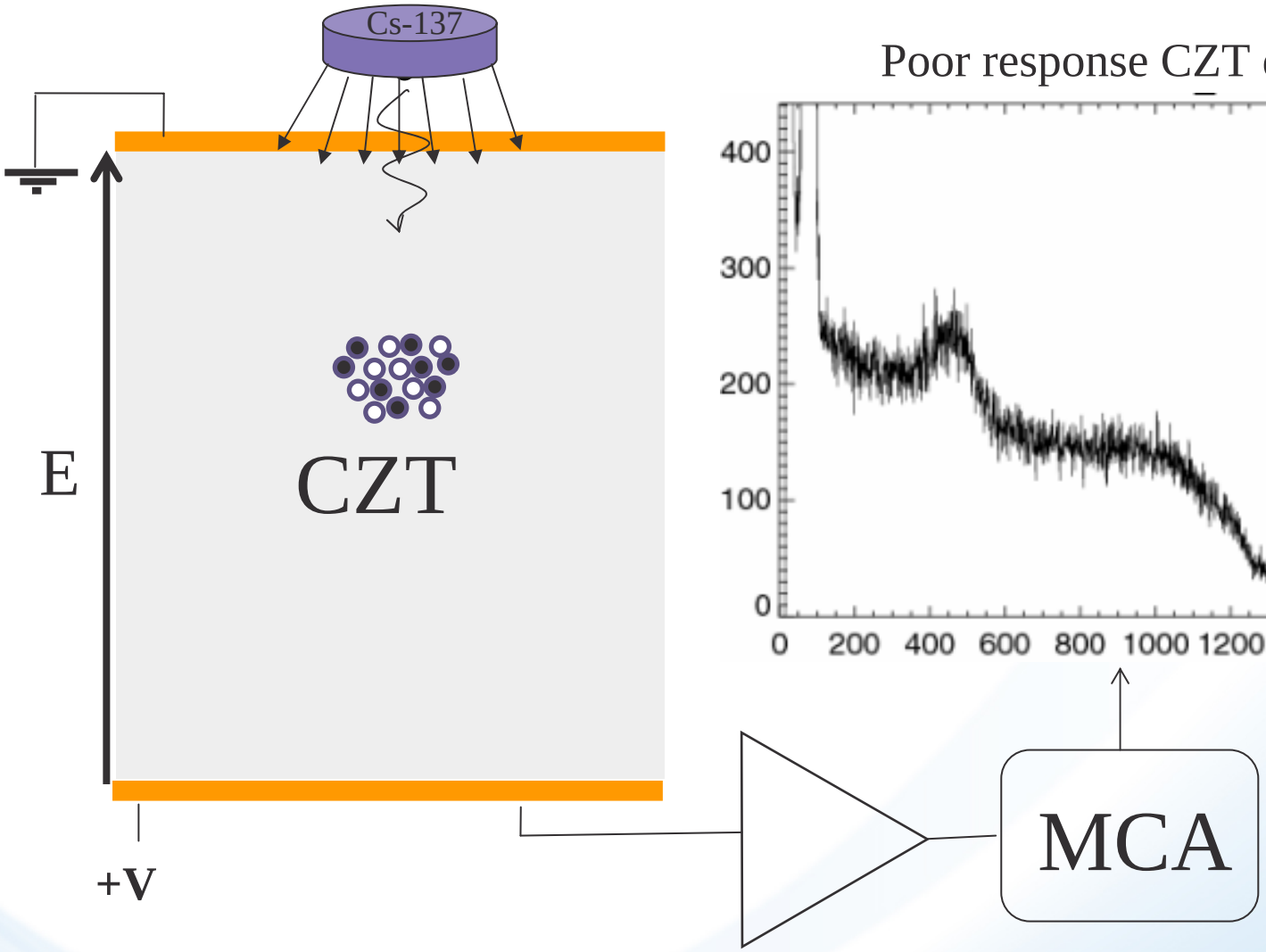

Poor response CZT detector

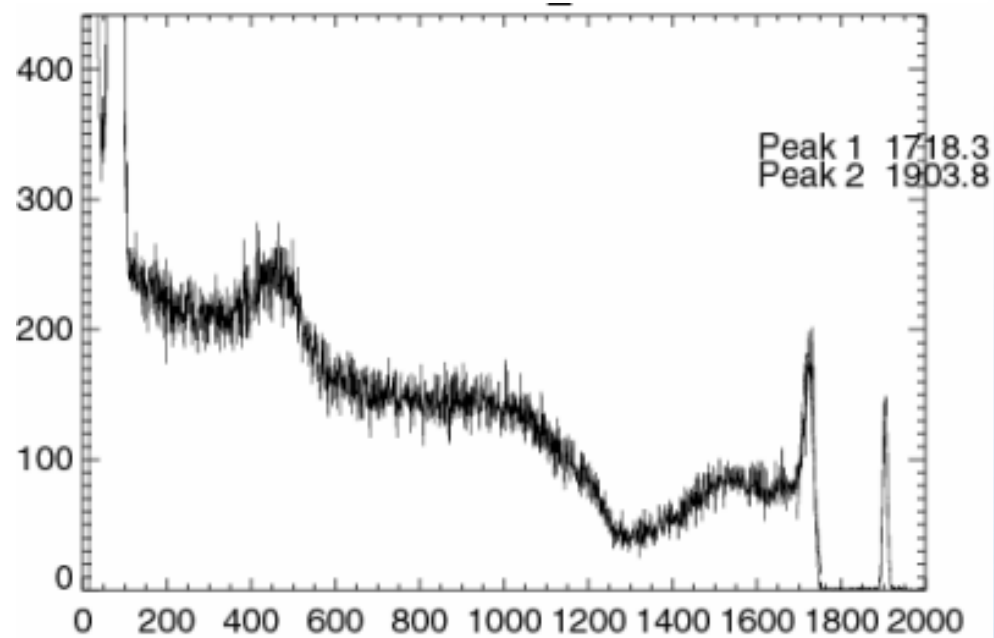

This source is **not collimated**; we need better spatial resolution to understand the degradation of detectors → Synchrotron Radiation (SR) of the National Synchrotron Light Source (NSLS)

Extended defects in CZT samples

Destructive method to reveal extended defects: Nakagawa etching

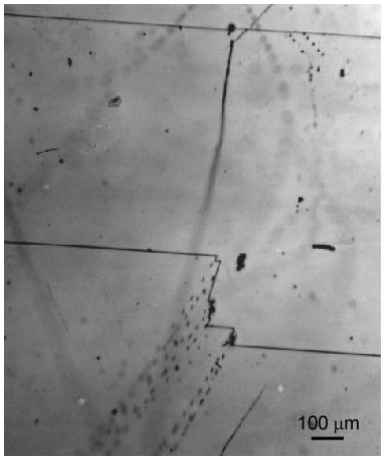

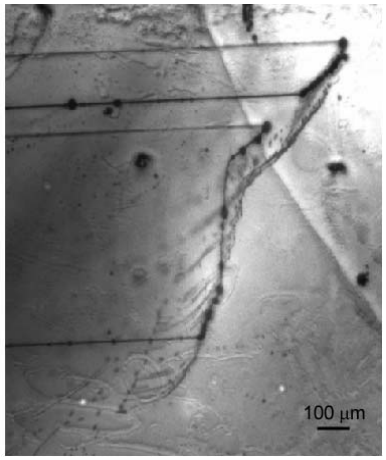

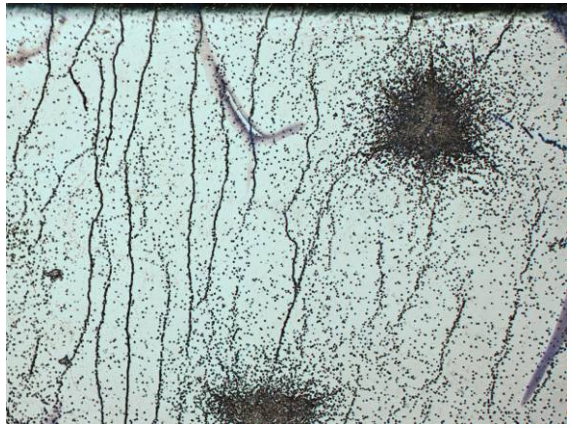

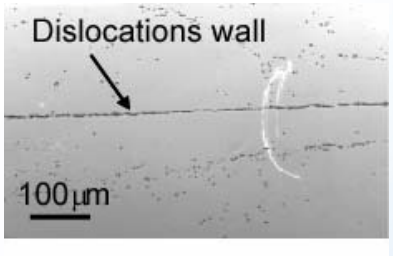

EPD image of a 12x5x3 mm^3 CZT sample

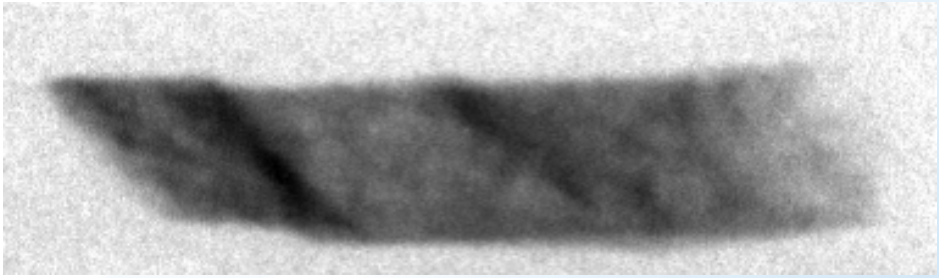

WXDT image of a 12x5x3 mm^3 CZT sample

They could be the reason why the internal E-field is not uniform

X-ray scans of the same 1.5-mm thick detector

20 V

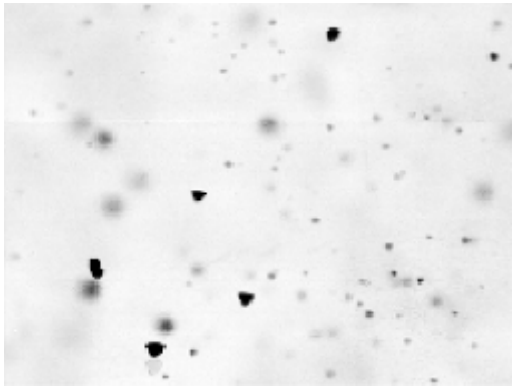

40 V

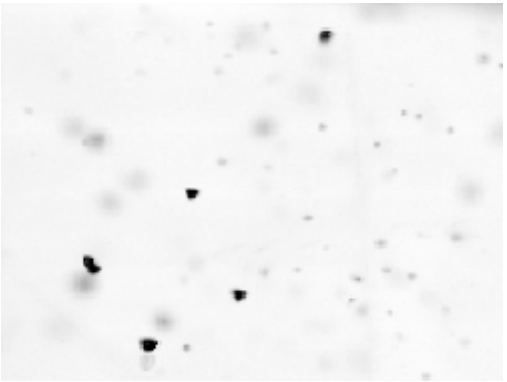

150 V

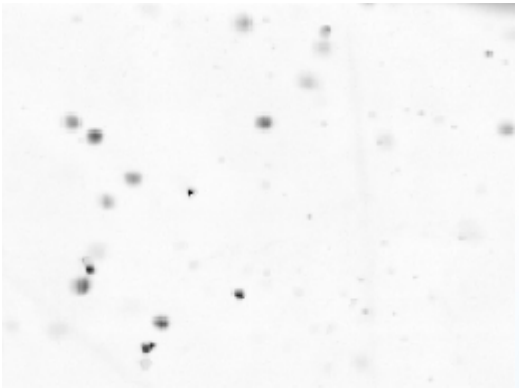

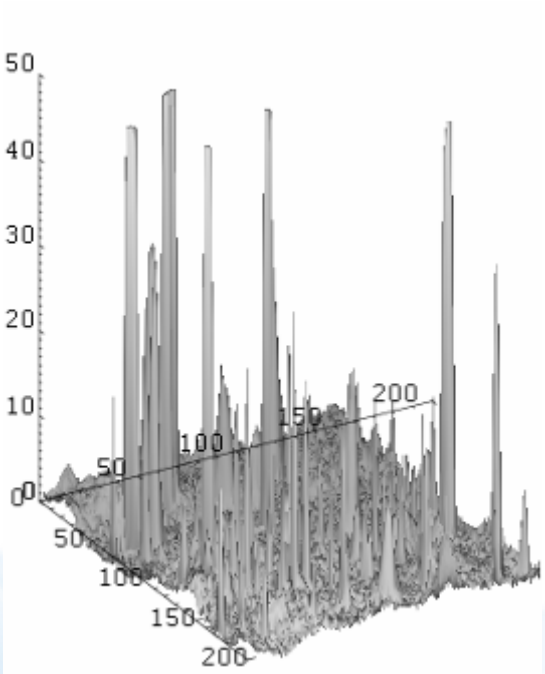

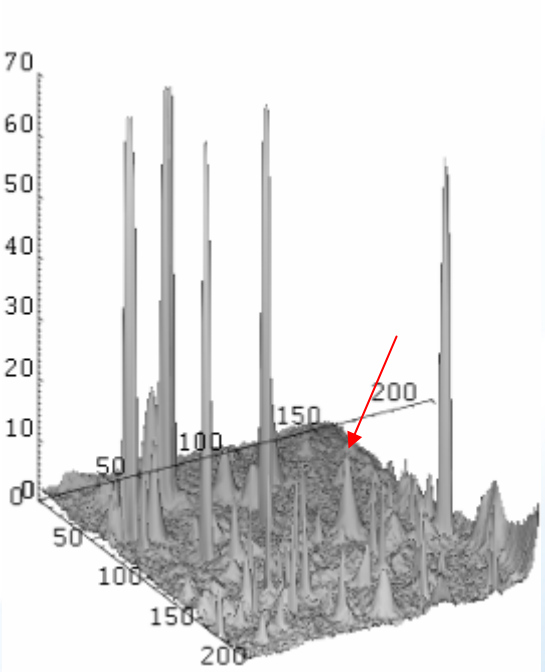

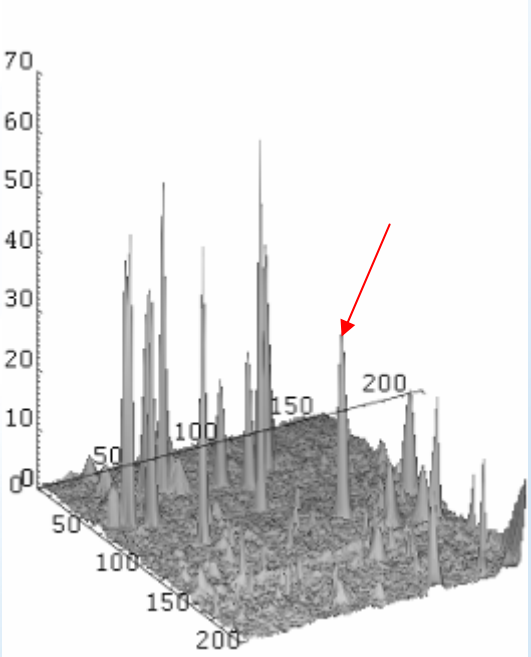

X-ray maps for one-pixel detector: uniform E-field

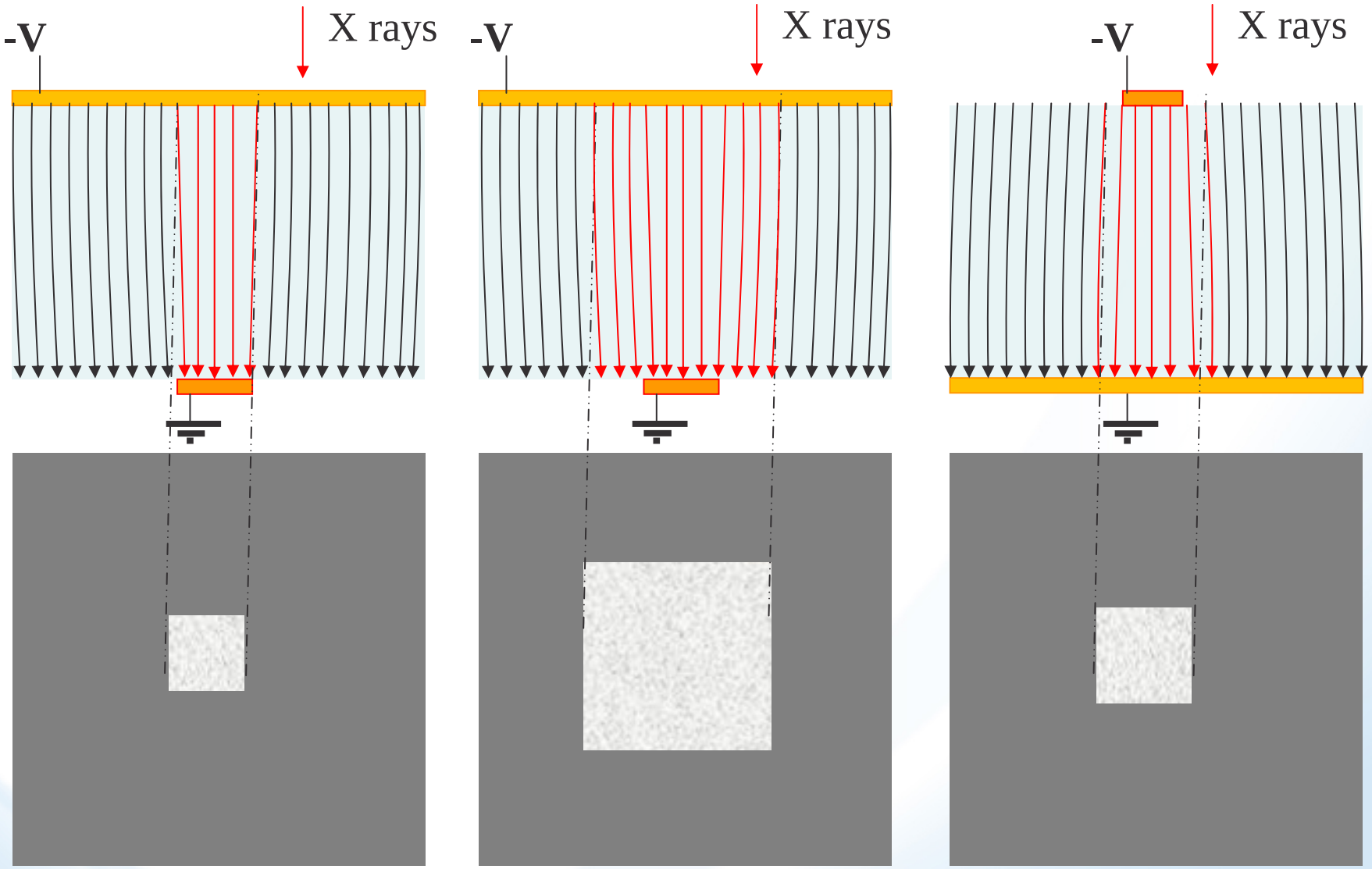

X-ray maps

X-ray maps for one-pixel detector: non-uniform E-field

Space charge could be the cause of internal E-field non uniformity

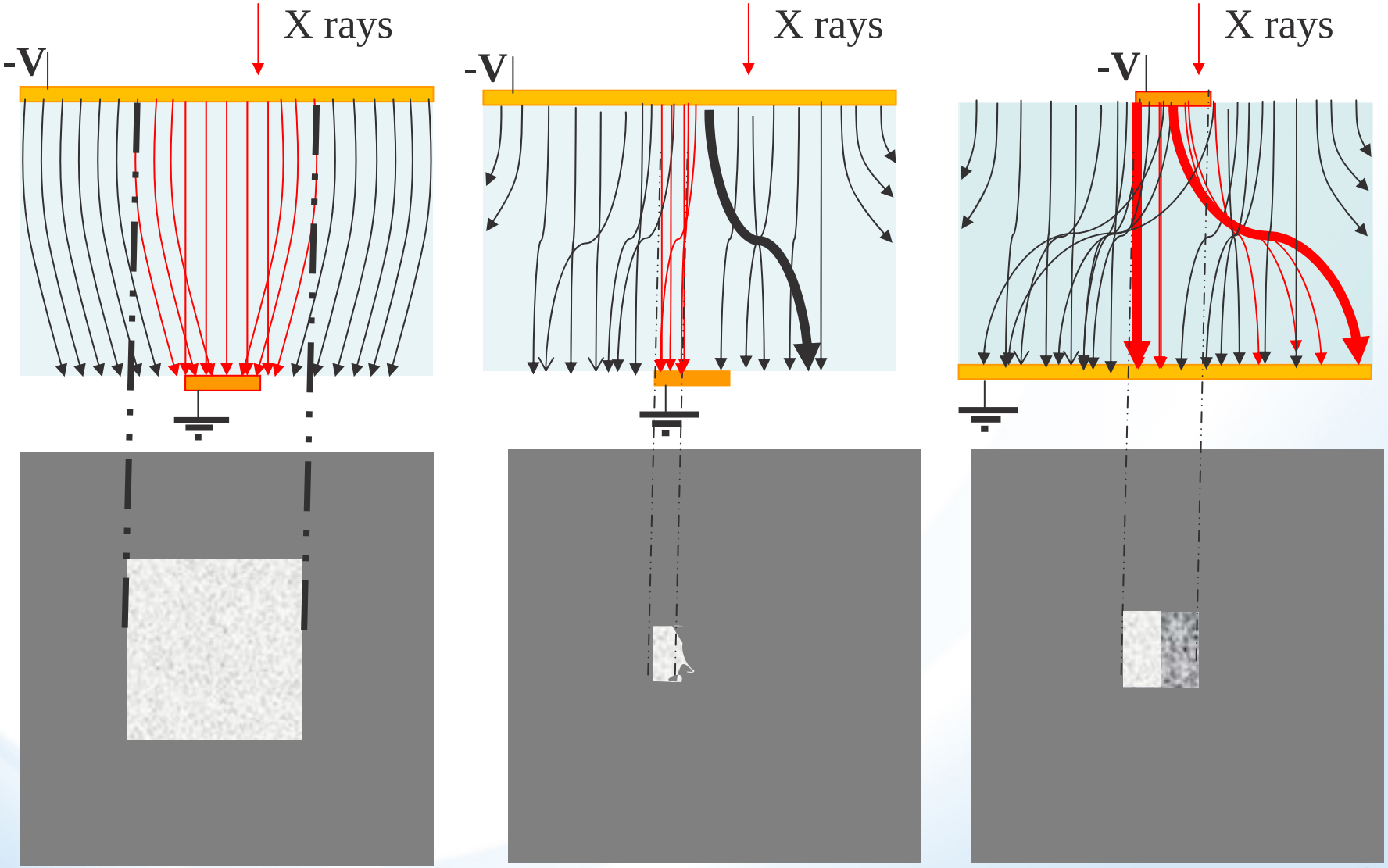

X-ray maps

Theory of Diffraction Topography

N.B. Not study of surfaces, the topography we are studying is that of the diffracting planes in the crystal

Transmission (Laue) topography.

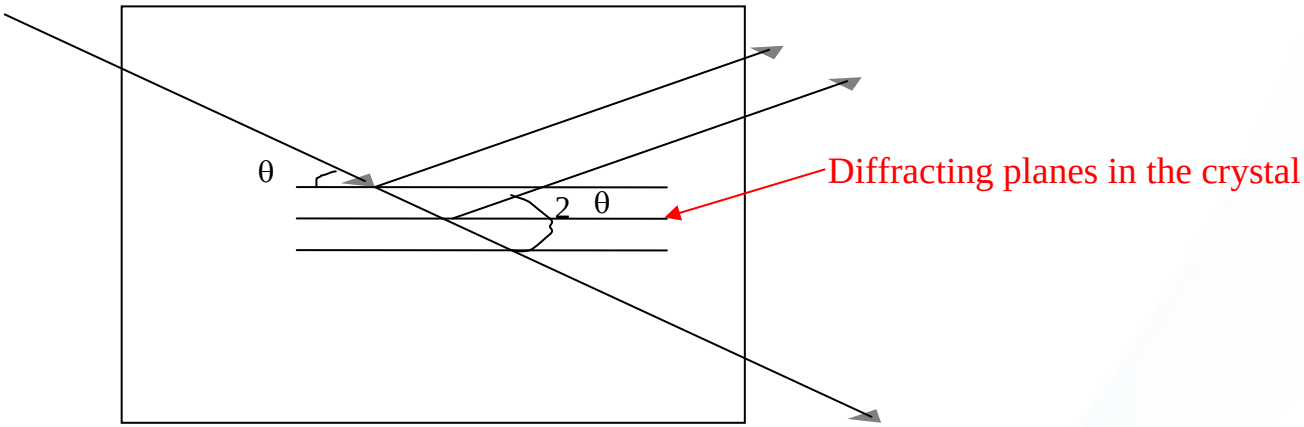

Reflection (Bragg) topography:

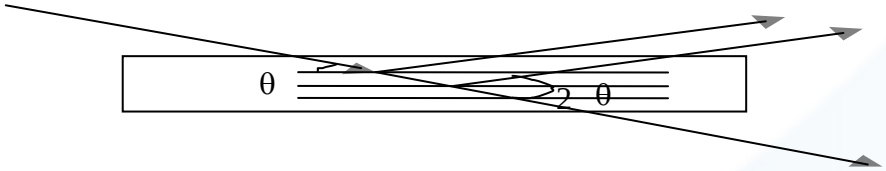

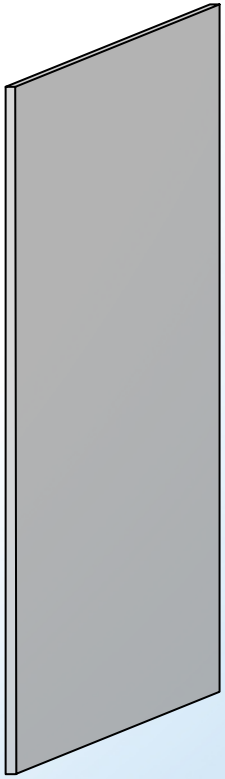
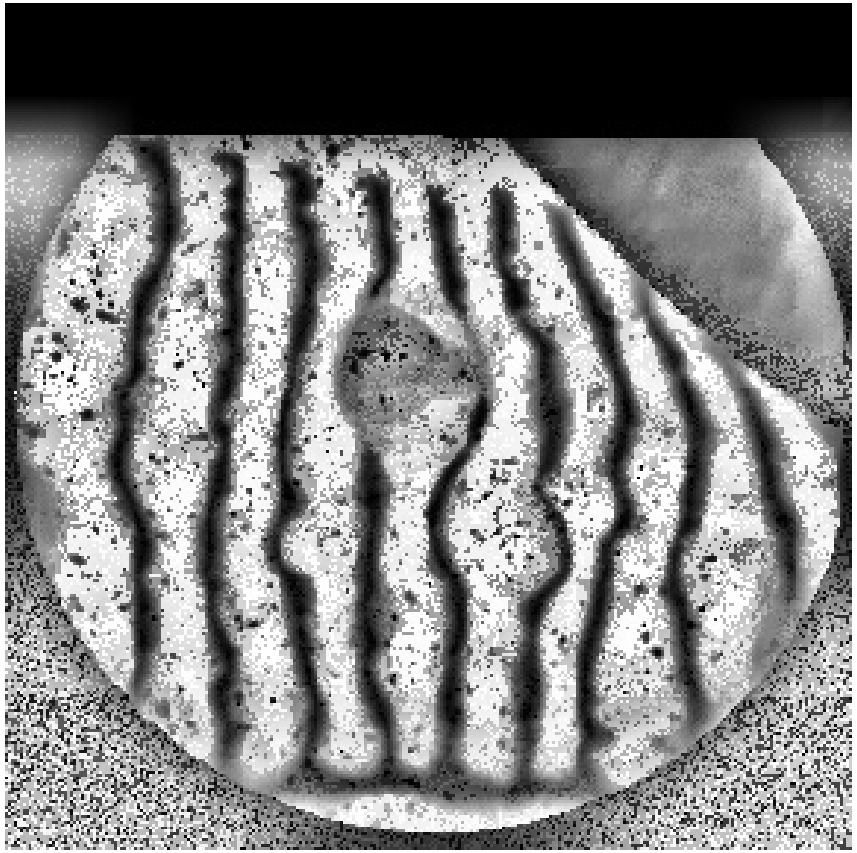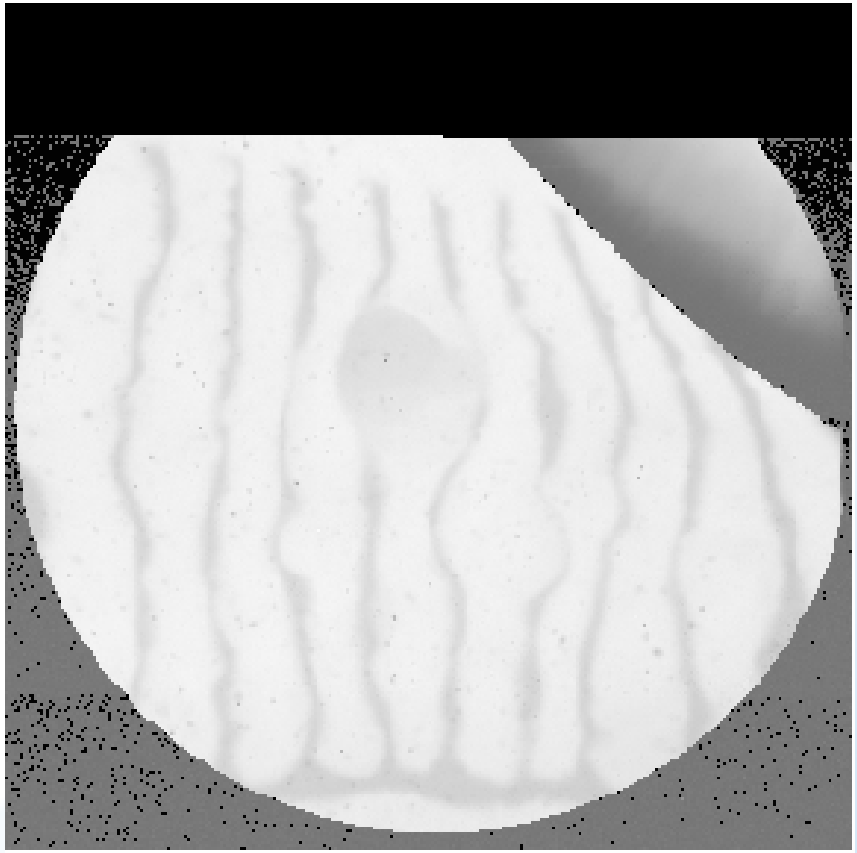
Bragg law $m\lambda = 2d \sin\theta$